REGULATION OF THE CARDIAC ISOFORM OF THE RYANODINE RECEPTOR BY S-ADENOSYL-L-LMETHIONINE

A Dissertation
Presented to
The Academic Faculty

by

Angela Kampfer Gaboardi

In Partial Fulfillment
of the Requirements for the Degree
Doctor of Philosophy in the
School of Applied Physiology

Georgia Institute of Technology
December 2011

REGULATION OF THE CARDIAC ISOFORM OF THE

RYANODINE RECEPTOR BY S-ADENOSYL-L-METHIONINE

Approved by:

Dr. Edward M. Balog, Advisor
School of Applied Physiology
Georgia Institute of Technology

Dr. Nael A. McCarty
Department of Pediatrics
Emory University

Dr. Thomas J. Burkholder
School of Applied Physiology
Georgia Institute of Technology

Dr. Raquel L. Lieberman
School of Chemistry & Biochemistry
Georgia Institute of Technology

Dr. T. Richard Nichols
School of Applied Physiology
Georgia Institute of Technology

Date Approved: October 18, 2011

This thesis is dedicated to Bob, Sue, Rob, Melissa & family who have taught me that the best things in life grow when shared.

ACKNOWLEDGEMENTS

I would first of all like to thank my committee members; my advisor, Dr. Ed Balog who has guided and encouraged me throughout my thesis work, and Dr. Tom Burkholder for all of his valuable insight. The unwavering enthusiasm of Dr. Neal McCarty and the knowledgeable perspectives of Drs Raquel Leiberman and Richard Nichols have been greatly appreciated. All of you have helped me to develop the skills and attitude necessary for the rigors of scientific research, for this I am very grateful.

I am so thankful for my parents Joan and Gert, who instilled in me early the value of hard work and inspired me to set high goals for myself. My sisters, Andrea and Stephanie have always been a loving support along the way. I would also like to thank Bob, Sue, and Melissa for their prayers and encouragement. A special thank you to my husband Rob, you are my best friend and greatest inspiration in life. I am forever thankful to God; it is only by his grace that I have arrived at the end of this journey.

TABLE OF CONTENTS

LIST OF TABLES

LIST OF FIGURES

LIST OF SYMBOLS AND ABBREVIATIONS

RyR2	Cardiac Ryanodine Receoptor
SR	Sarcoplasmic Reticulum
CSR	Cardiac Sarcoplasmic Reticulum
SAM	S-Adenosyl-L-Methionine
SAH	S-Adenosyl-L-Homocysteine
CaM	Calmodulin
FKBP	FK506 Binding Protein
ATP	Adenosine Triphosphate
AMPPNP	Adenosine 5'-(β,γ-imido)triphosphate
SERCA	Sarco/endoplasmic reticulum calcium ATPase
CICR	Calcium induced calcium release
DHPR	Dihydropyridine receptor
IP_3R	Inositol (1,4,5)-trisphosphate receptor
ENaC	Epithelial sodium channel
EM	Electron microscopy

SUMMARY

Activity of the Ryanodine Receptor (RyR2) (aka cardiac Ca^{2+} release channel) plays a pivotal role in contraction of the heart. S-adenosyl-l-methionine (SAM) is a biological methyl group donor that has close structural similarity to ATP, an important physiological regulator of RyR2. This work provides evidence that SAM can act as a RyR2 regulatory ligand in a manner independent from its recognized role as a biological methyl group donor. RyR2 activation appears to arise from the direct interaction of SAM, via its adenosyl moiety, with the RyR2 adenine nucleotide binding sites. Because uncertainty remains regarding the structural motifs involved in RyR2 modulation by ATP and its metabolites, this finding has important implications for clarifying the structural basis of ATP regulation of RyR2.

During the course of this project, direct measurements of single RyR2 activity revealed that SAM has distinct effects on RyR2 conductance. From the cytosolic side of the channel, SAM produced a single clearly resolved subconductance state. The effects of SAM on channel conductance were dependent on SAM concentration and membrane holding potential. A second goal of this work was to distinguish between the two possible mechanisms by which SAM could reduce RyR2 conductance: i) SAM interfering directly with ion permeation via binding within the conduction pathway (pore block), or ii) SAM binding a regulatory (or allosteric) site thereby stabilizing or inducing a reduced conductance conformation of the channel. It was determined that SAM does not directly interact with the RyR2 conduction pathway.

To account for these observations an allosteric model for the effect of SAM on RyR2 conductance is proposed. According to this model, SAM binding stabilizes an inherent RyR2 subconductance conformation. The voltage dependence of the SAM related subconductance state is accounted for by direct effects of voltage on channel conformation which indirectly alter the affinity of RyR2 for SAM. Patterns in the transitions between RyR2 conductance states in the presence of SAM may provide insight into the structure-activity relationship of RyR2 which can aid in the development of therapeutic strategies targeting this channel.

CHAPTER 1

INTRODUCTION

1.1 Ryanodine Receptors

1.1.1. Brief History:Elucidating the role of RyR in excitation-contraction coupling

In 1965 Alexander Sandow defined excitation-contraction coupling as "the function of the muscle fiber in which an electrical depolarization of the plasma membrane initiates a sequence of reactions that causes mechanical activation of the contractile myofibrils lying within the membrane"(*1*). The Ryanodine Receptor (RyR) is an ion channel most renowned for its critical role in this E-C coupling process. In the 1960s there was strong evidence to suggest that Ca^{2+} ions served as the direct chemical activator of muscle contraction. For example, Sidney Ringer found that isolated rat hearts beat perfectly when bathed in medium made with tap water, but when using distilled water, supplementation with Ca^{2+} ions was required to maintain contraction (*2*). Later, Heilbrunn and Wiercinski showed that the addition of Ca^{2+} to the cut ends of frog skeletal muscle fibers elicited contraction, and that of the various physiologically relevant ions applied directly to the cytoplasm, only Ca^{2+} elicited contraction (*3, 4*). However, 'the sequence of reactions' linking depolarization of the plasma membrane to a rise in cytoplasmic Ca^{2+} were poorly defined; the ryanodine receptor had not yet been discovered.

Striated muscle has an internal membrane system known as the sarcoplasmic reticulum (SR), which functions as an intracellular compartment for Ca^{2+} storage, and a

system of transverse tubules (T-tubules) which are invaginations of the plasma membrane. The SR consists of two distinct domains: the longitudinal SR and the junctional SR. The longitudinal SR surrounds the myofibrils as a network of interconnected tubules which coalesce at their ends into a single sac called terminal cisternae (i.e. junctional SR) (*5*). In 1962 Ebashi showed that SR extracted from muscle is able to accumulate Ca^{2+} from its external medium against very high electrochemical gradients and suggested a role for SR Ca^{2+} in the regulation of muscular contraction (*6*). Indeed, subsequent research would later reveal that the close apposition of the SR and T-tubule membranes establish the structural framework for E-C coupling in skeletal and cardiac muscle.

An early clue towards unraveling the E-C coupling mystery came in the 1980s through the work of Clara Franzini-Armstrong and colleagues. Using electron microscopy (EM), images of sectioned muscle revealed electron dense particles located at the junctions between the SR and T-tubules. These structures were given the name "foot" protein (*7, 8*). EM images also revealed that the junctional domains of the T-tubules were occupied by so called tetrads, each consisting of 4 intrinsic membrane particles (*7*). The positioning of tetrads in the junctional domain of T- tubules, and the feet in the SR suggested that these two proteins directly or indirectly interact possibly forming the link between excitation and contraction (i.e. electrical signals at the plasma membrane and the release of SR Ca^{2+}.)

Ryanodine proved invaluable in the identification and characterization of the junctional foot protein seen in EM images. Ryanodine, a natural plant alkaloid, was know to be toxic to animals, causing irreversible muscle contractions resulting in death

(*9*). At the time, it was not known that ryanodine binds with high specificity and affinity to the SR Ca^{2+} release channel (RyR) when it is open, thereby locking the channel an "open state" so that Ca^{2+} is not reaccumulated into the SR and the muscle cannot relax. Fleischer and colleagues showed that ryanodine blocked Ca^{2+} release from the SR, and direct binding studies with [^{3}H]ryanodine localized the receptors to the junctional region (terminal cisternae) of the SR (*10*). These findings supported previously accumulated evidence that Ca^{2+} release is localized to the junctional domain of the SR. EM images of the protein revealed a complex with fourfold symmetry having the overall dimensions and morphology consistent with the previously identified foot structure (*11, 12*), and when reconstituted into artificial bilayers the protein formed a high conductance Ca^{2+} channel (*13, 14*).

The present understanding of E-C coupling entails a critical interaction between the RyR SR Ca^{2+} release channel, and a voltage gated L-type Ca^{2+} channel, Cav1.1 (aka. dihydropyridine receptor, DHPR) within the T tubule membrane (previously seen in EM images as tetrads in the junctional region of T- tubules). The functional coupling between DHPR and RyR provides the link between depolarization of the surface membrane and release of SR Ca^{2+}. The mechanistic details of E-C coupling differ between skeletal and cardiac muscle. In skeletal muscle, a voltage induced conformational change in DHPR is transmitted to RyR via a physical interaction thereby activating Ca^{2+} release from the SR. In this system DHPR acts primarily as a voltage sensor rather than a Ca^{2+} channel; the influx of Ca^{2+} is not required. In cardiac muscle, E-C coupling occurs through a process of Ca^{2+} induced Ca^{2+} release (CICR) whereby the influx of external Ca^{2+} via the DHPR serves as the RyR activation signal. Thus the DHPR

and RyR do not physically interact. The sensitivity of Ca^{2+} induced activation of RyR forms the basis of CICR regulation in the heart.

1.1.2 Isoforms

There are three mammalian isoforms of the Ryanodine receptor encoded by three different genes; they are referred to as RyR1, RyR2, and RyR3. The isoforms exhibit ~70% overall sequence identity. The three isoforms differ in their tissue distribution. RyR1 and RyR2 are predominantly expressed in skeletal and cardiac muscle, respectively (*15, 16*), while RyR3 has a wide tissue distribution.

1.1.3. Structure and macromolecular complex

Two classes of intracellular ion channels have evolved to release Ca^{2+} from intracellular stores, the inositol (1,4,5)-trisphosphate receptor (IP_3R), and RyR. Both Ip_3R and RyR play important roles in fluctuations in intracellular Ca^{2+} concentrations which underlie a wide variety of physiological processes including cell division, memory and learning, and hormonal secretion. However, RyR has the singular claim to fame as the SR Ca^{2+} release channel in skeletal and cardiac muscle; a critical mediator of E-C coupling. RyRs were first observed as the 'foot' structures that bridge the approximate 12 nm (120Å) gap separating the T-tubule and SR membranes in cardiac and skeletal muscle (*17*). RyR is the largest of all ion channels and size is one of the greatest challenges faced in the elucidation of protein structure.

RyRs are high molecular weight homotetramers consisting of a C-terminal SR membrane spanning domain which forms an ion conduction pathway approximately 7

nM in length and 8 nM in diameter (*12*). The channel's large N-terminal cytoplasmic domain has the approximate dimensions 29x29x12 nM (*12, 15*). The quatrefoil structure of RyR arises from the symmetrical arrangement of four identical subunits of approximately 5,000 amino acids, or 560 kDa, each contributing to the formation of a single central ion conduction pathway. The tetrameric channel encompasses approximately 20,000 amino acids. Although the exact number remains to be determined, 6-8 transmembrane alpha helices are believed to form the channel's central pore. The pore may function in a manner analogous to the opening and closing of the iris of a camera. The pore dimensions are approximate, 2-3Å in width with a voltage drop of 10.4 Å in length (*18*).

Each RyR tetramer exists in its native membrane in complex with several accessory proteins. The best known RyR-interacting proteins are calmodulin (CaM), which tonically inhibits RyR2 activity and produces biphasic effects on RyR1(*19, 20*), FK506 binding proteins (FKBPs) which stabilize RyR in its closed state (*21, 22*), and the triadin-junctin-calsequestrin complex which senses luminal Ca^{2+} and modulates RyR activity by acting either as a Ca^{2+} reservoir or as a direct channel ligand (for review see (*23*). Additionally, anchoring sites for proteins involved in posttranslational RyR regulation have been identified. Protein kinase A (PKA), calmodulin-dependent protein kinase (CaMK)II, protein phosphatase (PP)1, and the cAMP-specific phosphodiesterase (PDE)4D3 are among the well characterized proteins which are critical to the physiological and pathological regulation of RyR (*15, 22, 24*). In addition to phosphorylation (*18*), a role for oxidation and nitration in RyR modification has been established (*25, 26*).

1.1.4. Functional assays

1.1.4.1. Ryanodine Binding

The purification of the Ryanodine Receptor (RyR) from skeletal and cardiac SR was made possible through the use of the plant alkaloid ryanodine, which binds to RyR with high specificity and affinity (nanomolar range). Ryanodine binds channels only in the open state, a property which has made [^{3}H]ryanodine binding a useful functional probe of the opening of RyRs by other ligands (*27, 28*). Effectors which activate the channel increase the rate of [^{3}H]ryanodine binding, while the rate of binding is decreased upon exposure of RyRs to channel inhibitors. Ryanodine binding is a straightforward assay that correlates well with RyR activation levels. Therefore, the [^{3}H]ryanodine binding assay is a sensitive and efficient method for investigating the function of a large number of RyR channels.

1.1.4.2. Reconstitution into planar lipid bilayers

Direct measurements of channel activity can provide mechanistic insights that would be otherwise undetected by [^{3}H]ryanodine binding. Because RyRs are located in the membrane of intracellular organelles, they are not directly accessible to patch pipettes, thus single RyRs are not easily studied by traditional patch techniques. Instead SR vesicles or purified RyRs are incorporated into an artificial lipid bilayer separating two ionic solutions. This setup allows considerable flexibility in manipulating experimental conditions.

The method used to form lipid bilayers is a modification of the film drainage method originally developed by Mueller et al (*29*). Lipids resuspended in a hydrophobic solvent such as n-decane are spread across a small aperture in a plastic septum producing a thin lipid film separating two fluid filled chambers. Both bilayer formation and channel incorporation are spontaneous processes. Ion channel protein is added to one side of the bilayer referred to as the *cis* (cytoplasmic) side because the channel will almost always incorporate with its large cytoplasmic domain exposed to the bath to which the protein was added. The luminal (SR lumen) side of the channel will face the opposite (*trans*) bath. Conditions which promote vesicle fusion include i) vigorous stirring of the *cis* bath (usually with a magnetic stirrer), ii) an osmotic gradient across the membrane (*cis* high), and iii) millimolar *cis* [Ca^{2+}]. When SR vesicles are incorporated into the bilayer, cesium methanesulphonate (CsMS) is commonly used as the principal salt in the chamber solutions. This is to prevent current signals from other ion channels from interfering with RyR recordings. RyR is quite permeable to Cs^+, whereas other ion channels in the SR do not conduct Cs^+ or MS^-. Once a channel incorporates it is possible to determine the ion conductance of a single channel (unitary conductance) and to monitor its opening and closing (gating) by measuring the current through the membrane in response to an applied electrochemical gradient.

Single RyR channel current signals appear as stochastic jumps typically between two stationary current levels representative of the channel in a closed, non conducting state, and an open, maximum conducting state. Less common intermediate current levels corresponding to subconductance states may also appear in RyR current records (see section 1.3.2). Stationary current levels are identifiable as peaks in amplitude histograms.

The peak width and the area under each peak reflect respectively, background noise, and time spent at that current level. Open probability (P_o), an overall measure of channel activity, is determined from current records as the fraction of time the channel is in a conducting state. An increase in P_o can arise from either an increased lifetime of the open state or a decreased lifetime of the closed state, also referred to as frequency of channel opening.

1.1.5. Biophysical properties

1.1.5.1. Gating and kinetic analysis

Descriptions of channel gating are based upon mathematical models that assume the existence of one or more closed state(s) and one or more open state(s). Figure 1A describes the kinetic behavior of a channel which can exist in only two states, open (O) and closed (C). For this 2 state channel, the time spent in any state is given by the reciprocal of the sum of the rate constants for leaving that state. Because the mean open time is $1/k_{-1}$ and the mean closed time is $1/k_1$, the rate constants can be obtained by measuring the mean open and closed times. The opening and closing of a single channel is well modeled by a Markovian or memoryless process meaning the state transition probability does not depend on previous states. As a consequence, channel lifetimes (open and closed times) are distributed exponentially (Fig. 1 B). With a single open (or closed) state as shown in Figure 1, the open (or closed) time distribution will follow a single exponential and the mean open (or closed) time will be given by the time constant of the distribution (i.e. τ_o or τ_c). It is not uncommon for channels to have several

kinetically distinguishable open (or closed) states, thus channel lifetimes may be best described by the sum of multiple exponential functions. In general the number of exponential components in the open (or closed) time distribution gives a lower estimate of the number of different states (i.e. channel conformations) associated with opening (or closing) events.

Analysis of single channel gating kinetics has provided insight into the mechanism underlying cytosolic Ca^{2+} activation of RyR. In the presence of 10 μM cytosolic Ca^{2+} the majority of channel openings are ≥1 ms in duration (*30*). The Ca^{2+}-induced increase in channel P_o arises from an increase in the frequency of channel openings, in other words, the progressive increase in P_o with increasing $[Ca^{2+}]$ is associated with a decrease in the duration of all closed dwell times (*30*). This has been attributed to Ca^{2+} ions binding to and thereby decreasing the dwell time of individual closed states. The behavior of RyR under physiological conditions has been well described by models which include two or three closed states and two open states (*31*). Using higher temporal resolution, up to three open and five closed states have been described for RyR (*30*). Correlation analysis of successive lifetimes suggested at least two distinct pathways exist between open and closed states. This finding lead to the proposition of a cyclic gating scheme for cytosolic Ca^{2+} activation of RyR2 (Fig. 2) (*31*).

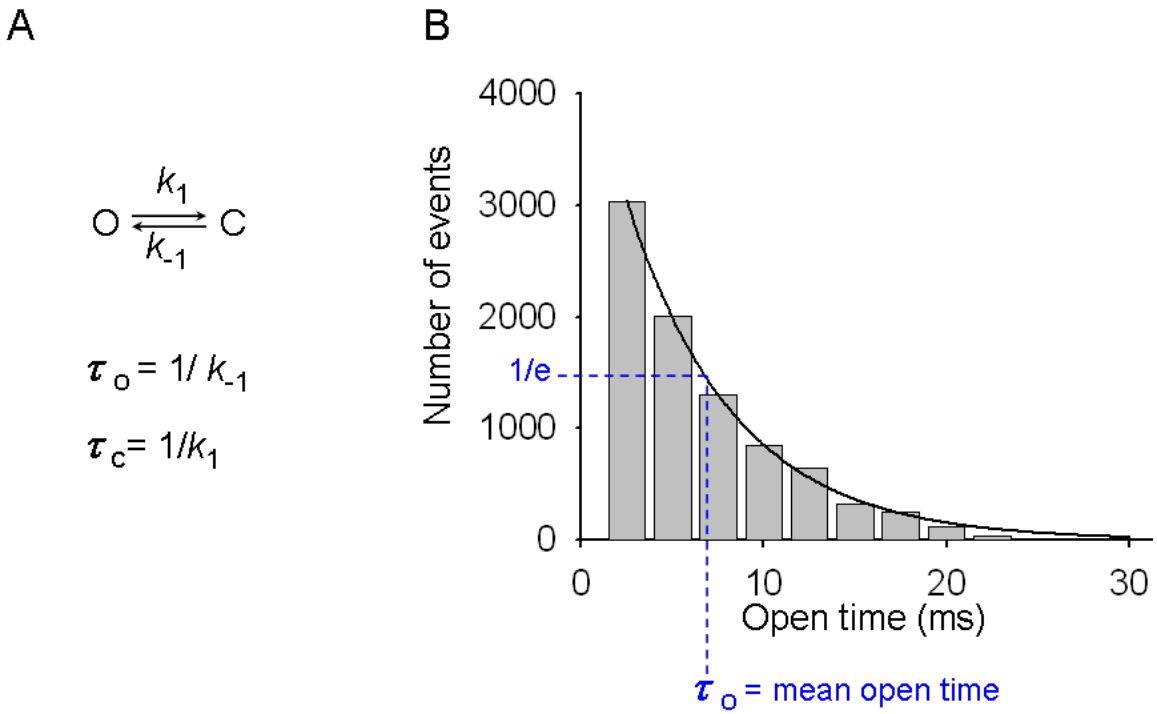

Figure 1. Kinetic analysis of single channel currents. A. Kinetic behavior of a hypothetical channel which can exist in either an open (O) or closed (C) state, where k_1 and k_{-1} are the rate constants (in sec^{-1}) for entering and leaving the open state, respectively. B. For a channel with one open state, the open times will follow a single exponential distribution. The time at which the number of events falls to 1/e of its maximal value represents the mean open time (τ_o).

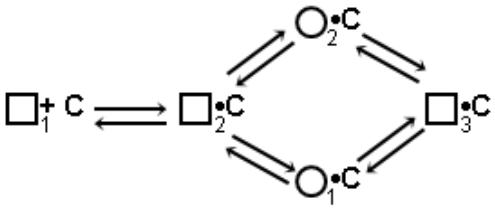

Figure 2. Minimal Kinetic Scheme for Ca^{2+} Activation of RyR. Ca^{2+} activated RyR2 has been described by a model which includes at least three closed states and two open states. This cyclical or branched gating scheme proposed by Ashley and Williams (1990) permits channel openings to two open states (O) from a single closed state (□). Ca^{2+} (C) activation of RyR has been attributed to a Ca^{2+}-induced decrease in the duration of closed times resulting from Ca^{2+} binding to one or more closed states.

1.1.5.2 Conductance and selectivity

Ion channels are highly permeable to some but not all ions. The ion selectivity of a channel arises partially from the shape of the ions and the channel pore, and partially from energy changes that accompany ion permeation. The ryanodine receptor is a poorly selective channel which has a high conductance for group Ia monovalent cations (Li^+, Na^+, K^+, Rb^+, Cs^+) and the alkaline earth divalent cations (Ba^{2+}, Sr^{2+}, Ca^{2+}, Mg^{2+}). The channel has a unitary conductance of ~750 pS in symmetrical 250 mM K^+ and ~150 pS in symmetrical Ca^{2+}. The channel's large Ca^{2+} conductance was originally demonstrated in recordings of native RyR channels (*13, 32*). Under bi-ionic conditions RyR is significantly more permeable to the alkaline earth divalent cations over K^+, however, there is little difference in permeability among the individual divalent cations or among the group Ia monovalent cations. Although the conductance of RyR for monovalent cations is higher than for Ca^{2+}, divalent cations are selected for over monovalent cations by a factor of 5-7 under physiological conditions (*33*).

RyR has a linear current-voltage relationship under symmetrical ionic conditions with monovalent cations as the permeant ions. With divalent cations as the permeant ions, the linear current-voltage relationship deviates slightly from ohmic behavior at high holding potentials.(*34, 35*). The Eyring rate theory has been used to model the movement of ions through channel pores. This theory conceptualizes the movement of ions as a series of jumps between binding sites thought of as energy minima or 'wells' separated by energy maxima or 'peaks'. Ion binding affinity depends on well depth and ion selectivity depends on differences in peak heights. Although rate theory is an

oversimplification of the underlying complex microscopic events, it can provide insight into the mechanisms of ion permeation in channels.

Investigations of the ionic conductance and selectivity properties of RyR2 from sheep cardiac muscle suggest that ions move in a single file through the RyR2 pore (*34, 35*). Conductance measurements in mixtures of K^+-Na^+ and K^+-Li^+ revealed no anomalous behavior as the mole fraction of the ions is varied, a finding consistent with single pore occupancy. Furthermore, the lack of rectification in the single channel current-voltage relationship implies a symmetric energy profile about a central axis. However, results from blocking experiments with a series of small tetraalkyl ammonium (TAA) cations suggested multiple pore occupancy (at least two cation binding sites). These blocking experiments also indicated that the RyR pore is most narrow close to the luminal face of the protein (*36*). A 4 barrier, 3 binding site model has been used to describe characteristics of ionic conductance in RyR2. Specifically, this model proposed the existence of a centrally located (within voltage drop) high affinity divalent binding site to account for the discrimination between divalent and monovalent cations (*33*).

1.1.6. RyR channel regulation

RyR is a Ca^{2+} gated channel. The sensitivity of Ca^{2+} induced activation of RyR forms the basis of CICR regulation in the heart. Several factors influence the sensitivity of RyR to activation by Ca^{2+}. Some of the best characterized RyR effectors include adenine nucleotides which activate the channel, and Mg^{2+} which has an inhibitory affect (*18, 27*).

RyR channel modulators are typically classified according to their effect on channel activity. Single channel current recordings provide the greatest mechanistic insight into the agonistic or antagonistic effects of RyR regulators. The majority of effectors act primarily by altering the opening and closing of the ion conduction pathway (through an allosteric mechanism), for example by increasing or decreasing the channels sensitivity to activation by Ca^{2+}. Some compounds are known to block RyR (i.e. physically obstruct the movement of ions through the channel pore; see section 1.3).

1.1.6.1. Ryanodine

Interaction of the plant alkaloid ryanodine with single RyR channels results in complex, concentration dependent modulation of channel conductance and gating. Ryanodine has three effects on channel activity. Submicromolar concentrations have been reported to increase channel P_o to the full conductance state (*37*). The more consistent finding, however, is for the channel to enter one or more relatively long lived subconductance states (most commonly to 50% of the full conductance level) in the presence of submicromolar concentrations of ryanodine. Micromolar or higher concentrations of ryanodine cause complete channel closure (*38*). The first two of the described effects are consistent with reports of a high affinity [^{3}H]ryanodine binding site and the third effect is consistent with the low affinity [^{3}H]ryanodine binding site/s (one or three low affinity sites have been suggested). The effects of ryanodine and several of its synthesized derivatives (ryanoids) on the K^+ conduction of RyR2 have been examined extensively. Unlike the control open state, the open probability of the ryanoid modified subconductance state is voltage dependent. The amplitude of the modified substate

induced by ryanoids varies, ranging from ~5 to 70% of the full conductance state (*39*). Although the molecular location of ryanodine binding sites remains unknown, a comparative molecular field analysis of the relationship between the structure of a group of ryanoids and their modulation of RyR conductance properties wase not consistent with a direct interaction of ryanodine with the ion permeation pathway. An allosteric mechanism has been proposed whereby ligand-induced conformational changes in the RyR mediate the interactions between ryanoids and permeant cations (see discussion in section 1.4.1) (*40*).

1.1.6.2. Calcium and Magnesium

RyR is a Ca^{2+} gated channel, thus functional assays of channel activity require Ca^{2+} in the medium in order for the channel to assume an open conformation. RyR displays a bell shaped Ca^{2+} activation/inactivation curve in the absence of other effectors. The biphasic regulation of RyR by cystolic Ca^{2+} is well characterized and has been demonstrated in SR vesicle Ca^{2+} efflux measurements, [^{3}H]ryanodine binding assays, and single channel recordings (*41*). RyRs are activated by Ca^{2+} within the μM range and inhibited by Ca^{2+} in the μM-mM range. The basis for this biphasic Ca^{2+} dependence is postulated to result from two distinct Ca^{2+} binding sites on the RyR channel, a high affinity binding site which when occupied opens the channel, and a low affinity binding site whose occupancy closes the channel. In single channel experiments, RyR has a P_o close to 0 in resting cytosolic Ca^{2+} (0.1 μM *cis* side). Micromolar concentrations of cytosolic Ca^{2+} cause near full activation of RyR, while millimolar concentrations have an inhibitory effect (*42*). Cytosolic Ca^{2+} is required for activation of the cardiac ryanodine

receptor (RyR2) (*43, 44*), but alone is not sufficient for maximal channel activity (*30, 31, 45*). P_o values for channels activated by cytosolic Ca^{2+} alone (up to 100 μM; roughly corresponding to maximum physiological [Ca^{2+}]) rarely exceed 0.5. RyR is also regulated by luminal Ca^{2+}, however whether this results from Ca^{2+} binding a luminal site or by gaining access to a cytoplasmic site (or both) remains unresolved (*46, 47*).

Magnesium inhibits RyR by two distinct mechanisms. Magnesium competes with Ca^{2+} for the high affinity Ca^{2+} activation site, although with much lower affinity (approximately 1 mmol/L affinity vs. 1 μmol/L affinity for Ca^{2+}). Additionally, Mg^{2+} and Ca^{2+} share a common inhibitory mechanism; at millimolar concentrations they both bind to the low affinity Ca^{2+} inhibitory site on the channel (*48*).

1.1.6.3. FK506 binding proteins

The family of FK506-binding proteins (FKBPs) bind the immunosuppressive drugs FK506 and rapamycin. The FKBP family has more than 20 members; the individual proteins are named according to their molecular mass. FKBP12/12.6 are tightly associated with RyRs in a stoichiometry of 1 per monomer (*21*). FKBP 12.6 is present in lower concentrations than FKBP12 in both cardiac and skeletal muscle (*49*). Although it was originally thought that only FKBP12.6 associated with RyR2 (*50*), recent studies have shown that the two FKBP isoforms bind both RyR1 and RyR2 (*51*). Due to its higher tissue concentration, FKBP12 is the predominant form bound to RyR1. The preferential interaction of FKBP12.6 with RyR2 results from the much higher affinity of RyR2 for FKBP12.6 compared to FKBP12 (*49*). FKBPs may have a role in coordinating interactions among the four RyR subunits, possibly stabilizing the maximum unitary

single channel conductance level. A controversial hypothesis, initially proposed by Andrew Marks, maintains that PKA mediated phosphorylation of RyR2 at serine 2808 (RyR2-S2808) causes FKBP12.6 dissociation thereby increasing channel open probability by inducing a long lived subconductance state(*21, 22*). According to this hypothesis, RyR2 hyperphosphorylation causes the elevated diastolic Ca^{2+} leak observed in heart failure (*22*). However, central tenets of this hypothesis have not always been reproduced. Several groups found that PKA phosphorylation of RyR2-S2808 neither caused FKBP12.6 dissociation nor significantly altered channel gating (*52-55*). At least two groups have failed to detect any effects of FKBP12.6 dissociation on RyR2 activity (*52, 56*).

1.1.6.4. Adenine nucleotides

Adenine nucleotides activate RyR2 in a concentration and Ca^{2+} dependent manner (*57*). In resting cardiac muscle, the basal ATP concentration is approximately 5-6 mM (*58*). This is sufficiently high for ATP to function as a principal cellular regulator of RyR2 (*59*). ATP, and its metabolites increase specific [^{3}H]ryanodine binding to RyR2 and increase channel open probability (*43, 57, 60, 61*). The efficacy of ATP and its metabolites follows the order ATP>ADP>AMP>adenine >adenosine (*43, 62*). ATP almost fully activates RyR2 with half-activating concentration (EC_{50}) in the high micromolar range in the presence of 10 μM cytosolic Ca^{2+} (*43*). ATP and other adenine based compounds are thought to bind to a poorly characterized adenine nucleotide binding site. The purine ring is important for agonist activity as the replacement of adenine with guanine destroys the ability of the nucleotide to modulate RyR (*57*).

However, the structural features of adenine based compounds which impart efficacy in activating RyR2 are unknown. Comparative molecular field analysis studies investigating correlations between ligand structure and efficacy in activating RyR2 have attributed the high efficacy of ATP to its negatively charged phosphate groups. This conclusion was based on the observation that decreasing the number of phosphate groups decreases the ability of adenine nucleotides to open the channel (*61*).

Questions also remain regarding the number and location of ATP binding sites on RyR. Depending on isoform and species the consensus sequence for an ATP binding site, GXGXXG, occurs between three and six times in the RyR sequence. A study investigating the direct effects of ATP of RyR2 gating showed that in the presence of 10 μM Ca^{2+} half maximal activation of RyR2 occurred at 0.22 mM ATP, and maximal channel activation occurred at 2 mM ATP. A hill coefficient of 1.5 for the ATP dose-response curve indicates that at least two molecules of ATP bind to the channel to cause maximal activation (*43*). By monitoring the direct binding of a spin-labeled ATP, another group showed that a total of eight nucleotide binding sites are located on RyR1 (*63*). Together the characteristics of RyR activation by ATP, and direct binding studies suggest the presence of two ATP sites per RyR monomer.

1.2. Molecular recognition of ATP in proteins

Although there is no universal fingerprint for ATP binding in proteins, a number of signature motifs are involved in the binding of nucleotide phosphate groups and their associated metal ions. The phosphate-binding loop (P-loop) or Walker A motif consists of a glycine rich sequence followed by a conserved lysine and a serine or threonine

(GXXXXGK[TS])(*64*). The conserved lysine is thought to be important for loop conformation and may interact directly with β and γ phosphates of ATP via hydrogen bonding, while the conserved serine/threonine is believed to coordinate associated Mg^{2+} ions. This sequence typically forms a flexible loop between a β-strand and an α-helix, therefore, a prudent search for potential ATP binding sites would consider the structural context in which identified glycine rich motifs are located. Not all ATP binding proteins contain a P-loop within their primary sequence; these include the E1/E2 type ATPases, actin, tubulin, and gylcolytic kinases.

Non-bonded intermolecular interactions are also important molecular determinants for recognition of the adenine moiety of ATP by proteins(*65*). These interactions occur between the adenine base and its surrounding residues in binding pockets of adenylate-binding proteins. The three most important interactions are hydrogen bonding (adenine base has the capacity to form five H-bonds), π-π stacking interactions between the adenine base and aromatic residues (Phe, Tyr, and Trp), and cation-π interactions between the adenine base and positively charged residues (Lys, and Arg).

The inositol (1,4,5)-trisphosphate receptor (IP_3R) and the ryanodine receptor are members of the intracellular Ca^{2+} channel super family. ATP regulates both RyRs and IP3Rs in a manner, which does not require hydrolysis. The activity of all three IP_3R channel isoforms is increased by micromolar concentrations of ATP and decreased with millimolar concentrations(*66*). Two putative adenine nucleotide binding sites designated ATPA and ATPB have been identified within the regulatory domain of the type 1 IP_3R at residues 1773-1780 and 2016-2021 respectively (*66*). The glycine rich motifs within

these segments are believed to underlie the stimulatory effect of ATP on the IP_3R channel. The ATPA site is unique to the type 1 IP_3R, ATPB is conserved among all 3 channel isoforms, and a third sequence (ATPC) is formed upon the removal of the S2 splice site from the type 1 IP_3R (*67*). The inhibitory effect of ATP at higher concentrations has been attributed to its action as a competitive antagonist at the IP_3 binding site (*68*).

A sequence alignment of the mouse type 1 IP_3R with either the human or mouse RyR2 was performed with protein BLAST. Neither IP_3R consensus adenine nucleotide-binding motif (residues 1773-1780 or 2016-2021), however, was among the 5 or 6 BLAST hits producing significant sequence alignments. Electron-spin resonance (ESR) spectroscopy on RyR1 has been used to monitor the interaction of a spin-labeled ATP with the intact RyR1 protein. These studies suggested that each RyR1 monomer has 2 functionally distinct ATP binding sites (*63*). Sequence analysis of RyR1 predicts at least eight adenine nucleotide consensus binding motifs (GXGXXG) (*69*); a number, which greatly exceeds the two binding sites per monomer suggested by ESR studies. The GXGXXG motif is present within the residues 2-7, 699-704, 1195-1200, 2264-2269, 2370-2375, 4449-4454, 4452-4457, and 4602-4607 in RyR1. Brandt and colleagues identified a RyR1 peptide fragment photo-labeled with 8-azido[α-^{32}P]ATP containing the amino acids 2370-2375 providing additional evidence that this sequence may be a functional ATP binding site(*70*). Four additional sequences, amino acids 1081-1084, 2935-2938, 3503-3506, and 3937-3940, conform to the consensus ATP-binding sites Y[GAST][VG][KTQSN] reported to bind the purine ring of ATP in the chaperone protein GroES. This motif has been proposed to form potential ATP binding sites in

RyRs as neither ATP bound to this site in GroES, nor ATP which activates RyRs is hydrolysed (*71*). Otsu and colleagues predicted only one putative GXGXXG consensus site in the rabbit RyR2 sequence, residues 2619-2652. This sequence was predicted to be preceded by a beta strand and followed by an alpha helix. An additional GXGXXG sequence was found but not considered as an acceptable ATP binding site due to its inappropriate structural context (*72*).

Presumably only a subset, if any of the predicted consensus motifs in RyR confer sensitivity to ATP, yet this remains to be established. Interestingly, a recent study demonstrated that mutation of the ATPA and ATPB sites in IP_3R did not eliminate the ability of ATP to activate the channel, while mutation of ATPB in the type 2 and type 3 IP_3R eliminated the enhancing effects of ATP on the type 2 but not type 3 channels (*73*). Furthermore, mutagenesis of two predicted ATP binding sequences, GXGXXG (amino acids 2370-2375 of RyR1), and YSGK (amino acids 3937-3940 of RyR1), which are conserved among all RyR isoforms, did not alter ATP induced increase in [^{3}H]ryanodine binding to any of the RyR1 mutants. Mutations in the GXGXXG motif did, however, reduce caffeine and 4-chloro-m-cresol sensitivity of RyR1 (*69*). Therefore ATP regulation of ion channel activity may involve a novel mechanism, and/or sequence analysis may be an inaccurate means of predicting putative adenine nucleotide binding sites in ion channels.

1.3. Multiple conductance states in ion channels

The simplest model for an ion channel has an open (conducting) and closed (non-conducting) state (i.e. conformation). Therefore traditionally, gaiting refers to transitions

between the one open and one closed state (Fig 1). The RyR regulators Ca^{2+}, Mg^{2+}, and adenine nucleotides discussed above under *RyR channel regulation* are classified as gating modifiers. Adenine nucleotides, for example, increase overall time spent in the open state by stabilizing and destabilizing the channel open and closed conformations, respectively. However, measurements of single channel activity have shown that many types of ion channels exhibit multiple open (and closed) states, thus not conforming to a simple two state model. Indeed, the number and variety of ion channels for which subconductance behavior has been described suggests that channel gating is a dynamic process which involves transitions among a multitude of protein conformations having different energy minima and maxima.

1.3.1. Ion channels exhibit subconductance behavior

Subconductance states have been described for a variety of ion channels including the acetylcholine receptor channel from embryonic rat muscle (*74*), the voltage dependent K^+ channel from *Torpedo* electroplax (*75*), the Ca^{2+} dependent K^+ channel of rat muscle (*76*), the serotonin dependent K^+ channels from *Aplysia* sensory neurons (*77*), and RyR. Both GABA- and glycine- activated chloride channels display a range of conductance states (*78*). Additionally, rapid voltage dependent transitions between subconductance states have been reported for type 1 and type 3 IP_3R channels in *Xenopus* oocyte nuclei (*79, 80*). Together these observations lend support to the theory that, even in the absence of regulatory ligands, channel proteins adopt multiple conformations having distinct ion permeation properties.

1.3.2. Subconductance behavior in RyRs

Ryanodine receptors are in part characterized by their large unitary single channel conductance (~750 pS in symmetrical 250 mM K^+ and ~150 pS in symmetrical Ca^{2+}), however, less prevalent subconductance states have been observed, and are especially evident in purified channels (*81*). Ahern and colleagues observed brief openings to multiple conductance states in rabbit skeletal muscle RyRs, and that openings to an inherent conductance level ~30% of the maximum single channel conductance were prolonged in the presence of the immunosuppressant FK506 (*82*). Similar subconductance behavior has been reported by others (*21, 22*). The loss of RyR accessory proteins during enrichment of SR fractions by sucrose-gradient centrifugation may contribute to the greater prevalence of subconductance states in purified channels. Generally speaking substates are rarely observed in RyR; however, regulation of their occurrence may have physiological significance. For example the level of RyR phosphorylation has been shown to influence channel gating between multiple open conductance states (*83*).

1.4. Mechanisms of channel 'block': Classic pore block vs. allosteric mechanism

Several venoms, herbs, food poisons, and drugs are known to affect the excitability of cell membranes by acting on ion channel proteins (*84*). By inhibiting the ionic current through channels these agents can decrease membrane excitability. Small charged species such as metal and organic cations can reduce whole cell currents by interfering directly with ion permeation via binding within the conduction pathway (i.e. pore block). An allosteric mechanism has also been proposed whereby the binding of a

molecule at a regulatory or allosteric site stabilizes closed or reduced conductance conformations of the channel, essentially casing the pore to block itself. Nature exploits both mechanisms, and it can be difficult to distinguish then unambiguously. Depending on the ion channel and the nature of the interacting molecule, various lines of evidence can provide insight into the mechanism (classical pore block or allosteric) underlying ion channel 'block'. Included among these are: voltage dependence, effect of driving force, kinetic analysis, site directed mutagenesis, and structural data.

1.4.1. Voltage dependence

In 1973 Ann Woodhull proposed a pore block model to explain the voltage dependent reduction of Na^+ channel current produced by internal hydrogen ions (*85*). Woodhull reasoned that because the H^+ induced reduction of sodium channel currents was dependent on the potential across the nerve cell membrane, H^+ ions may bind to a site located within the pore partway into the electric field across the channel. The rate constants for H^+ binding and unbinding would therefore be voltage dependent because the proton needs to move through the electric field to get to its binding site in the channel pore.

Inhibition of ionic current through a variety of ion channels, including RyR, is consistent with Woodhull's theory of direct pore block. Block of RyR by TEA^+ was manifest as a smooth, voltage dependent reduction in single channel current amplitude. Calculations from the Woodhull model suggest a single TEA^+ binding site is located in the channel pore approximately 90% into the electric field across the channel from the cytosolic side (*36*). The large tetra alkyl ammonium cation tetra butyl ammonium

(TBA^+), the charged local anesthetic lidocaine, and two quaternary amines (QX572 and QX314) also reduced RyR channel conductance via a direct interaction with the permeation pathway. From the cytosolic side TBA^+ induced rapid current fluctuations between the maximum single channel conductance level and a low amplitude (~21% of maximum conductance) subconductance state. This blocking phenomenon was dependent on TBA^+ concentration, and only observed at positive membrane potentials (which promote *cis* to *trans* ion fluxes), and prevalence of the TBA^+ related subconductance state increased as the potential across the channel is made increasingly positive(*86*). Lidocaine, QX572, and QX314 likewise blocked only from the cystolic face of the channel and produced similar concentration, and voltage dependent subconductance behavior in RyR. In contrast, the local anesthetics tetracaine and procaine are thought to inhibit RyR via an allosteric mechanism due to their lack of voltage dependence and membrane sidedness (*87, 88*). Proposed binding site(s) for these compounds lie in or close to the lipid bilayer (*87*).

The Woodhull theory of pore block is a plausible mechanism which allows for definite predictions to be made and tested. One testable prediction of this model is that the steepness of the voltage dependence depends upon the valence of the blocking species and the location of the binding site within the electric field across the channel. Therefore, the voltage dependence of block is expected to vary with the charge of the blocking species. This line of evidence has been used to determine the mechanism by which transmembrane potential influences the probability of RyR modification by ryanodine. Ryanodine modification of RyR produces a long-lived subconductance state. Several ryanodine derivatives known a ryanoids also induced a subconductance state by

competing with ryanodine for a high affinity site on the channel (*89-91*). The interaction of one such positively charged ryanoid (21-amino-9α-hydroxyryanodine) with the channel was strongly influenced by transmembrane voltage (*92*). Both the rate of association and dissociation were voltage dependent. This voltage dependent interaction could result from translocation of the ryanoid to a site within the voltage drop across the channel (i.e. direct pore block), or a voltage-driven alteration in binding site affinity for the ryanoid (i.e. allosteric mechanism). The extent of equilibrium [^{3}H]ryanodine binding is increased by activating ligands such as ATP and decreased by inhibitory ligands such as Mg^{2+} suggesting the high affinity binding site is only accessible when the channel is open (*27, 28*). Additionally, the rate of association of 21-amino-9α-hydroxyryanodine with RyR was linearly dependent on channel P_o (*92*). Together these features of the interaction of ryanoids with RyR are consistent with location of a binding site within the conduction pathway accessible only when the channel is open. However, a study comparing the interactions of a positively charged and neutral ryanoid with RyR showed the rate constants for ryanoid association and dissociation were unchanged by valence (*93*). The lack of an effect of valence on the voltage dependence of ryanoid interaction is inconsistent with the Woodhull model and thus difficult to reconcile with a mechanism of direct pore block. Therefore, the mechanism by which ryanodine modifies RyR conductance is unclear as evidence to support either an allosteric or direct block mechanism exists.

Predictions based on the Woodhull model have also provided insight into the mechanism underlying 'block' of Na^+ channels by saxitoxin and related compounds. Saxitoxin produces voltage dependent all-or-none 'blocking' events in single Na^+

channels (*94*). Several natural derivatives of saxitoxin (i.e. guanidinium toxins) 'block' Na^+ channels with varying affinities and kinetics of action. Importantly, these toxin derivatives have different net charges ranging from 0 to +2 (*94*). Contrary to expectations for the case of toxin binding to a site within the electric field (presumably within the pore), toxin charge was shown to have no effect on the voltage dependence of blocking rates. Therefore, direct pore block was abandoned, and the alternatively theory of voltage-driven changes in channel conformation was proposed to account for the effects of voltage on toxin binding.

1.4.2. Varying driving force for ion flux

Another line of evidence to suggest that a 'blocker' binding site is actually within the pore involves competition with permeant ions. By changing the concentration of permeant ions on one side of the channel, one can manipulate the driving force for ion flux through the channel pore. If a 'blocking' species binds to a site within the permeation pathway, varying driving force is expected to affect the binding, and thus the 'blocking' effect. In a series of experiments (*95-97*) Clay Armstrong investigated the mechanism underlying block of inward rectifier K^+ channels by intracellular TEA. His experiments suggest that the TEA binding site lies within the channel pore, and is only accessible from the cytoplasmic side when the channel gate is opened by a depolarizing pulse. A pivotal finding was that the TEA dissociation rate increased by external K^+ especially at membrane potentials that elicit inward K^+ currents. This finding suggested that the voltage driven movement of K^+ ions through the pore effectively 'knock' TEA ions off a binding site in the pore located near the cytoplasmic end of the channel.

1.4.3. Kinetic behavior of 'blocking' events

It is possible, with kinetic analysis of single channel activity, to obtain very detailed information about mechanisms determining channel conductance and gating. Thus, models describing kinetic behavior of channels in the presence of a 'blocking' agent are instructive. Analysis is based upon the assumption that 'blocking' events represent the residence time of the 'blocking' agent at its binding site on the channel. Figure 3 depicts a simple two state model describing a reversible binding reaction. The significance of this model is that it is only realistic in the case of direct pore block (i.e. the physical interaction the 'blocking' species with the permeation pathway). According to this scheme the blocker (X) binds to and blocks the open channel (O). Therefore, lifetime of the open state (O) is inversely proportional to the rate of X binding, which in turn is dependent on the concentration of X. Lifetime of the blocked state (B) is determined by the residence time of X at its site, a parameter which is independent of [X]. Thus for the case of direct pore block, the lifetime of the open and blocked states should be inversely proportional to [X] and independent of [X], respectively.

Often, predictions based on a reversible binding scheme (Fig. 3) do not fit the measured kinetics of 'block', and are more adequately described by an allosteric model (Fig 4). Figure 4 depicts a hypothetical allosteric model describing voltage driven changes in channel conformation analogous to the mechanisms proposed for the voltage dependent 'block' of Na^+ channels by guanidinium toxins, and the voltage dependent modification of RyR by ryanodine (discussed above).

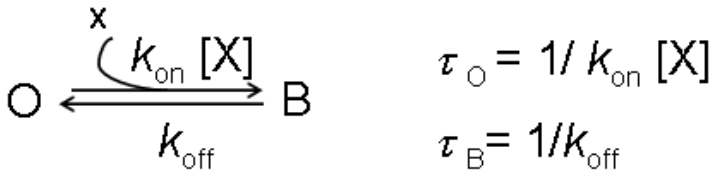

Figure 3. Reversible binding scheme for classic open channel block. The species (X) produces a blocked state (B) by entering the pore of the open channel (O). This scheme predicts that the lifetime of the open state (O) to be inversely proportional to the concentration of X and the lifetime of the blocked state (B) to be independent of [X].

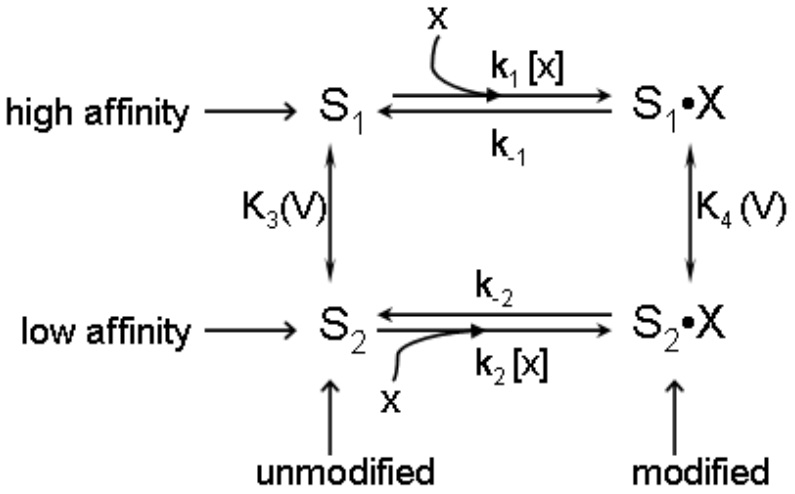

Figure 4. Hypothetical Scheme to explain voltage dependent modification of channel conductance. S represents a ligand binding site on the channel which exists in either a high affinity (S_1) or low affinity (S_2) form. The rate constants for X binding (k_1, k_2) and unbinding (k_{-1}, k_{-2}) are not voltage dependent. Voltage dependent equilibrium (K_3 and K_4) between the high and low affinity channel conformations accounts for the apparent voltage dependence of modification.

The allosteric theory of channel 'block' states that non-conducting or subconductance events represent distinct channel conformations with altered ion permeation properties. Two possibilities can be envisioned i) induced fit and ii) prior isomerization. Induced fit describes a situation in which ligand binding produces a change in pore structure, with the conformation of the pore determined by the structure of the binding ligand. Prior isomerization proposes that ligand binding stabilizes a channel conformation that has a very low probability of occurrence in the absence of ligand. The allosteric scheme depicted in Figure 4 describes the situation of prior isomerization. An important implication of this model is that conductance changes are intrinsic properties of ion channels which represent conformational changes in the channel protein. This model describes the case in which the channel may adopt a minimum of two conformations, denoted by the subscripts 1 and 2, to which the ligand can bind. The ligand binding site (S) is available on the channel in either a high affinity (S_1) or low affinity (S_2) form depending on channel conformation. The apparent voltage dependence of the ligand interaction arises from a voltage dependent equilibrium between the two intrinsic channel conformations (the equilibrium constants K_3 and K_4 are voltage dependent). Take for example the interaction of ryanoids with RyR. Both rates of association and dissociation of ryanoids vary with applied holding potential; k_{on} increases and k_{off} decreases as the potential is shifted to more positive values. In this scheme, positive potentials shift the equilibrium towards S_1, the high affinity conformation, thus accounting for the increased rate of ryanoid association with increasing positive potentials.

An analogous circular 4 state model (Fig. 5) was proposed by Schild and colleagues to describe Zn^{2+} induced subconductance events in cardiac Na^+ channels (*98*).

In the presence of external zinc ions, Na^{2+} channels transitioned between at least four distinct current levels. The primary effect of Zn^{2+} was the induction of flickery closings to a low amplitude subconductance state. The rate of Zn^{2+} association with Na^{+} channels was voltage dependent; k_{on} increased with hyperpolarization (increasing negative membrane potential) suggestive of a pore block mechanism. However, the observed dependence of both k_{on} and k_{off} on Zn^{2+} concentration was incompatible with a simple blocking model (Fig. 2). As Zn^{2+} concentration was increased the lifetime of the open full conductance state (O) decreased and the lifetime of the open subconductance state (S) increased indicating that Zn^{2+} can bind to O, but preferentially binds to and stabilizes an intrinsic subconductance conformation (S). These findings are consistent with the allosteric mechanism of prior isomerization, implying that the subconductance state is an inherent characteristic of Na^{+} channel gating.

Kinetic evidence has provided insight into the mechanism underlying ruthenium red block of RyR. Ruthenium red (RR) has a linear structure consisting of three ruthenium atoms which serve as a nucleus for a total of 14 amino groups ($[(NH_3)_5Ru\text{-}O\text{-}Ru(NH_3)_4\text{-}O\text{-}Ru(NH_3)_5]^{6+}$; it is one of the most potent inhibitors of SR Ca^{2+} release (*99*). Both the pore block and allosteric mechanism has been proposed by (different groups) to account for the effects of RR on single RyR channel currents. At the single channel level, RR caused long term closure which was irreversible on the time scale of single channel recordings and thus incompatible with kinetic analysis (*13*). Two different approaches have been used to circumvent this difficulty: investigating the kinetics of RR interaction with ryanodine modified channels, or channels maximally activated by Ca^{2+} and ATP.

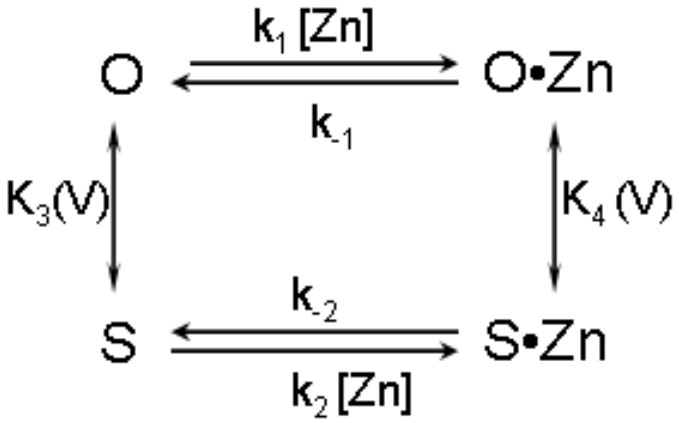

Figure 5. Allosteric mechanism of the Zn^{2+} induced subconductance state in cardiac Na^{+} channels. Zn^{2+} can bind to the full open (O) and subconductance (S) channel conformations. The Zn^{2+} binding site has a high affinity for Zn^{2+} when the channel is in the S conformation, and a lower affinity for Zn^{2+} when the channel is in the O conformation. A voltage dependent equilibrium between O and S gives rise to the apparent voltage dependence of Zn^{2+} binding (modified from ref (*98*)) .

Cytosolic RR produced voltage dependent "all-or-none flickery block of ryanodine activated channels"(*100*). 'Block' became more pronounced at large positive potentials which favored movement of RR into the conduction pathway of the channel. From the luminal face, rather than producing flicker block, RR caused voltage dependent reduction of the amplitude of the long lived ryanodine modified subconductance state. Luminal (*trans* RR) only reduced current flow at negative potentials which favor movement of luminal RR into the pore. A hill coefficient of two for the dose response curve suggested that multiple RR molecules are involved in the inhibition. In ryanodine-modified channels, the rate of RR 'block' (k_{on}) but not the 'unblocking' rate (k_{off}) showed dependence on RR concentration, consistent with a reversible binding reaction (Fig. 2). Ma proposed that multiple positively charged RR molecules enter the pore, resulting in reduction of single channel current.

In the ryanodine-unmodified RyR (maximally activated by Ca^{2+} and ATP) RR produced several subconductance states, which were dependent on channel activity, membrane potential, and sidedness of RR addition (*101*). However, Xu and colleagues identified a voltage independent component to RR inhibition which they attributed to an interaction between Ca^{2+} regulatory and RR inhibition sites. This mechanism may have been 'masked' in the previous study as ryanodine modification renders RyR insensitive to Ca^{2+} regulation. Based on the observation that the rate of formation, but not the amplitude, of the RR-related subconductance states was dependent on RR concentration, Xu and colleagues disagreed with the pore block mechanism proposed by Ma. Rather stating that "an alternative explanation is that the substates are the result of voltage- and

RR-dependent changes in channel protein conformation." Thus the mechanism underlying RR inhibition of RyR is still unclear.

1.4.4. Mutagenesis and structural data

Results from classical biophysical experiments may be indicative of a mechanism of action; however, effects of mutations within the pore on block, and visualization of blocking species in the pore in crystallized structures of channels provide the most compelling evidence for distinguishing between a pore block and allosteric mechanism. Several venoms used by organisms for defense purposes contain peptides that target ion channels. As discussed previously, the effect of guanidinium toxins on Na^+ channel conductance was not adequately described by a simple model of pore block. Similarly, apamin modification of K^+ channels, and the effect of scorpion toxins on RyR appear to involve an allosteric mechanism.

Apamin is an 18 amino acid peptide toxin isolated from bee venom which inhibits Ca^{2+} activated K^+ channels (K_{Ca}) with high affinity and specificity. A recent study employe site directed mutagenesis, ^{125}I-apamin binding, and molecular modeling of ligand-channel interactions suggested that apamin 'blocks' via an allosteric mechanism (*102*). In mutant channels, the replacement of a basic histidine residue located in the outer pore region with an uncharged asparagine abolished ^{125}I-apamin binding. Functional studies showed that currents of mutant channels were no longer 'blocked' by apamin. Molecular modeling of apamin interacting with the outer pore histidine positioned the toxin a large distance from the ion conduction pathway, making it unlikely for apamin to physically occlude the passage of ions through the selectivity filter. A prior

study showed that H^+ ions likely inhibit macroscopic currents through K_{Ca} via an allosteric mechanism involving protonation of the outer pore histidine residue (*103*). Via an analogous mechanism, positively charged residues on apamin may mimic protons and interact with the outer pore histidine residue to promote a conformational change in the channel which affects ion permeation.

Toxins isolated from scorpion venom bind with high affinity to RyRs. Imperatoxin activator ($IpTx_a$) and maurocalcin (MCa) from the venom of the scorpions *Pandinus imperator* and *Scorpio maurus palmatus* selectively activate RyRs by inducing a long lived subconductance state. $IpTx_a$ and MCa are basic peptides composed of 33 amino acids and possess 82% sequence identity. Their three dimensional structure is stabilized by disulfide bridges formed between three pairs of cysteine residues (*104, 105*). They modulate RyR gating from the cytoplasmic side in voltage and concentration dependent manner (*106-108*). Although studies have not conclusively distinguish between a pore block and allosteric mechanism, experimental evidence is most consistent with a ligand-induced conformational change as the mechanism underlying the subconductance states produced by $IpTx_a$ and MCa (*107, 108*). There is also structural support for an allosteric mechanism of action. Cryo-electron microscopy and three-dimensional image analysis suggesed the $IpTx_a$ binding site is far (~11 nm) from the center of the cytoplasmic side of the transmembrane region of the RyR channel (*109*).

1.4.5. Summary of ion channel block

Evidence for entry into the pore varies depending on the channel 'blocking' species. Open channel block is expected to be voltage dependent, reversed by ions from

the opposite side of the membrane, and consistent with a reversible binding kinetic scheme. Results from classical biophysical experiments may strongly support one theory over the other. However, effects of mutations within the pore on block, and visualization of blocking species inside (or ouside) the pore in crystallized structures of channels provide the most compelling evidence for a direct pore block (or allosteric) mechanism.

1.5. S-Adenosyl-L-Methionine

S-Adenosyl-L-Methionine is formed from the essential amino acid methionine and adenosine triphosphate (ATP). It functions as a methyl group donor in a vast number of reactions catalyzed by a diverse class of enzymes known as methyltransferases (*110*). SAM plays an important role in cellular metabolism as a precursor molecule to three main pathways: methylation, transulfuration, and aminopropylation (*111*). The aminopropylation pathway leads to the synthesis of polyamines, and the transulfuration pathway leads to the synthesis of glutathione.

1.5.1. Structure and Chemistry

SAM is present in cells at a concentration of 60-90 μM (*112, 113*). Although all cells synthesize SAM, the liver serves as the major site for its synthesis and degradation (*111*). The synthesis of SAM is catalyzed by methionine adenosyl transferase (MAT, aka S-adenosyl-l-methionine synthetase). This reaction involves the transfer of the adenosyl moiety of ATP to methionine forming a sulfonium ion which readily transfers its methyl group to a large variety of acceptor substrates including nucleic acids, proteins, phospholipids, and a long list of small molecules (*110*).

The first step in mammalian methionine metabolism is its conversion to SAM and transfer of the methyl group to a variety of methyl acceptors. Up to half of the daily intake of methionine is converted to SAM and about 85% of methylation reactions take place in the liver. Factors influencing intracellular SAM levels include availability of methionine, SAM utilization for polyamine synthesis, and the type of MAT expressed (*111*). Most of the SAM synthesized is used in transmethylation reactions. A diverse class of enzymes known as methyltransferases catalyze the transfer of the methyl group from the sulfonium of SAM to the oxygen, nitrogen, or sulfur atom of biological targets (*114*). The end products of this reaction are a methylated substrate, and S-adenosyl-L-homocysteine (SAH), which is a potent inhibitor of methyltransferase activity. A decrease in the SAM to SAH ratio resulting from either an increase in SAH level or a decrease in the SAM level, has been shown to inhibit transmethylation reactions (*115*).

1.5.2. Role in protein methylation

SAM serves an important biological function as the sole methyl donor in a multitude of cellular methylation reactions (*110, 116*). Methylation of biological molecules is a mechanism for regulating a diverse array of physiological processes including, protein localization, and intermolecular interactions (*117, 118*). Protein methylation can occur on the side chains of several amino acids: N-methylation of arginine, lysine, and histidine, O-methylation of glutamate and isoaspartate, and S-methylation cysteine and methionine. These reactions are catalyzed by highly protein- and amino acid-specific methyltransferases. Most cells contain numerous SAM-dependent methyltransferases that transfer the methyl group of SAM to the oxygen,

nitrogen, or sulfur atoms of target molecules. Protein methylation can have a global effect on protein function via alterations in steric orientation, charge, or hydrophobicity (*117*). Although protein methylation is regarded as a salient posttranslational regulator of protein function, relatively little has been reported on ion channel methylation.

The epithelial sodium channel (ENaC) was reportedly activated by methylation via a mechanism which involved regulation by the steroid hormone aldosterone (*119, 120*). However the site of methylation and enzyme involved remain to be determined. More recently, a proteomic study identified methylation of the α subunit of the cardiac sodium channel ($Na_v1.5$) at three arginine residues. Although the functional relevance of $Na_v1.5$ methylation is unknown, two of the identified residues are known Nav1.5 mutations causing Brugada and long QT type 3 syndromes (R526H and R680H respectively) (*121*).

1.5.3. SAM regulation of Ryanodine Receptors

Interventions designed to increase cellular concentrations of SAM were shown to have a positive inotropic effect on the heart. This effect was attributed to lipid-methylation which in turn stimulated the Sarco(endo)plasmic reticulum Ca^{2+} pump (SERCA) (*122, 123*). However, the effects of this intervention on RyR2 were not investigated. RyRs from coronary artery myocytes were reportedly activated by SAM (*124*). However, smooth muscle expresses RyR1, RyR2 (*125, 126*), and RyR3 (*127*), therefore the results reported by Chen and colleagues reflect effects of SAM acting on multiple RyR isoforms (*124*). FKBP was proposed to be the sole target of methylation resulting in its dissociation from RyR2 causing channel activation. This is analogous to

the mechanism by which RyR2 hyperphosphorylation putatively results in FKBP12.6 dissociation and channel activation (*22*). The possibility that SAM regulation of RyRs involves a direct interaction with the channel has not been addressed.

1.6. Introduction to research question: SAM regulation of Ryanodine Receptors

SAM has been shown to enhance cardiac contractile performance via effects on the SERCA pump (*122, 123*). Ryanodine receptors from coronary artery myocytes were reportedly activated by SAM via an indirect mechanism involving protein methylation (*124*). However, smooth muscle expresses RyR1, RyR2 (*125, 126*), and RyR3 (*127*), therefore the effects of SAM on a defined RyR isoform are unclear.

This work was undertaken to characterize the effects of SAM on a specific RyR isoform, RyR2, and to clarify the mechanism underlying RyR2 regulation by SAM. Initial work described in chapters 2 and 3 distinguish between SAM regulation of RyR2 via its established role as a biological methyl group donor and SAM acting as a regulatory ligand with consideration of SAM binding to the well-established RyR2 adenine nucleotide binding site(s). The potential interaction of SAM with the RyR2 adenine nucleotide regulatory sites has important implications for clarifying the structural basis of ATP regulation of the channel. During the course of this project the novel observation of a SAM related RyR2 subconductance state was made, thus work described in chapter 4 distinguishes between the two possible mechanisms by which SAM could reduce RyR2 conductance: i) SAM interfering directly with ion permeation via binding within the conduction pathway, or ii) the binding of SAM at a regulatory (or allosteric) site which stabilizes or induces a reduced conductance conformation of the channel.

Chapter 5 summarizes the major findings and proposes future directions.

CHAPTER 2

S-ADENOYL-L-METHIONINE ACTIVATES THE CARDIAC RYANODINE RECEPTOR

Kampfer, A. J., and Balog, E. M. (2008), *Biochem Biophys Res Commun 371*, 606-609.

2.1. Abstract

S-Adenosyl-L-methionine (SAM) is the biological methyl-group donor for the enzymatic methylation of numerous substrates including proteins. SAM has been reported to activate smooth muscle derived ryanodine receptor calcium release channels. Therefore, we examined the effects of SAM on the cardiac isoform of the ryanodine receptor (RyR2). SAM increased cardiac sarcoplasmic reticulum [^{3}H]ryanodine binding in a concentration-dependent manner by increasing the affinity of RyR2 for ryanodine. Activation occurred at physiologically relevant concentrations. SAM, which contains an adenosine moiety, enhanced ryanodine binding in the absence but not in the presence of ATP. S-Adenosyl-L-homocysteine (SAH) is the product of the loss of the methyl-group from SAM and inhibits methylation reactions. SAH did not activate RyR2 but did inhibit SAM-induced RyR2 activation. SAH did not alter adenine nucleotide activation of RyR2. These data suggest SAM activates RyR2 via a site that interacts with, but is distinct from, the adenine nucleotide binding site.

2.2. Introduction

In the heart, ryanodine receptor calcium release channels (RyR2) are the efflux pathway by which calcium is released from the sarcoplasmic reticulum (SR) to initiate cardiac contraction. RyR2 is regulated primarily by Ca^{2+}, although the biphasic Ca^{2+}

dependence of channel activation can be modified by numerous endogenous ligands and post-translational modifications (*18, 128*).

S-Adenosyl-Lmethionine (SAM) is the biological methyl-group donor for a multitude of methylation reactions including protein methylation which alters protein-protein interactions and protein function (*117, 118*). Experimental interventions designed to elevate cellular SAM concentrations had a positive inotropic effect on the heart (*122, 123*). This work attributed the effect to increased activity of the SR Ca^{2+} ATPase but did not explore possible affects on RyR2. Recently, Chen et al (*124*) showed that SAM activated RyR channels derived from bovine coronary smooth muscle. The activation was attributed to the methylation and subsequent dissociation of the RyR accessory protein FKBP12. Because smooth muscle RyR expression is heterogenous, with cells containing all three RyR isoforms (*125-127*), one aim of the present work was to use cardiac sarcoplasmic reticulum to determine the affects of SAM on a defined channel isoform, RyR2.

SAM is produced when the adenosyl moiety of adenosine triphosphate (ATP) is transferred to methionine, forming a sulfonium ion which can easily transfer its methyl group to numerous biological substrates including proteins and phospholipids. Methyl-group transfer converts SAM to S-adenosylhomocysteine (SAH), a potent competitive inhibitor of transmethylation reactions (*111*).

Adenine nucleotides are important endogenous RyR regulators. Among these nucleotides, ATP is the most potent channel activator and the efficacy of channel activation decreases as phosphate groups are lost (*60, 61*). Thus, it appears that the number of phosphates are critical determinates of activation efficacy. Indeed, adenosine

binds RyR2 with high affinity but fails to open the channel causing adenosine to be a competitive inhibitor of ATP activation (*60, 61*); but see (*129*) for conflicting results]. The presence of an adenosine moiety in SAM raises the possibility that the SAM-induced RyR activation may be due to SAM binding to the RyR adenine nucleotide binding site. Thus, the second aim of this work was to determine whether there is an interaction between RyR2 activation by SAM and adenine nucleotides.

2.3. Methods

2.3.1. Materials

Pigs were purchased from Clemson University Research Farm Services. Unlabeled ryanodine was obtained from Calbiochem (La Jolla, CA). Adenosine 5′-(β,γ-imido)triphosphate tetralithium salt (AMPPNP), S-(5'-adenosyl)-L-methionine chloride (SAM) and S-(5'-adenosyl)-L-homocysteine were obtained from Sigma (St. Louis, MO). [^{3}H]Ryanodine was obtained from PerkinElmer (Waltham, MA).

2.3.2. Isolation of Cardiac Sarcoplasmic Reticulum (CSR) vesicles

Animals were euthanized in accordance with *Public Health Service Policy on Humane Care and Use of Laboratory Animals* and with the approval of the Institutional Animal Care and Use Committee of the Georgia Institute of Technology. Animals were first anesthetized by subcutaneous injection of ketamine (20 mg/kg) and xylazine (2 mg/kg) followed by euthanasia by intravenous injection of sodium pentobarbital (100 mg/kg). Hearts were rapidly excised and rinsed in ice-cold 10 mM sodium bicarbonate

buffer. Ventricles were trimmed of excess fat and connective tissue. Minced ventricular tissue was homogenized in 10 mM $NaHCO_3$ and centrifuged for 5 mins at 4,000 x g. The supernatant was filtered through gauze, centrifuged for 20 mins at 4,000 x g, filtered a second time and centrifuged 30 mins at 80,000 x g. Pelleted membranes were extracted in 0.6 M KCl and 20 mM Tris (pH 6.8) on ice for 45 mins then centrifuged 30 min at 120,000 x g. The pellets were resuspended in 10% sucrose, centrifuged 30 mins at 120,000 x g and resuspended in a minimal volume of 10% sucrose. CSR was frozen in liquid N_2 and stored at -70^{o}C. All buffers contained 1 μg/ml aprotinin, 1 μg/ml leupeptin, 1 μg/ml pepstatin A, 1 mM benzamidine, and 1 mM phenylmethylsulphonylfluoride.

2.3.3. [^{3}H]Ryanodine Binding

Ryanodine binds with high affinity and selectively to RyRs in the open state; thus, CSR vesicle [^{3}H]ryanodine binding measurements are sensitive indicators of RyR2 channel activity (*28, 130*). CSR vesicle (0.4 mg/ml) binding media contained 7 nM [^{3}H]ryanodine, 150 mM KCl, 20 mM K-Pipes, pH 7.0, 0.1 mg/ml bovine serum albumin, 1.0 μg/ml leupeptin, 1.0 μg/ml aprotinin, and Ca-EGTA buffer to achieve the desired free Ca^{2+} concentration (*131*). Estimates of maximal [^{3}H]ryanodine binding capacity of CSR vesicle preparations were made in parallel with each experiment in media that in addition contained 600 mM KCl, 10 mM ATP, 100 μM Ca^{2+} and 50 nM [^{3}H]ryanodine. Nonspecific binding was measured in binding media that also contained 10 mM $MgCl_2$ and 20 μM nonradioactive ryanodine. After 20 hrs at room temperature (20-22^{o}C) CSR vesicles were collected on Whatman GF/B filters and washed with 8 mls of ice-cold 100

mM KCl buffer. Radioactivity retained by the filters was determined by liquid scintillation counting. All assays were performed in duplicate.

2.3.4. Analysis

The Ca^{2+} dependence of ryanodine binding was fit with an equation that assumes a high affinity Ca^{2+}-binding site, which when bound will activate the RyR, and a lower affinity Ca^{2+} binding site, which when bound will inhibit channel opening (*132*). The effects of SAM on maximal CSR vesicle [^{3}H]ryanodine binding capacity (B_{max}) and dissociation constant (K_d) were determined by saturation analysis using non-linear curve fitting of equation 1 to binding isotherms.

Equ. 1:

$$[^3H]\text{Ryanodine Bound} = (B_{max} \text{ X } [\text{Ryanodine}])/(K_d + [\text{Ryanodine}])$$

All curve fitting was performed using SigmaPlot 9.0 (Systat Software, Point Richmond, CA).

2.3.5. Statistics

Data are presented as mean ± S.E.M. CSR [^{3}H]ryanodine binding in the presence and absence of SAM, SAH, and AMPPNP, was analyzed using a one-way ANOVA with a Holm-Sidak multiple comparison as a *post-hoc* test or by Student's paired or unpaired t-tests as appropriate. Statistical analysis was performed using SigmaStat 3.1 (Systat Software, Point Richmond, CA). The level of significance was $p<0.05$.

2.4. Results

In media containing 10 μM Ca^{2+}, SAM increased CSR vesicle [^{3}H]ryanodine binding in a concentration-dependent manner (Figure 6A). Binding in media containing ≥ 75 μM SAM was significantly ($p<0.05$; n=5) increased compared to media lacking SAM. Binding increased 58, 63, and 113% in media containing 75 μM, 100 μM and 1 mM SAM respectively. To determine whether SAM activation of RyR2 was Ca^{2+}-dependent, the Ca^{2+} concentration dependence of CSR ryanodine binding was performed in media containing either no SAM, 0.1 or 1.0 mM SAM (Figure 6B). In media containing 0.1 mM SAM the extent of CSR ryanodine binding at optimally activating Ca^{2+} was increased approximately 90% from 20.5±1.0% to 39.0±2.6% of maximal ($p<0.05$). Including 0.1 mM SAM in the binding media did not alter the Ca^{2+} concentration required for half-maximal ryanodine binding (EC_{50}; No SAM: 2.92±0.29 μM, 0.1 mM SAM: 3.09±0.62 μM), the Hill coefficient for Ca^{2+} activation (n_a; No SAM: 2.1±0.5, 0.1 mM SAM 1.3±0.3) or Ca^{2+} inhibition (n_i; No SAM: 1.3±0.2, 0.1 mM SAM:1.7±0.5). Including 0.1 mM SAM caused a non-significant increase in the Ca^{2+} concentration required to half-inhibit (IC_{50}) ryanodine binding from 3.12±0.45 mM to 7.16±1.24 mM. Raising the SAM concentration in the binding media to 1.0 mM CSR caused a 160% increase in CSR ryanodine binding at optimal Ca^{2+} to 53.4±2.4% of maximal. In media containing 1 mM SAM, the Ca^{2+} IC_{50} was further increased to 12.8±2.3 mM and was significantly different from the Ca^{2+} IC_{50} in the absence of SAM ($p<0.05$). Compared binding in the absence of SAM, including 1.0 mM SAM in the binding media did not significantly alter the Ca^{2+} EC_{50} (2.92±0.38 μM), the n_a (1.4±0.2) or the n_i (1.4±0.4). In media containing 100 nM Ca^{2+} SAM did not significantly increase CSR vesicle ryanodine binding (0.03±0.17,

0.77±0.21 and 1.32±0.56% of maximal in media containing no SAM, 0.1 mM SAM and 1.0 mM SAM respectively). Thus, SAM increased RyR2 Ca^{2+} activation but did not alone activate RyR2 and at 1 mM SAM increased the Ca^{2+} concentration required to inhibit ryanodine binding.

Saturation analysis was then carried out to determine whether SAM enhanced CSR vesicle ryanodine binding by increasing the affinity of RyR2 for ryanodine or if SAM increased the number of channels which bind ryanodine. Figure 7 summarizes these experiments. In media containing 30 μM Ca^{2+}, SAM significantly increased CSR affinity for ryanodine, decreasing the K_d from 13.8±1.5 nM in the absence of SAM to 9.5±0.8 nM in media containing 0.1 mM SAM ($p<0.05$, $n=7$). Including 0.1 mM SAM in the CSR ryanodine binding media did not significantly alter the maximal ryanodine binding (B_{max}). In the absence of SAM B_{max} was 1.16±0.04 pmol/mg and in media containing 0.1 mM SAM B_{max} was 1.29±0.04 pmol/mg.

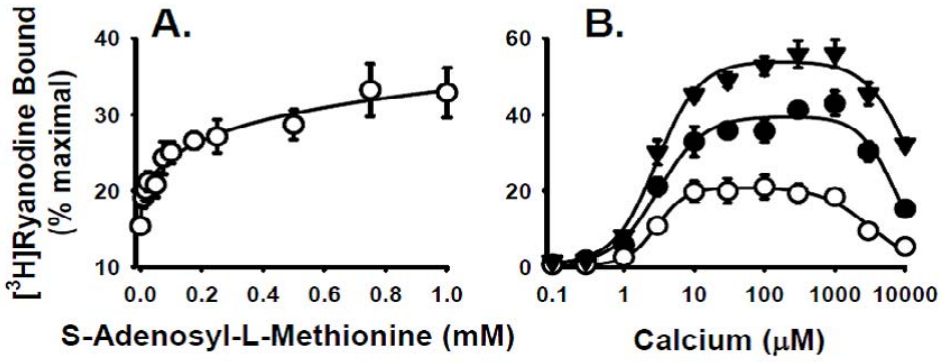

Figure 6. S-Adenosyl-L-methionine increased CSR vesicle ryanodine binding. **A.** S-Adenosyl-L-methionine concentration dependence of CSR vesicle [^{3}H]ryanodine binding. Binding was performed as described in the Methods in media containing 10 μM Ca^{2+} and the indicated concentration of SAM. SAM significantly increased ryanodine binding at all concentrations ≥75 μM ($p<0.01$, n=5). **B**. Ca^{2+} concentration dependence of CSR vesicle ryanodine binding. Binding was performed as described in the Methods in media containing the indicated concentration of Ca^{2+} and either no SAM (○), 0.1 mM SAM (●) or 1.0 mM SAM (▼), n=4.

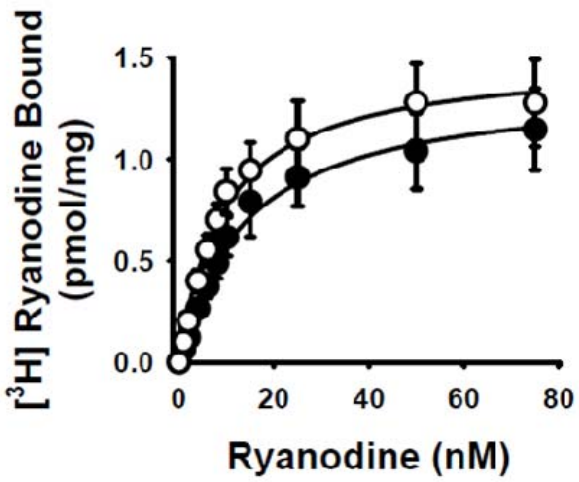

Figure 7. Saturation analysis of the effects of SAM on CSR [^{3}H]ryanodine binding (○ No SAM;● 0.1 mM SAM) . Binding was performed as described in the Methods in media containing 3 μM Ca^{2+} and the indicated concentration of ryanodine. SAM (0.1 mM) significantly increased CSR affinity for ryanodine; Kd: No SAM=13.8±1.5 nM; 0.1 mM SAM=9.5±0.8 nM, $p<0.05$. The maximal CSR ryanodine binding was not significantly altered by SAM (Bmax: No SAM=1.16±0.04 pmol/mg; 0.1 mM SAM= 1.29±0.04 pmol/mg). Lines are fits to equation 1; n=7.

Adenine nucleotides are well characterized endogenous RyR2 regulators. Because SAM is an adenosine containing compound the possibility that SAM activates RyR2 via the adenine nucleotide binding site was investigated. AMPPNP, the non-hydrolyzable analog of ATP, was used in these experiments to avoid the potential confounding effect of RyR2 phosphorylation. To determine whether there is an interaction between SAM and AMPPNP activation of RyR2, the AMPPNP concentration dependence of CSR ryanodine binding was performed in the absence and presence of 0.1 mM SAM (Figure 8). In the absence of SAM, AMPPNP increased ryanodine binding with an EC_{50} of 90±10 μM and a Hill coefficient of 0.91±0.05. Ryanodine binding was increased from 13.5±1.3% of maximal in the absence of AMPPNP to 40.6±3.9% in 1 mM AMPPNP. Including 0.1 mM SAM in the binding media did not significantly alter either the AMPPNP EC_{50} (100±7 μM) or the Hill coefficient (0.66±0.24). In media containing 0.1 mM SAM, ryanodine binding increased from 21.5±2.7% in the absence of AMPPNP to 43.9±3.6 in 1 mM AMPPNP. The addition of 0.1 mM SAM to the binding media significantly increased CSR vesicle ryanodine binding in the absence of AMPPNP and in combination with the lowest concentration (0.01 mM) AMPPNP but did not alter the maximal extent of CSR ryanodine binding in media containing ≥0.3 mM AMPPNP. The lack of an additive effect of SAM plus AMPPNP suggests that either SAM and AMPPNP act via a common site or they act via distinct but interacting sites.

SAH differs from SAM only by the loss of a methyl group and is a competitive inhibitor of methyltransefrase reactions. However, its use in examining methylation-induced activation of RyR2 is complicated by its possible interaction with the adenine nucleotide binding site. Thus, we determined the affects of SAH on both SAM and

AMPPNP activation of RyR2. The dependence of CSR vesicle [^{3}H]ryanodine binding on the SAM concentration, the SAH concentration, and SAM concentration in media containing 0.4 mM SAH is shown in Figure 9A. CSR vesicle ryanodine binding was significantly increased in media containing ≥0.1 mM SAM ($p<0.05$, n=8). In contrast, including up to 0.4 mM SAH in the binding media did not significantly increase ryanodine binding. Importantly, including 0.4 mM SAH in the ryanodine binding media prevented the SAM-induced increase in CSR ryanodine binding. This is consistent with the previously reported SAH block of SAM-induced activation of vascular smooth muscle RyRs [10]. If SAM activates RyR2 via the adenine nucleotide binding site, a possibility raised by the results shown in Figure 8 and SAM activation is prevented by SAH, then SAH should also block AMPPNP activation of the channel. Thus, the AMPPNP concentration dependence of ryanodine binding was determined in the absence of SAH and in media containing 0.4 mM SAH. Figure 9B shows that including ≥0.2 mM AMPPNP in the ryanodine binding media significantly increased CSR ryanodine binding ($p<0.05$, n=3). However, in contrast to SAH block of the SAM-induced increase in CSR ryanodine binding, including 0.4 mM SAH in the binding media had no effect on the AMPPNP-induced increase in CSR ryanodine binding.

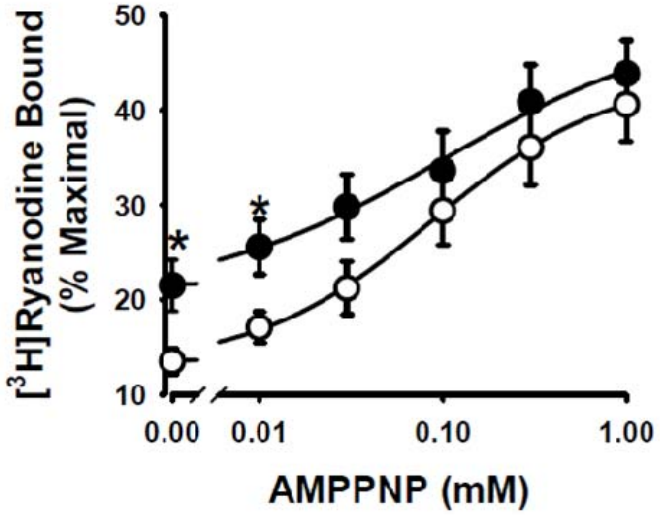

Figure 8. AMPPNP concentration dependence of CSR vesicle [^{3}H]ryanodine binding in the presence (●) and absence (○) of SAM. Ryanodine binding was performed as described in the Methods in media containing 3 μM Ca^{2+} and the indicated concentration of AMPPNP ± 0.1 mM SAM. AMPPNP (≥0.1 mM) significantly increased CSR ryanodine binding. The addition of 0.1 mM SAM to the binding media significantly increased CSR [^{3}H]ryanodine binding in media containing ≤ 0.01 mM AMPPNP (* $p<0.05$, n=8).

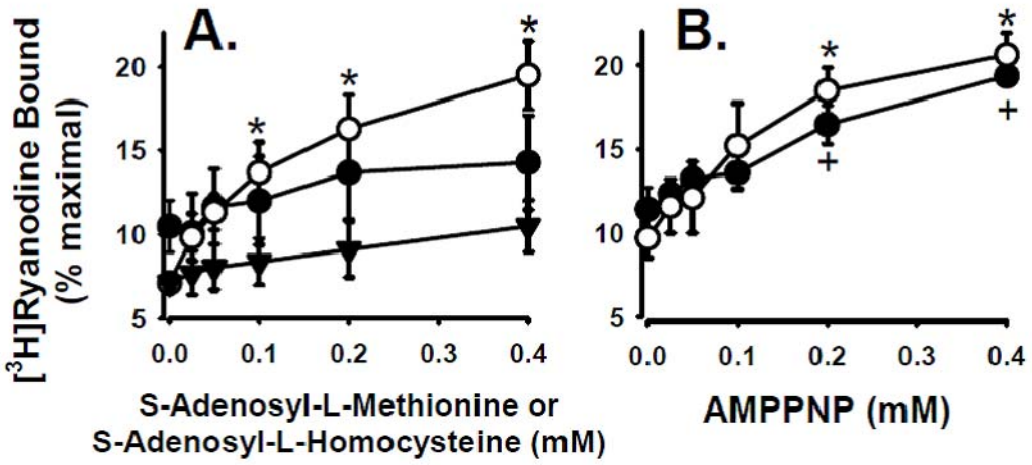

Figure 9. SAH blocked SAM activation but not AMPPNP activation of RyR2. **A.** CSR vesicle ryanodine binding was performed as described in the Methods in media containing 1 μM Ca^{2+} and the indicated concentration of SAM (○), SAH (▼) or SAM + 0.4 mM SAH (●); n=8. SAM at concentrations ≥ 0.1 mM significantly increased CSR vesicle ryanodine binding (* indicates significantly different from 0 SAM, $p<0.05$). CSR vesicle [^{3}H]ryanodine binding in media containing up to 0.4 mM SAH was not significantly different from binding in media containing no SAM. Including 0.4 mM SAH in media containing increasing concentrations of SAM prevented the SAM-induced increase in CSR ryanodine binding. **B.** Ryanodine binding was performed as described in the Methods in media containing 1 μM Ca^{2+}, and the indicated concentration of AMPPNP (○) or the indicated concentration of AMPPNP + 0.4 mM SAH (●). * Significantly different from 0 AMPPNP ($p<0.05$, n=3). + Significantly different from 0.4 mM SAH + 0 AMPPNP ($p<0.05$, n=3).

2.5. Discussion

SAM is the biological methyl-group donor for a multitude of methylation reactions. Protein methylation was noted over 40 years ago (*133*) and has come to be appreciated as a common and important post-translational reaction regulating protein-protein interaction and protein function (*117, 118*). Indeed, epithelial Na^+ channels are regulated via a methylation reaction (*134*) and plant aquaporin channels have recently been shown to be methylated (*135*). RyRs may also be regulated by protein methylation. Chen et al (*124*) attributed the SAM-induced increase in the open probability of vascular smooth muscle RyRs to the methylation and subsequent dissociation of the RyR accessory protein FKBP. However, determining the mechanism of RyR activation by SAM is complicated by the possibility that SAM, via its adenosine moiety, binds the RyR adenine nucleotide binding site.

We examined the effects of SAM on [^{3}H]ryanodine binding to SR vesicles derived from cardiac ventricles, a tissue in which RyR expression is nearly exclusively RyR2 (*136*). We found that SAM concentrations $\geq$ 75 μM increased CSR vesicle ryanodine binding (Figure 6A**)** by increasing the affinity of RyR2 for ryanodine (Figure 7). The concentration of SAM in mammalian cells has been reported to be 60 – 90 μM (*112, 113*). Thus concentrations of SAM required to activate RyR2 *in vitro* are within the physiological concentration range.

RyR2 activation by SAM was similar to activation by adenine nucleotides in that both compounds enhance Ca^{2+} activation of the channel but have minimal effects of channel activity in the absence of Ca^{2+} (*32, 45*). SAM did not increase ryanodine binding in sub-micromolar Ca^{2+} or decrease the Ca^{2+} EC_{50} but rather increased the Ca^{2+} IC_{50}

(Figure 6B). Thus SAM activation required the presence of activating concentrations of Ca^{2+}.

If SAM and adenine nucleotides share a common activating site or the two sites are allosterically coupled, activation by the two compounds should be less than additive. Indeed, that is what is shown in Figure 9, SAM increased CSR ryanodine binding in media containing ≤0.01 mM AMPPNP but in media containing ≥0.03 mM AMPPNP, SAM did not enhance binding. Thus, there appears to be an interaction between RyR2 activation by SAM and AMPPNP. SAH differs from SAM simply by the loss of the sulfonium methyl group. Thus, like SAM, SAH could potentially bind to the RyR adenine nucleotide binding site. However, it is clear from Figure 9 that in spite of the close structural similarities between SAM and SAH, SAH did not activate RyR2. It is possible that SAH at higher concentrations may increase CSR ryanodine binding, however, because of the low solubility of SAH we were limited to the concentration range shown in Figure 4. Consistent with the previous report by Chen et al (*124*) SAH did however block RyR2 activation by SAM. A plausible hypothesis is that SAM activates RyR2 via the adenine nucleotide binding site and that the loss of the methyl group converts SAM from an agonist to an antagonist at the adenine nucleotide binding site. If SAH is indeed an antagonist, it should decrease AMPPNP activation of RyR2. As shown in Figure 9, AMPPNP significantly enhanced CSR ryanodine binding. This activation of RyR2 was not altered by SAH, suggesting SAH does not interact with the adenine nucleotide binding site. Thus the SAH block of SAM activation and lack of affect of SAH on AMPPNP activation suggests SAM activation of RyR2 occurred via a mechanism distinct from, but interacting with, the adenine nucleotide binding site.

The results presented here show that RyR2 can be activated by physiologically relevant concentrations of the biological methyl-group donor SAM. Thus, SAM may be a novel regulator of RyR2 channel function.

CHAPTER 3

S-ADENOSYL-L-METHIONINE REGULATION OF THE CARDIAC RYANODINE RECEPTOR INVOLVES MULTIPLE MECHANISMS

Kampfer, A. J., and Balog, E. M. (2010), *Biochemistry 49*, 7600-7614.

3.1. Abstract

Cardiac contraction is triggered by the release of Ca^{2+} via the ryanodine receptor (RyR2), a sarcoplasmic reticulum (SR) resident ion channel. RyR2 channel activity is modulated through ligand binding and posttranslational regulatory mechanisms. S-adenosyl-L-methionine (SAM), the primary methyl group donor for enzyme-mediated methylation of proteins and other biological targets, activates RyR2 via an unknown mechanism (*137*). Here we show that the SAM induced increase in cardiac SR (CSR) vesicle [^{3}H]ryanodine binding is unaffected by methyltransferase inhibitors, and immunoprecipitation of RyR2 from S-adenosyl-L-[methyl-^{3}H]-methionine ([^{3}H]SAM) pre-treated CSR indicate that RyR2 is not a target of SAM mediated protein methylation. Because SAM contains an adenosine moiety and RyR2 is activated by ATP, we investigated whether SAM exerts its effects through the adenine nucleotide binding sites on the RyR2 channel. In support of this hypothesis, the SAM and ATP concentration dependence of CSR vesicle [^{3}H]ryanodine binding virtually overlap. Furthermore, ryanodine binding assays show that SAM competes with adenine nucleotide activation of RyR2, and the effects of SAM on mean channel open and closed times follow similar trends as those observed for ATP. Interestingly, SAM but not ATP activation of RyR2 was associated with a marked increase in the percent of channel openings to a sub-conductance level ~ 60% of the maximal single channel conductance. This work highlights the complexity underlying

SAM regulation of RyR2, and suggests ligand binding is among the multiple mechanisms responsible for SAM regulation of RyR2.

3.2. Introduction

The ryanodine receptor (RyR) is an intracellular Ca^{2+} channel located in the sarcoplasmic reticulum (SR) membrane which serves as a gated efflux pathway for stored Ca^{2+}. Mobilization of intracellular Ca^{2+} via the cardiac isoform of the channel (RyR2) is the event which triggers contraction, thus, RyR2 plays a critical role in the contractile performance of the heart. RyRs are high molecular weight homotetramers consisting of a C-terminal SR membrane spanning domain, and a large N-terminal cytoplasmic domain (*15*). Each RyR tetramer exists in its native membrane as part of a macromolecular complex in association with a number of signaling molecules involved in posttranslational protein modification. The RyR is also subject to complex allosteric regulation by metabolites, ions, and pharmacological agents (*27*). Physiological RyR regulatory ligands include Ca^{2+}, Mg^{2+}, ATP, and the accessory proteins calmodulin (CaM) and FK506 binding proteins (FKBPs).

ATP activates RyR2 in a concentration and Ca^{2+} dependent manner (*57*), and is present in resting muscle at a concentration sufficiently high for it to function as a principal cellular regulator of RyR2 (*59*). Although the degree to which adenine nucleotides (e.g. ATP and its metabolites) activate RyR2 varies, all are thought to interact with the same class of binding sites on the channel. The purine ring is important for agonist activity at these sites, as the replacement of adenine with guanine destroys the

ability of the nucleotide to modulate RyR (*57*). However, other structural features that determine the ability of adenosine based compounds to activate RyR2 are poorly defined.

The biological methyl group donor S-adenosyl-L-methionine (SAM) participates in transmethylation reactions whereby the methyl group of SAM is transferred to proteins, nucleic acids, or lipids thereby altering the localization and/or function of the methylated target (*112, 117, 138*). Previous reports of a SAM-induced enhancement of cardiac contraction did not investigate the effects of SAM on RyR2 (*122, 123*). More recently Chen *et al* (*124*) attributed SAM activation of RyRs from coronary artery myocytes to protein methylation causing the dissociation of the RyR accessory protein FKBP12. However, smooth muscle expresses RyR1, RyR2 (*125, 126*), and RyR3 (*127*), therefore the effects of SAM on RyRs from artery myocytes reflect SAM acting on multiple channel isoforms (*124*).

In contrast to the effects of SAM observed by Chen and colleagues (*124*), our prior work suggests SAM activates RyR2 through a direct interaction with the channel (*137*). Importantly, SAM is an adenosine based compound which raises the possibility that SAM, like ATP, regulates RyR2 via the adenine nucleotide binding site/s. In the present study we have examined the effects of SAM on a defined RyR isoform by utilizing cardiac SR (CSR) vesicle ryanodine binding and current recordings from native RyR2 channels incorporated into phospholipid bilayers. Our primary aim was to clarify how SAM exerts its effect on RyR2 activity, specifically, whether SAM acts via a direct (e.g. ligand binding) or an indirect (e.g. posttranslational modification) mechanism. In addition to the previously reported activation of RyR2 by SAM, we observe a distinct SAM induced channel sub-conductance state. Our data indicate that SAM directly

activates RyR2 through the adenine nucleotide binding site/s and suggests that sub-conductance states result from an indirect effect of SAM on RyR2.

3.3. Materials and Methods

3.3.1. Materials

Pigs were purchased from Clemson University Research Farm Services. Unlabeled ryanodine and 3-[(3-Cholamidopropyl)dimethylammonio]-1-propanesulfonate (CHAPS) were obtained from Calbiochem (La Jolla, CA). Adenosine 5'-(b,c-imido)triphosphate tetralithium salt (AMPPNP), S-(5'-adenosyl)-L-methionine chloride (SAM), S-(5'-adenosyl)-L-homocysteine (SAH), sinefungin, FK506, ATP, and ADP were obtained from Sigma (St. Louis, MO). [^{3}H]Ryanodine and S-adenosyl-L-[methyl-^{3}H]-methionine ([^{3}H]SAM) were obtained from Perkin-Elmer (Waltham, MA). FKBP12.6 antibodies were obtained from R&D Systems (#AF4174, Minneapolis, MN). RyR2 monoclonal antibody (clone C3-33) was from Sigma-Aldrich (St. Louis, MO). Horseradish preoxidase conjugated antibodies donkey anti-goat and goat anti-mouse were obtained from Santa Cruz Biotechnology (Santa Cruz, CA) and Millipore (Billerica, MA) respectively. EcoLite scintillation fluid and protease inhibitors were purchased from MP Biomedicals (Solon, OH). ECL Plus Western Blotting detection system was from GE Healthcare. BioMax light film was obtained from KODAK. Whatman GF/B filters were from Brandel, Inc. (Gaithersberg, MD), and BioTrace PVDF membranes were from Life Sciences (Pensacola, FL). Recombinant Protein-G sepharose 4B beads were obtained

from Invitrogen (Carlsbad, CA). Phosplolipids were purchased from Avanti Polar Lipids (Alabaster, AL).

3.3.2. Isolation of cardiac sarcoplasmic reticulum vesicles

Cardiac SR (CSR) vesicles used for [^{3}H]ryanodine binding were prepared from porcine ventricular tissue as previously described (*139*). Animals were euthanized in accordance with the Public Health Services Policy on Humane Care and Use of Laboratory Animals and with the approval of the Institutional Care and Use Committee of the Georgia Institute of Technology. Briefly, animals were euthanized by intravenous injection of sodium pentobarbital (100 mg/kg) following sedation by subcutaneous injection of ketamine (20 mg/kg) and xylazine (2 mg/kg). Muscle was homogenized in ice-cold 10 mM $NaHCO_3$ buffer and the supernatant from a 4,000 × g centrifugation was filtered through cheesecloth, re-centrifuged and retained. Membranes pelleted at 80,000 × g from the supernatant were extracted in 0.6 M KCl and 20 mM Tris (pH 6.8), centrifuged at 120,000 × g, and resuspended in a minimal volume of 10% sucrose. Heavy CSR vesicles isolated based on the method of Sitsapesan and Williams (*140*) were used for channel recordings as they incorporated more readily into phospholipid bilayers. Muscle was homogenized in a buffer containing 300 mM sucrose, and 20 mM piperazine-N,N'-bis(2-ethanesulfonic acid) (PIPES) (pH 7.4), centrifuged at 10,000 × g, and the retained supernnatant was centrifuged a second time at 87,000 × g. The pelleted membranes were resuspended in a salt solution (400 mM KCL, 0.5 mM $MgCl_2$, 0.5 mM $CaCl_2$, 0.5 mM EGTA, 25 mM PIPES, pH 7.0) containing 10% sucrose w/v. The mixed membrane suspension was layered upon discontinuous sucrose-density gradients

consisting of identical salt solutions containing 20%, 30%, and 40% sucrose w/v and sedimented at 100,000 × g. Heavy CSR membrane vesicles collected at the 30-40% sucrose interface were diluted in 400 mM KCl, pelleted at 87,000 × g, and resuspended in a minimal volume of buffer containing 400 mM sucrose, and 5 mM 4-(2-hydroxyethyl)-1-iperazineethanesulfonic acid (HEPES) (pH 7.2). All isolation buffers contained a mixture of protease inhibitors (aprotinin, leupeptin, pepstatin A, benzamidine, and phenylmethylsulphonyl-fluoride). Vesicles were frozen rapidly in liquid N_2 and stored at -80ºC.

3.3.3. [^{3}H]SAM/SAM pretreatment of CSR vesicles and determination of [^{3}H]methyl incorporation

CSR vesicles (4 mg/mL) were incubated in media containing 20 mM PIPES (pH 7.0), 150 mM KCl, 0.285 μM (3 μ Ci) S-adenosyl-L-[methyl-^{3}H]-methionine ([^{3}H]SAM), ± 1 mM S-adenosyl-L-homocysteine (SAH) and/or 500 fold excess unlabled SAM for 30 min at 37^{o}C. In a subset of experiments CSR was incubated as described above but in the presence of 0.1 or 2 mM unlabled SAM rather than [^{3}H]SAM. Treated CSR vesicles were pelleted by centrifugation through 15% sucrose. Pellets were washed by resuspension in 10% sucrose followed by centrifugation at 100,000 × g. Washed CSR vesicles were resuspended in a minimal volume of 10% sucrose, flash frozen in liquid N_2, and stored at -80ºC. SAM treated heavy CSR used for channel recording experiments was resuspended in a minimal volume of buffer containing 400 mM sucrose, and 5 mM HEPES (pH 7.2). All buffers contained a mixture of protease inhibitors. For determining [^{3}H]methyl incorporation, an aliquot of treated CSR vesicles (100 μg) was collected by

filtration onto Whatman GF/B filters, washed with 8 mL ice-cold 100 mM KCl, and the activity retained was measured by liquid scintillation counting.

3.3.4. RyR2 Immunoprecipitation and determination of [^{3}H]methyl incorporation

Control or [^{3}H]SAM pretreated CSR vesicles (200 μg) were solubilized overnight at 4^{o}C in buffer containing 3% CHAPS, 1.0 M NaCl, 20 mM Tris-HCl (pH 7.4), 1 mM dithiothreitol, and protease inhibitors and centrifuged at 12,000 × g for 10 min. Solubilized CSR was incubated for 2 hrs at 4ºC with or without a RyR2 specific antibody (1:100) with rotary mixing and for an additional 2 hrs followed by the addition of Protein G-Sepharose CL-4B beads (20 μl). Beads were pelleted by centrifugation at 14,000 × g and washed twice with IP buffer containing 20 mM Tris-HCl (pH 7.4), 1.0 M NaCl, 0.4% CHAPS, and protease inhibitors. Proteins were eluted from the affinity beads by boiling in sodium dodecyl sulfate (SDS)-sample buffer containing 10% SDS. For determining [^{3}H]methyl incorporation into immunoprecipitated samples, radioactivity of an aliquot (20 μL) of eluted proteins was determined by liquid scintillation counting.

3.3.5. FK506 treatment of CSR vesicles

Treatment of CSR vesicles was based on the method of Ahern et. al. for the removal of FKBP12 from RyRs (*141*). CSR vesicles (2 mg/mL) were incubated at 37 ºC for 30 min in media containing 20 mM Imidazole (pH 7.4), 300 mM sucrose, protease inhibitors, and 10 uM FK506 (in ethanol) or an equivalent volume of ethanol as control. Vesicles were pelleted at 24,000 × g, washed in buffer, and repelleted before resuspension in a minimal volume of buffer.

3.3.6. Western Blotting

CSR vesicles and immunoprecipitated RyR2 samples were separated on 5% or 5-20% gradient SDS-polyacrylamide gels using the buffer system of Laemmli (*142*) and transferred to PVDF membranes for 18 hrs at 30 V followed by 60 min at 200 V using a buffer of 25 mM Tris pH 8.3, 192 mM glycine, 20% methanol and 0.05% SDS at 4ºC. After blocking for 1 hr at room temperature in fresh 5% BSA in PBS containing 0.1 % Tween-20 (PBS-T), membranes were exposed to FKBP12.6 antibodies diluted to 1:1,000 in PBS-T, 5% BSA and 0.5 M NaCl overnight at 4^{o}C. After washing and incubating in horseradish peroxidase conjugated conjugated donkey anti-goat IgG (1:100,000) for 1 hr at room temperature, reacted bands were visualized using enhanced chemiluminescence. Antibody complexes were stripped from the membrane by incubation in 100 mM 2-mercaptoethanol, 2% SDS and 62.5 mM tris(hydroxymethyl)amino-methane pH 6.7 at 50^{o}C for 30 min. RyR2 was detected either after transfer of proteins to PDVF membranes or after stripping membranes previously probed for FKBP12.6. RyR2 monoclonal C3-33 was used at a dilution of 1:50,000. The secondary horseradish peroxidase conjugated goat anti-mouse antibody was used at a dilution of 1:20,000.

3.3.7. [^{3}H]Ryanodine binding

[^{3}H]Ryanodine binding measurements are sensitive indicators of RyR2 channel activity as ryanodine binds with high affinity and selectively to RyRs in the open state (*28, 130*). Ryanodine binding buffer contained 0.4 mg/ml CSR vesicles, 7 nM [^{3}H]ryanodine, 150 mM KCl, 20 mM K-PIPES (pH 7.0), 0.1 mg/ml BSA, 1.0 μg/ml leupeptin, 1.0 μg/ml aprotinin, and Ca^{2+}–EGTA buffers to achieve the desired free Ca^{2+}

concentrations (*131*). Estimates of maximal [^{3}H]ryanodine binding capacity of CSR vesicle preparations were made in parallel with each experiment in media that in addition contained 500 mM KCl, 5 mM ATP, 100 μM Ca^{2+}, and 50 nM ryanodine. Nonspecific CSR vesicle [^{3}H]ryanodine binding was determined by inclusion of 10 mM $MgCl_2$ and 20 μM unlabled ryanodine in the binding media. After 20 hr at room temperature (20–22 ºC) CSR vesicles were collected on Whatman GF/B filters and washed with 8 ml of ice-cold 100 mM KCl. Radioactivity retained by the filters was determined by liquid scintillation counting. The Ca^{2+} dependence of ryanodine binding was fit with an equation that assumes a high affinity Ca^{2+}-binding site, which when bound will activate the channel, and a lower affinity Ca^{2+} binding site, which when bound will inhibit channel opening (*132*). All curve fitting was performed using SigmaPlot 9.0 (Systat Software, Point Richmond, CA). All assays were performed in duplicate and were repeated using at least 4 different CSR vesicle preparations.

3.3.8. Single channel recordings

Muller-Rudin bilayers were formed by painting a lipid mixture (phosphatidylethanolamine, phosphatidylserine, phosphatidylcholine, 5:3:2 ratio by wt, 50 mg/ml dissolved in *n*-decane) across a 100 - 250 μm aperture in a Delrin cup. To assist in vesicle fusion, an osmotic gradient was established across the bilayer. Heavy CSR vesicles were added to the *cis* chamber which contained 250 mM cesium methanesulfonate, 10 mM HEPES (pH 7.4), and 1 mM $CaCl_2$. The *trans* chamber contained 50 mM cesium methansulfonate and 10 mM HEPES pH 7.4. After incorporation of channels into the bilayer, the concentration of cesium methansulfonate in

the *trans* chamber was raised to 250 mM and the *cis* chamber Ca^{2+} concentration adjusted by adding small aliquots of concentrated EGTA and $CaCl_2$ (*131*). Small aliquots of concentrated channel regulators were added to the *cis* chamber with stirring prior to data acquisition. Voltage was controlled and channel currents were recorded using an Axoclamp 200B patch clamp amplifier (Molecular Devices). The *cis* and *trans* chambers were connected to the amplifier head stage by Ag/AgCl electrodes and agar salt bridges. The *trans* chamber was held at ground and current was applied to the *cis* chamber. Current was monitored on an oscilloscope, recorded at 5 kHz and signals were filtered at 1 kHz. Channel data were collected using a pulsing protocol in which the potential was held at 0 mV for 120 ms between steps of 4-s duration to -70 mV (CLAMPEX program, pCLAMP software, Axon instruments).

3.3.9. Analysis of data

Only channels having a conductance of at least 400 pS were used for analysis. Single-channel current amplitudes were measured from digitized data using manually controlled cursors. Channel open probability (P_o), open times, and closed times were determined by the half-amplitude threshold method with a threshold set so that openings to the maximum single channel conductance level (γ_{max}) and openings to the SAM related sub-conductance level (γ_{sub}) were included in the analyses. Single channel P_o was calculated from at least 30 4-s sweeps using FETCHAN and PSTAT analysis programs (pCLAMP software). Frequently two channels incorporated into the bilayer, indicated by current amplitudes of twice the expected magnitude, and P_o was estimated as the average P_o of the two channels, calculated as [P_o level 1 + (P_o level 2 × 2)]/2. Bilayers in which 3

or 4 channels had incorporated were treated similarly. The probability of openings to γ_{sub} (P_o sub-state; ~20 pA) was calculated as time spent in γ_{sub} / total recording time. The percentage of channel openings to sub-conductance levels was given by [P_o sub-state / (P_o sub-state + P_o maximum single channel conductance level (≥ 20 pA)) × 100].

3.3.10. Statistics

CSR [^{3}H]ryanodine binding and [^{3}H]methyl-group incorporation data are presented as means ± SEM and were analyzed using a one-way ANOVA with a Holm-Sidak multiple comparison as a post-hoc test or by Student's t-tests as appropriate. Occasionally data did not fit the assumptions required for a t-test, in which case a non-parametric test was performed. Single channel open probabilities and dwell times are presented as means ± SEM analyzed using Student's paired t-tests or Mann-Whitney Rank Sum test. Statistical analysis was performed using SigmaStat 3.1 (Systat Software, Point Richmond, CA). The level of significance was $p < 0.05$ unless otherwise noted.

3.4. Results

3.4.1. Effects of SAM on CSR vesicle [^{3}H]Ryanodine binding

S-adenosyl-L-methionine (SAM) is a ubiquitous methyl group donor which is present in cells at a concentration of 60-90 μM (*112, 113*). Previously we have shown that SAM (≥ 75 μM) significantly increases CSR vesicle [^{3}H]ryanodine binding in a concentration dependent manner (*137*). Thus, RyR2 is activated by a physiological concentration of SAM. The effects of SAM on the Ca^{2+} concentration dependence of CSR vesicle [^{3}H]ryanodine binding revealed that SAM activation of RyR2 is Ca^{2+}

dependent (Fig 10). The effects of 0.1 and 1 mM SAM on the maximal Ca^{2+}-induced CSR vesicle [^{3}H]ryanodine binding (%B_{max}), Ca^{2+} concentrations required to half-maximally activate (EC_{50}) and half-inhibit (IC_{50}) binding, and the Hill coefficients for activation (n_a) and inhibition (n_i) are given in Table 1. In the presence of 0.1 mM SAM the B_{max} and IC_{50} of CSR vesicle ryanodine binding increased significantly. Inclusion of 1 mM SAM in the binding media increased the %B_{max}, IC_{50}, and caused additional effects, significantly increasing the n_a, and decreasing the EC_{50}. SAM did not significantly increase CSR [^{3}H]ryanodine binding in media containing sub-activating Ca^{2+} concentrations (< 0.1 μM). Thus, SAM did not alone activate RyR2 but enhanced Ca^{2+} activation of RyR2, and increased the Ca^{2+} concentration required to inhibit ryanodine binding.

Table 1. Parameters from fits to Ca^{2+} concentration dependence of CSR vesicle [^{3}H]Ryanodine binding. The Ca^{2+} concentration dependence of CSR vesicle ryanodine binding was performed as described in "Materials and Methods" in media containing the indicated Ca^{2+} concentration and either No Addition, 0.1 mM SAM, or 1 mM SAM. [^{3}H]Ryanodine binding is expressed as percent of maximal [^{3}H]ryanodine 0.2 binding. Significantly different from No Addition (* $p \leq 0.05$, # $p \leq 0.005$, , † $p \leq 0.001$).

	% B_{max}	EC_{50} (μM)	IC_{50} (mM)	n_a	n_i
No Addition	26.7 ± 1.52	1.37 ± 0.33	4.0 ± .83	1.01 ± 0.20	1.21 ± 0.59
0.01 mM SAM	38.0 ± 1.66#	1.13 ± 0.26	9.69 ± 1.46*	0.88 ± 0.15	1.77 ± 1.31
1 mM SAM	55.3 ± 1.23†	0.46 ± 0.04*	10.73 ± 1.75*	1.82 ± 0.23*	0.97 ± 0.19

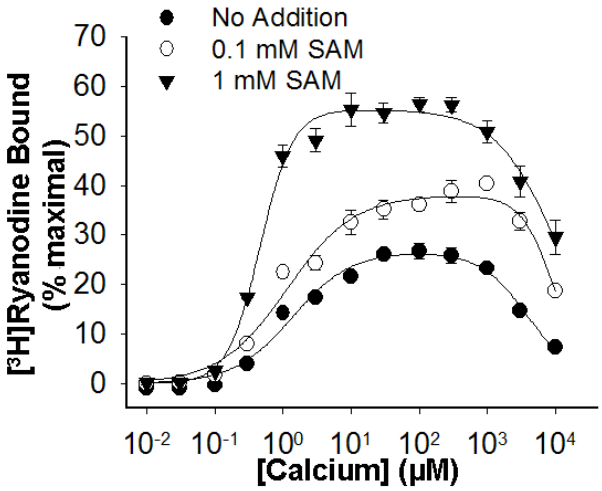

Figure 10. Effects of SAM on Ca^{2+}-dependent activation of RyR2. The Ca^{2+} concentration dependence of CSR vesicle ryanodine binding was performed as described in "Materials and Methods" in media containing the indicated Ca^{2+} concentration and either No Addition , 0.1 mM SAM, or 1 mM SAM. [^{3}H]Ryanodine binding is expressed as percent of maximal [^{3}H]ryanodine binding. The *solid lines* are the fits to the Ca^{2+} concentration dependence (B_{max} = 1.4 ± 0.18 pmol/mg; n= 4).

3.4.2. Methyltransferase inhibitors do not block the SAM-induced increase in CSR vesicle ryanodine binding

SAM is the primary methyl group donor for the enzyme-mediated methylation of biological macromolecules. Activation of RyR2 by SAM may therefore be the result of protein methylation. S-adenosyl-L-homocysteine (SAH), a product of methyl group transfer from SAM to an acceptor molecule, inhibits methyltransferase activity by mass action, while sinefungin inhibits transmethylation reactions by competing for the SAM binding site on methyltransferases. Figure 11 A shows the effect of 1 mM SAM on CSR vesicle [^{3}H]ryanodine binding in the absence or presence of increasing concentrations of sinefungin (*top panel*) or SAH (*bottom panel*). Including 1 mM SAM in the binding media significantly increased CSR ryanodine binding which was not blocked by SAH up to 1.8 mM or sinefingin up 3 mM. Due to low solubility of SAH, higher concentrations of the compound were not used. Importantly, neither SAH nor sinefungin alone significantly altered CSR ryanodine binding from control. These results suggest activation of RyR2 by SAM is not the result of enzyme-mediated methylation

3.4.3. RyR2 methylation is not detected following incubation of CSR vesicles with [^{3}H]SAM

Additional experiments were performed to determine if RyR2 is methylated under conditions in which SAM activation of CSR [^{3}H]ryanodine binding is observed. CSR vesicles were pretreated with S-adenosyl-L-[methyl-

^{3}H]-methionine ([^{3}H]SAM) in the presence or absence of SAH and/or excess unlabled SAM, followed by centrifugation and washing to remove unincorporated [^{3}H]SAM. Radioactivity associated with pretreated CSR and retained in respective immunoprecipitates was determined as an indicator of methyl group incorporation (Table 2, Fig. 11 B). The inset in Figure 11 B shows a representative Western blot as an indication of RyR2 protein yield obtained by our immunoprecipitation protocol. Inclusion of SAH and/or excess unlabled SAM in the incubation buffer during [^{3}H]SAM treatment reduced the amount of radioactivity incorporated into CSR by ≥ 95%. Less than 6% of the radioactivity incorporated into pretreated CSR was retained by immunoprecipitation, and was unaffected by inclusion of methyltransferase inhibitors in the incubation media. Furthermore, there was no difference in the amount of radioactivity recovered by immunoprecipitation performed in the presence or absence of a RyR2 specific antibody. RyR2, therefore, is not among the SR components methylated during SAM treatment.

Table 2. Scintillation counts from [^{3}H]SAM pretreated CSR and Immunoprecipitated RyR2. CSR was incubated as described in "Materials and Methods" Data are means ± SE from 3 experiments (all assays were performed in duplicate). Significantly different from [^{3}H]SAM alone (* $p \leq 0.001$, † $p \leq 0.01$, # $p \leq 0.05$).

Incubation conditions	CSR (CPM)	RyR2 IP with antibody (CPM)	RyR2 IP without antibody (CPM)
[^{3}H]SAM alone	54676 ± 4823	196.7 ± 37.12	175.17 ± 17.14
+ unlabled SAM	1183 ± 92.26*	69.33 ± 25.39†	40.67 ± 11.08#
+ SAH	2407 ± 299.5*	53.83 ± 13.57†	28.83 ± 3.77#
+ unlabled SAM + SAH	1750 ± 163.5*	46.17 ± 11.26†	33.67 ± 6.99#

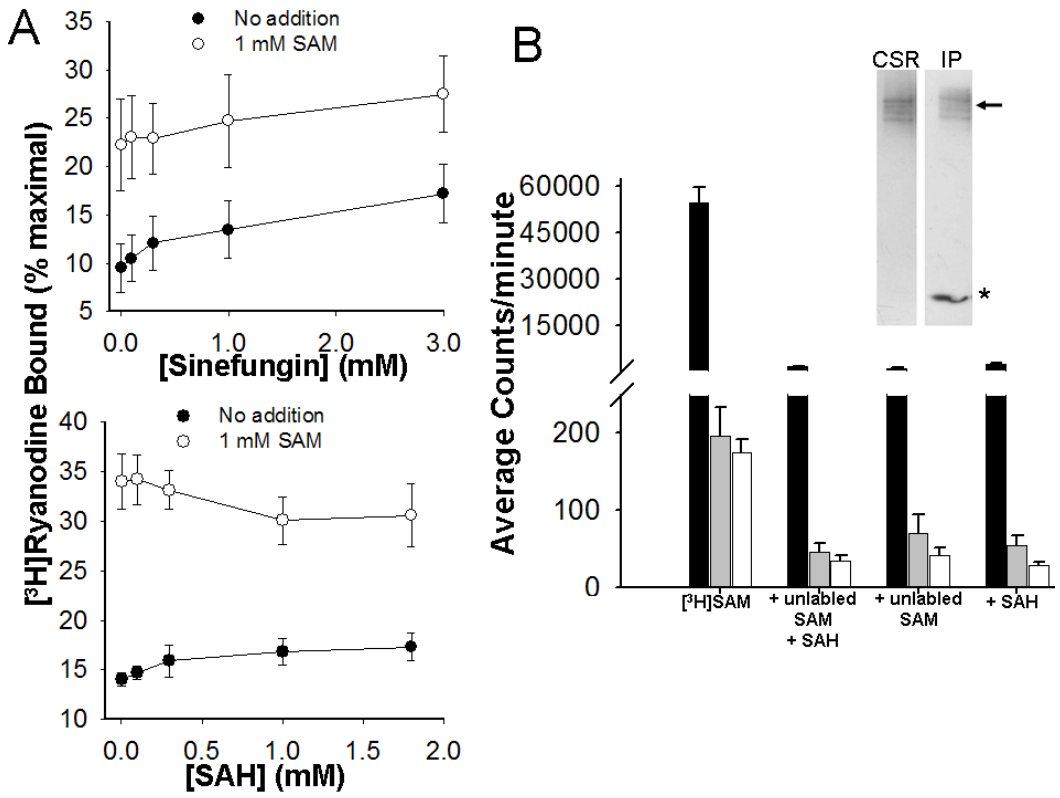

Figure 11. Methyltransferase inhibitors do not block SAM activation. (A) CSR vesicle ryanodine binding was performed as described in "Materials and Methods" in media containing 3 µM Ca^{2+}, the indicated concentrations of sinefungin (*top panel*; B_{max}= 2.9 ± 0.2 pmol/mg; n= 4) or S-adenosyl-l-homocysteine (SAH) (*bottom panel*; B_{max}= 2.5 ± 0.3 pmol/mg; n= 4), with or without (No Addition) 1 mM SAM. [^{3}H]Ryanodine binding is expressed as percent of maximal [^{3}H]ryanodine binding. (B) CSR was incubated as described in "Materials and Methods" in the presence of 0.285 µM (3 µCi) [^{3}H]SAM and No Addition or 1 mM SAH and/or 3.2 mM unlabled SAM (>1000 fold excess). CSR vesicles were centrifuged through sucrose, washed and resuspened 10% sucrose. RyR2 was immunoprecipitated from treated CRS either in the presence or absence of anti-RyR,. Liquid scintillation counting was used to measure radioactivity associated with 100 µg treated CSR (black bars), and 20 µl aliquots of samples immunoprecipitated from treated CSR in the presence (grey bars) or absence (white bars) of anti-RyR2. Inset shows a Western blot demonstrating typical protein yield from RyR2 immunoprecipitations performed as described in "Materials and Methods". The position of RyR2 and RyR antibody are indicated with an arrow and asterisk respectively. Data are means ± SE from 3 experiments (all assays were performed in duplicate).

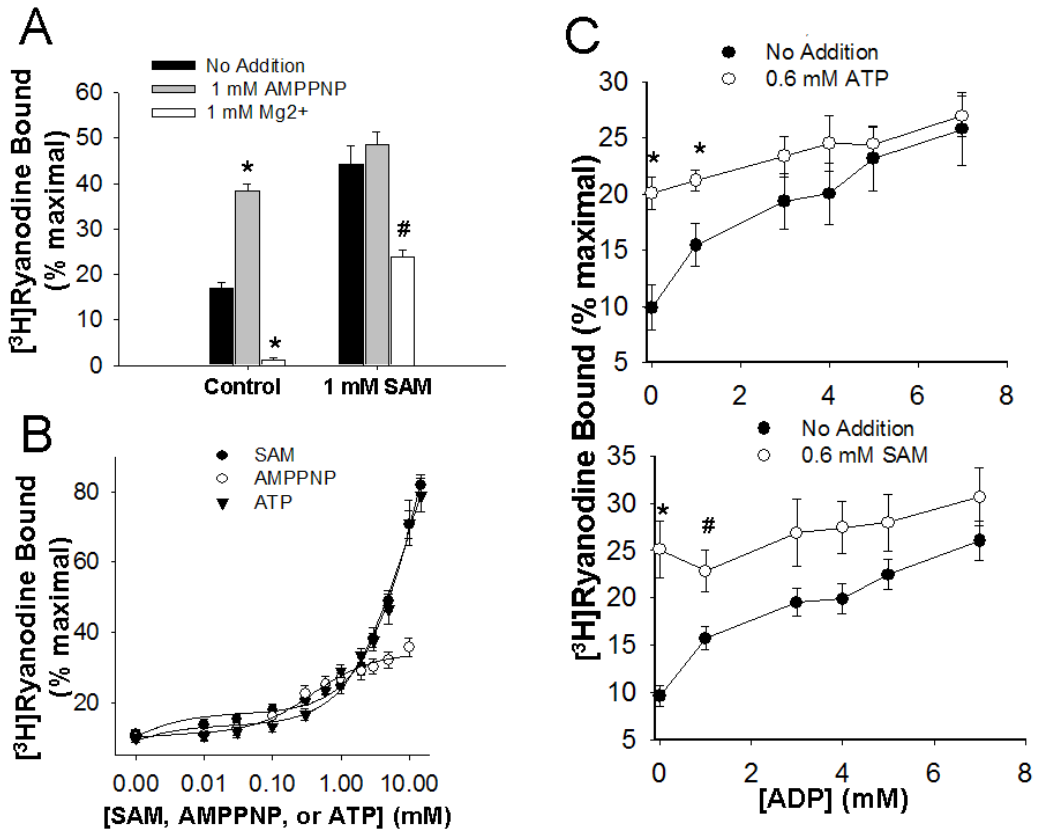

Figure 12. Interaction between SAM and ATP activation of RyR2. CSR vesicle ryanodine binding was performed as described in "Materials and Methods" (A-C) and is expressed as a percent of maximal [^{3}H]ryanodine binding. (A) Effects of SAM on modulation of cardiac SR vesicle ryanodine binding by established RyR2 regulators. Ryanodine binding was performed in media containing 3 µM Ca^{2+} in the presence or absence (control) of 1 mM AMPPNP or 1 mM Mg^{2+} with or without (No Addition) 1 mM SAM (B_{max} = 1.5 ± 0.4 pmol/mg; n= 5). Significantly different from control (*$p \leq 0.001$, # $p \leq 0.01$). (B) Comparison of the SAM, AMPPNP, and ATP concentration dependence of CSR ryanodine binding performed in the presence of 3 µM Ca^{2+} (B_{max} = 2.4 ± 0.3pmol/mg; n= 5). (C) Competition between the ADP and SAM or ATP induced increase in CSR ryanodine binding was performed in media containing 3 µM Ca^{2+} and the indicated concentrations of ADP with or without (No Addition) 0.6 mM ATP (B_{max} = 3 ± 0.3pmol/mg; n= 4) (*top panel*) or 0.6 mM SAM (B_{max} = 2.7 ± 0.15 pmol/mg; n= 5) (*bottom panel*). Significantly different from No Addition (*$p \leq 0.001$, # $p \leq 0.05$).

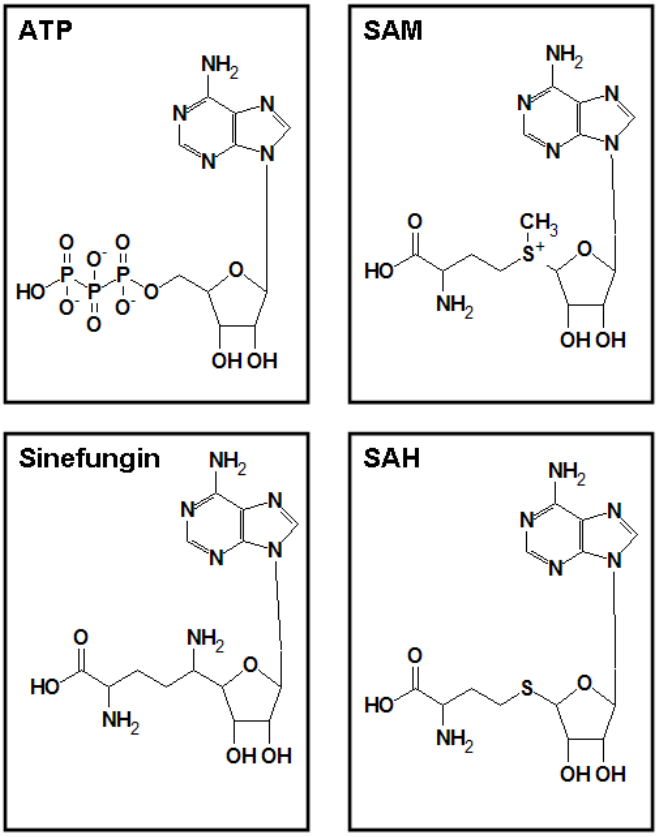

Figure 13. Chemical structures of ATP, s-adenosyl-l-methionine (SAM), s-adenosyl-l-homocysteine (SAH), and sinefungin. SAM is synthesized from methionine and ATP, which serves as an adenosine "donor". Note the sulfonium of SAM imparts a net positive charge to the molecule in contrast to the electronegative phosphates of ATP. The methyltransferase inhibitors SAH and sinefungin have no net charge, and have no effect on CSR ryanodine binding.

3.4.4. Effects of SAM on CSR vesicle ryanodine binding in the presence of other physiological RyR2 effectors

To further characterize SAM activation of RyR2 we investigated the effects of SAM on RyR2 regulation by Mg^{2+} and the non-hydrolyzable ATP analogue, AMPPNP (Fig. 12 A). In the absence of other RyR2 regulators (3 μM Ca^{2+} alone) 1 mM SAM significantly increased CSR [^{3}H]ryanodine binding over control from 17.0 ± 1.2% to 44.2 ± 4.1 % of maximal. The addition of 1 mM Mg^{2+} to the binding media caused a reduction in CSR ryanodine binding both in the presence (23.8 ± 1.7%) and absence (1.1 ± 0.6%) of SAM. CSR vesicle [^{3}H]ryanodine binding was significantly enhanced by 1 mM AMPPNP to 38.3 ± 1.7 % of maximal, however, in media containing 1 mM SAM, the addition of AMPPNP did not cause a further increase CSR ryanodine binding (48.6 ± 2.7%). Thus, SAM activation of RyR2 reduced channel activation by the ATP analogue AMPPNP.

3.4.5. SAM competes with adenine nucleotide–induced increase in CSR vesicle ryanodine binding

Importantly, SAM contains an adenosine moiety, and is therefore structurally similar to ATP and other adenine based compounds (Fig. 13). Thus, the interaction between SAM and AMPPNP activation of RyR2 provoked us to investigate more thoroughly whether SAM regulation of RyR2 results from SAM interacting with the adenine nucleotide binding site/s. The substitution of AMPPNP for ATP avoids the potential confounding effect of RyR2

phosphorylation, however, differences in the efficacy of RyR activation by ATP and its non-hydrolysable analogues have been noted (*57, 60*). Thus, we compared the SAM, ATP, and AMPPNP concentration dependence of CSR vesicle ryanodine binding (Fig. 12 B). The SAM and ATP concentration dependence of CSR [^{3}H]ryanodine binding paralleled one another and did not plateau up to 10 mM. Binding was significantly increased over control by all SAM concentrations $\geq$ 0.1 mM and by all ATP concentrations $\geq$ 0.3 mM. The extent of CSR [^{3}H]ryanodine binding was not different between SAM and ATP at any of the concentrations investigated. In contrast, the AMPPNP-induced increase in binding reached a plateau at ~2 mM. The discrepancy between the ATP and AMPPNP concentration dependence of CSR ryanodine binding motivated the use of ATP in subsequent experiments.

To determine whether there is an interaction between SAM and adenine nucleotide activation of RyR2, the ADP concentration dependence of CSR ryanodine binding was performed in the absence (No Addition) and presence of either 0.6 mM ATP or SAM. In media containing 3 μM Ca^{2+}, ADP increased CSR ryanodine binding in a concentration dependent manner and ATP enhanced binding in the absence and presence of 1 mM ADP, but had no further effect on binding at higher concentrations of ADP (Fig. 12 C, *top panel*). The lack of an additive effect of ADP plus ATP is consistent with two ligands acting via a common site (the adenine nucleotide binding site/s). Figure 12 C (*bottom panel*) shows that SAM enhanced CSR ryanodine binding in the absence and presence of 1 mM ADP, but had no additional effect on binding in the presence of higher

concentrations of ADP. Taken together, the data presented in Figure 3 suggest that SAM and adenine nucleotides act through a common binding site.

3.4.6. SAM activates RyR2 and increases sub-conductance level openings

As a more direct measure of SAM-induced channel opening we examined the effects of SAM on native RyR2 channels incorporated into phospholipid bilayers. Consistent with results from CSR ryanodine binding, 0.1 mM SAM activated RyR2, which was reflected by a significant increase in channel open probability (P_o). In the experiment shown in Figure 14 channel P_o increased from 0.087 in the presence of 10 μM *cis* Ca^{2+} to 0.271 after the addition of 0.1 mM *cis* SAM. The increase in P_o could be attributed to both an increase in the mean open time (Control = 0.45 ms; 0.1 mM SAM = 1.00 ms) and to a decrease in the mean closed time (Control = 6.35 ms; 0.1 mM SAM = 2.66 ms). The summary data presented in Table 3 and Figure 16 support the conclusion that 0.1 mM SAM caused a significant increase in mean open time. Additionally, mean channel closed time was decreased in the presence of 0.1 mM SAM in 3 out of 4 experiments.

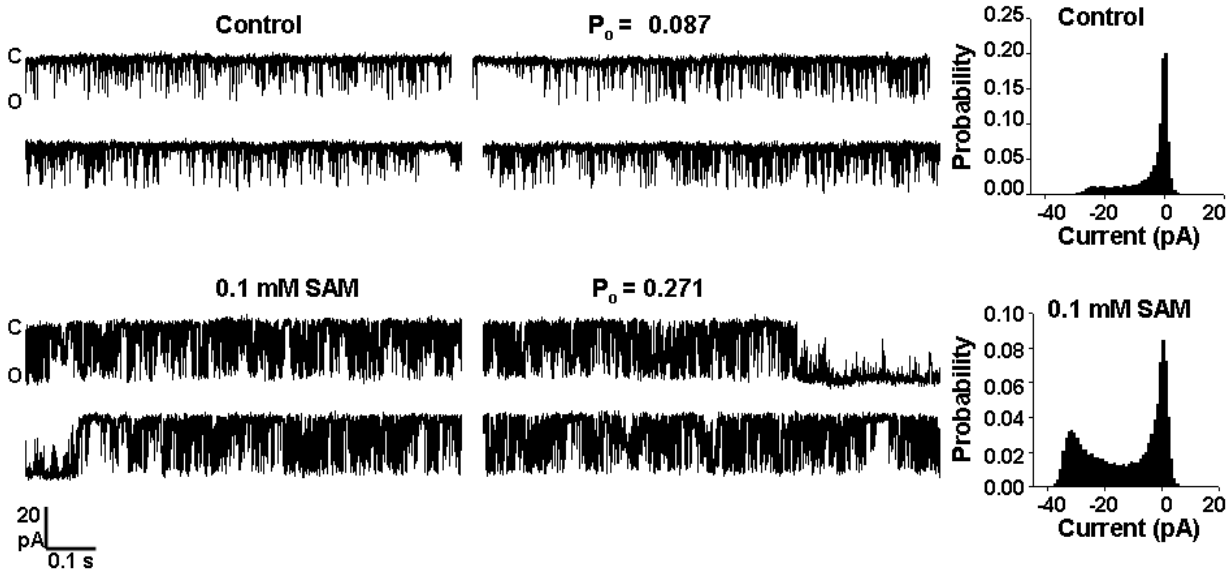

Figure 14. SAM activates native RyR2 channels. Currents were recorded in symmetrical 250 mM Cs^+ using a pulsing protocol consisting of steps to -70 mV. Closed (*C*) and full conductance open (*O*) levels are indicated to the left of the traces and corresponding amplitude histograms from ≥ 2 min recording time are shown to the right. Channel open probability (P_o) is indicated above each trace. The t*op* trace shows a representative channel activated by 10 μM *cis* Ca^{2+} and the *bottom* trace shows activity of the same channel immediately following the addition of 0.1 mM *cis* SAM.

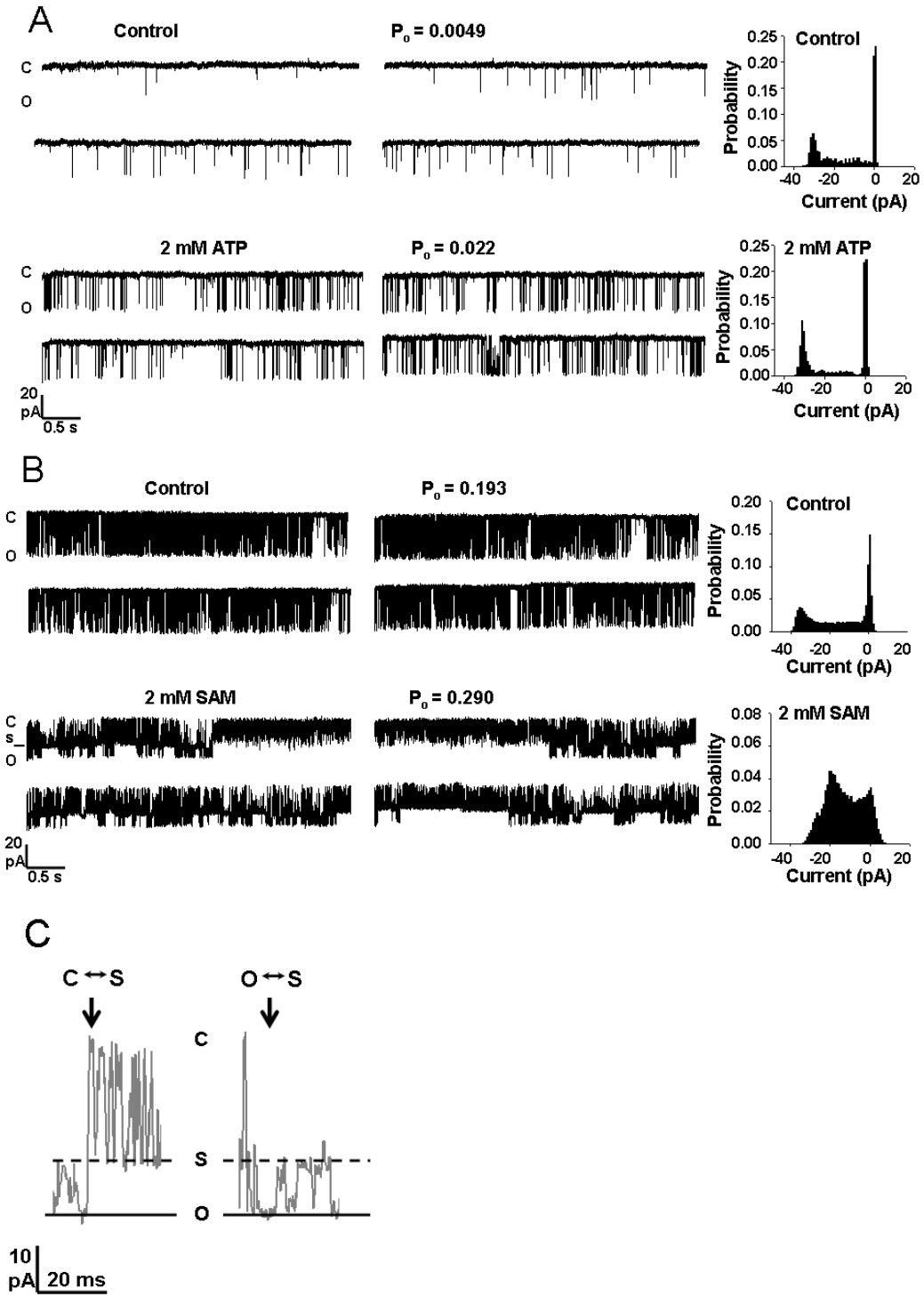
A
Control
P_o = 0.0049
C
O
Control
Probability
0.25
0.20
0.15
0.10
0.05
0.00
-40 -20 0 20
Current (pA)
2 mM ATP
P_o = 0.022
2 mM ATP
20
pA
0.5 s
B
Control
P_o = 0.193
0.20
2 mM SAM
P_o = 0.290
0.08
0.06
0.04
0.02
C
C ↔ S
O ↔ S
S
10
pA
20 ms

Figure 15. Comparison of SAM and ATP activation of native RyR2 channels. Currents were recorded in symmetrical 250 mM Cs^+ using a pulsing protocol consisting of steps to -70 mV. Closed (*C*), full conductance open (*O*) and sub-conductance open (*s*) levels are indicated to the left of the traces and corresponding amplitude histograms from ≥ 2 min recording time are shown to the right. Channel open probability (P_o) is indicated above each trace. *Top* traces in each panel show a representative channel activated by 10 μM *cis* Ca^{2+} and *bottom* traces show channel activity immediately following the addition of (A) 2 mM *cis* ATP or (B) 2 mM *cis* SAM. The SAM-induced sub-conductance state in B is typical and was observed in all experiments (6 single channel recordings) upon addition of 2 mM SAM, but was extremely rare upon the addition of 2 mM ATP. (C) Segments of channel recording following the addition of 2 mM *cis* SAM are shown on an expanded time scale. Transitions from the closed state (*C*) to the sub-conductance state (*S and dotted line*) and from the full conductance (*O and solid line*) to the sub-conductance state were frequently observed (*arrows*). The sequence of transitions between states is indicated above each arrow.

To further investigate whether SAM interacts with the RyR2 adenine nucleotide binding site we compared the effects of SAM and ATP on the activity of native RyR2 channels. An identical concentration of SAM and ATP shown to substantially activate RyR2 (2 mM) was chosen for comparison given the overlap in the SAM and ATP concentration dependence of CSR vesicle ryanodine binding (Fig. 12 B). Activation of RyR2 was reflected by a significant increase in channel P_o after the addition of either ATP or SAM to the *cis* chamber (Fig. 16 A). Representative RyR2 channel current recordings are shown in Figure 6. Channel P_o increased from 0.0049 in the presence of 10 μM *cis* Ca^{2+} to 0.022 after the addition of 2 mM *cis* ATP (Fig. 15 A). The increase in P_o was due to an increase in the mean open time (Control = 0.94 ms; 2 mM ATP = 1.57 ms) and a decrease in the mean closed time (Control = 205 ms; 2 mM ATP = 96.8 ms). Although the channel shown in Figure 15 B was activated to a greater extent by Ca^{2+} alone (P_o= 0.193) compared to the previous channel in A, the addition of 2 mM *cis* SAM caused an immediate increase in P_o to 0.290. In contrast to ATP, however, SAM activation of RyR2 was associated with a marked change in channel conductance which is evident in the current trace and corresponding amplitude histogram (Fig. 15 B, *bottom trace*). Average maximal single RyR2 channel unitary conductance (γ_{max}) in 250 mM symmetrical Cs^+ recorded at -70 mV was 513 ± 10, 514 ± 15, 507 ± 16, 528 ± 28 pS for control, 0.1 mM SAM, 2 mM SAM, and 2 mM ATP respectively. The average conductance of sub-state openings in the presence of 2 mM SAM was 294 ± 22 pS corresponding to ~ 60% of γ_{max}. The summary data in Figure 16 B show that in the presence of 2 mM

SAM the percent of channel openings to a predominant sub-state ~ 60% γ_{max} increased from 1.7 ± 1.2 to 31.3 ± 5%, while ATP had no effect on the percent of sub-state openings (control: 1.2 ± 0.5%; 2 mM ATP: 0.4 ± 0.2%). Sub-states detected under control conditions likely reflect very brief openings that were not fully resolved. The percent of RyR2 sub-state openings also increased in the presence of 0.1 mM SAM (Control = 0.14 ± 0.08 %; 0.1 mM SAM = 1.54 ± 0.15 % sub-state openings) (Fig. 16 B), however due to the low frequency of occurrence, these events are difficult to resolve visually (Fig. 14 A). RyR2 channel transitions between the closed, maximum conductance, and the SAM-induced sub-conductance state are more clearly resolved in segments of channel recording shown on an expanded time scale (Fig. 15 C). In the presence of 2 mM *cis* SAM, entry into the sub-conductance state occurred either from the closed or from the fully open state. Both of these transitions were commonly observed (*arrows* in Fig. 15 C). In agreement with previously described effects of ATP on RyR2 (*43*), single channel data indicate that 2 mM *cis* ATP enhanced channel P_o through both an increase in mean open time and a decrease in mean closed time. In the representative single channel experiment shown in Figure 6 A, mean channel open time increased from 0.94 to 1.57 ms and mean closed time decreased from 205 to 96.8 ms after the addition of 2 mM *cis* ATP. For the channel shown in Figure 14, 0.1 mM SAM increased the mean open time from 0.45 to 1.00 ms and decreased the mean closed time from 6.35 to 2.66 ms. After the addition of 2 mM *cis* SAM (Fig. 15 B) mean channel open time increased from 0.919 to 3.13 ms and mean closed time decreased from 4.1 to 1.45 ms.

Thus, the effects of 0.1 mM and 2 mM SAM on RyR2 mean open and closed times followed similar trends to those observed for ATP (Table 2, Fig. 16 C-E).

3.4.7. Potential Mechanisms of the SAM-induced sub-conductance state

Attempts were made to remove SAM by perfusion of the *cis* chamber, however, this procedure produced inconsistent results including substantial increases and declines in channel P_o. Thus, as an alternative approach to test the reversibility of the SAM-induced RyR2 sub-state we performed a subset of experiments in which native RyR2 from SAM treated heavy CSR were incorporated into phospholipid bilayers. Representative current recordings from these experiments are shown in Figure 8. Prior incubation with 2 mM SAM altered RyR2 conductance with 5 out of 7 channel recordings exhibiting a predominant sub-state of ~ 60% γ_{max} (Fig. 17 B). This predominant sub-state was not observed in any channel recordings (5 recordings) from CSR incubated in the absence of SAM (Fig. 17 A), thus suggesting SAM alters RyR2 conductance via an indirect mechanism. In a previous study, Chen and colleagues proposed that SAM activation of RyRs from smooth muscle occurs via dissociation of FKBP (*124*). We therefore investigated whether SAM induced the dissociation of FKBP12.6 from the channel. After pretreatment of CSR vesicles with SAM (0, 0.1 or 2 mM) at 37ºC for 30 min, the amount of FKBP12.6 associated with CSR vesicles was visualized by Western blots of CSR proteins immunostained with RyR2 or FKBP12.6 specific antibodies (Fig. 18 B, *top panel*). Immunostaining of the FKBP12.6 band (~12 kDa) was not reduced by incubation of CSR with 0.1 or

2 mM SAM. We also investigated whether the association between FKBP12.6 and RyR2 was required for the SAM-induced increase in CSR vesicle ryanodine binding. For this purpose, CSR vesicles were incubated in the absence (No addition) or presence of FK506, an immunosuppressant which has been show to cause dissociation of FKBPs from RyRs (*143*). FK506 treatment did not affect the SAM concentration dependent increase in CSR ryanodine binding (Fig. 18 B, *bottom panel*), further supporting the conclusion that FKBP12.6 dissociation is not the mechanism underlying SAM regulation of RyR2. We therefore envision that SAM reduces channel conductance by causing a conformational change in the RyR2 protein.

Table 3. Effects of ATP and SAM on mean channel open and closed times. Single RyR2 channel currents were recorded in the presence of 10 μM *cis* Ca^{2+} and analyzed for mean open and closed times as described in "Materials and Methods" before and after the addition of 2 mM ATP, 2 mM SAM, or 0.1 mM SAM to the *cis* chamber. Data in each cell are means ± SE from 4 experiments. Significantly different from mean open time before addition (* $p \leq 0.05$).

	Mean open time Before addition (ms)	Mean open time After addition (ms)	Mean closed time Before addition (ms)	Mean closed time After addition (ms)
2 mM ATP	0.73 ± 0.16	1.32 ± 0.33	87.77 ± 58.65	36.13 ± 30.39
2 mM SAM	0.86 ± 0.10	2.47 ± 0.82	28.17 ± 19.11	6.13 ± 3.33
0.1 mM SAM	0.57 ± 0.11	1.12 ± 0.20*	6.73 ± 2.44	2.89 ± 1.23

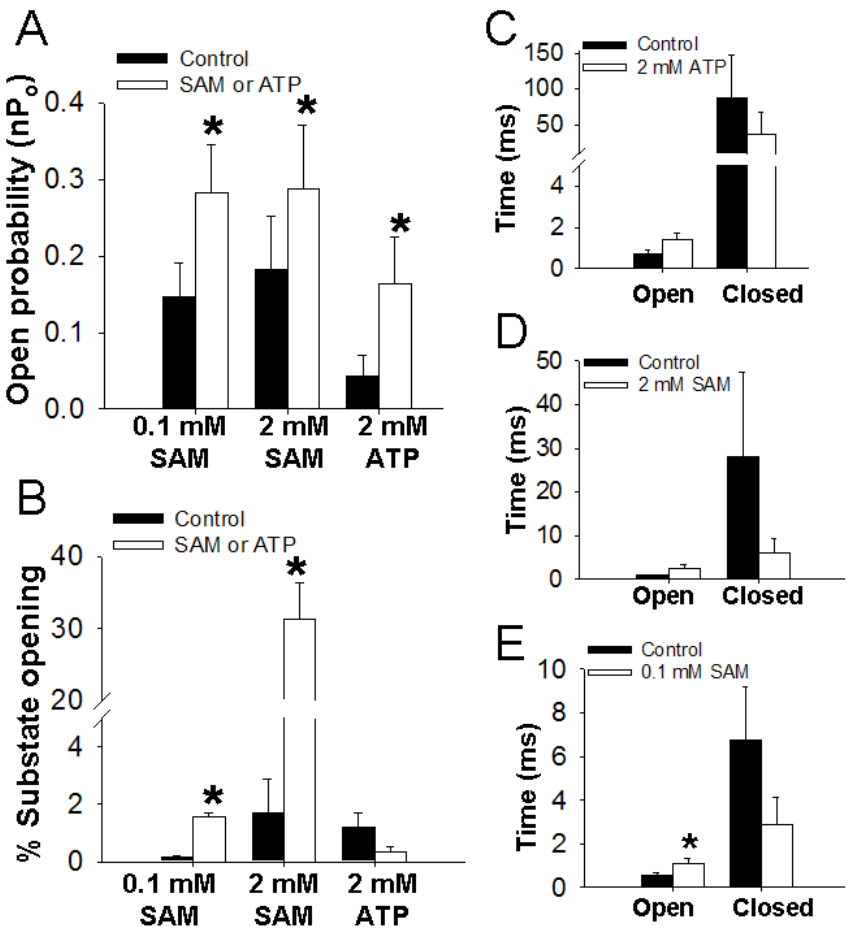

Figure 16. Effects of SAM and ATP on RyR2 activation and conductance. RyR2 channel currents were recorded in the presence of 10 µM *cis* Ca^{2+} (control) and following the addition of the indicated concentrations of *cis* ATP or SAM and analyzed as described in "Materials and Methods" for the following parameters: (A) Channel P_o (n = 6-12), (B) single RyR2 % sub-state opening (n = 4-5), and (C-E) single RyR2 mean open and closed times (n = 4). Significantly different from control (*$p \leq 0.05$).

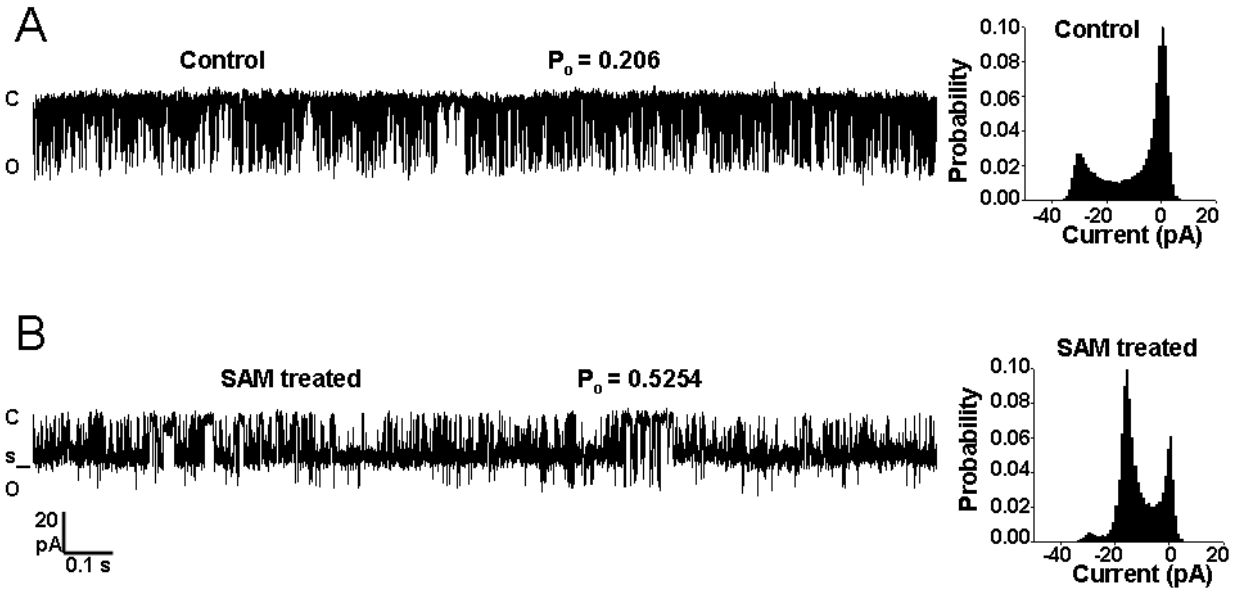

Figure 17. RyR2 from SAM treated CSR exhibit altered conductance. Native RyR2 from heavy CSR incubated as described in "Materials and Methods" in the (A) absence or (B) presence of 2 mM SAM were incorporated into phospolipid bilayers. Currents were recorded in symmetrical 250 mM Cs^+ using a pulsing protocol consisting of steps to -70 mV. Closed (*C*), full conductance open (*O*) and sub-conductance open (*s*) levels are indicated to the left of the traces and corresponding amplitude histograms from ≥ 2 min recording time are shown to the right. Channel open probability (P_o) is indicated above each trace.

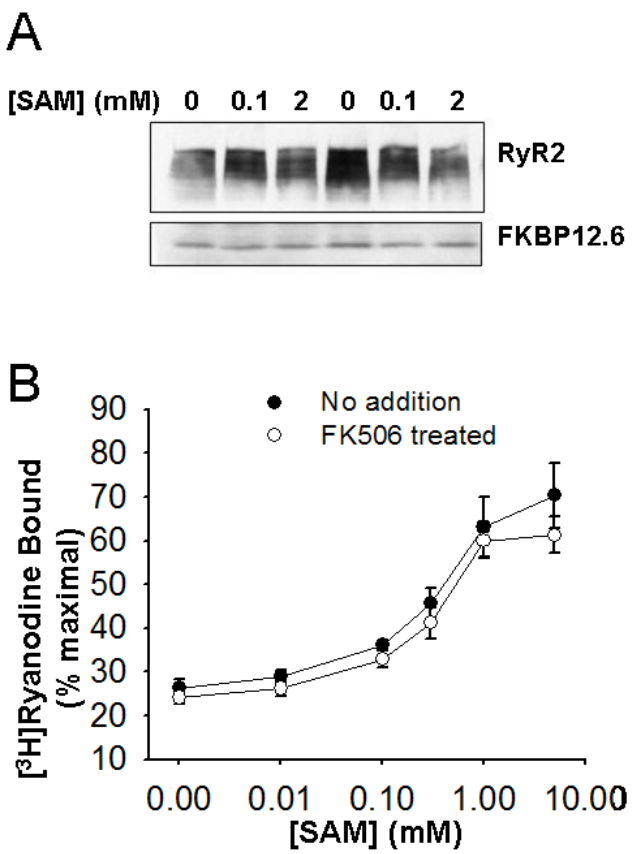

Figure 18. FKBP12.6 dissociation does not underlie the SAM related RyR2 sub-conductance state. (A) CSR vesicles were incubated as described in "Materials and Methods" in the presence of 0, 0.1, or 2 mM SAM. Treated CSR vesicles were centrifuged through 15% sucrose, washed, and resuspended in a minimal volume of 10% sucrose. CSR was subjected to SDS-PAGE followed by Western blot analysis using antibodies specific for RyR2 and FKBP12.6. Western blot analysis indicates that SAM did not induce the loss of FKBP12.6 from CSR. CSR vesicles were treated with or without 10 μM FK506, pelleted, washed, and resuspended in a minimal volume of buffer. (B) Ryanodine binding to pretreated CSR was performed as described under "Materials and Methods" in media containing 10 μM Ca^{2+} and the indicated concentration of SAM. [^{3}H]Ryanodine binding is expressed as a percent of maximal [^{3}H]ryanodine binding (B_{max}= 2.3 ± 0.4; n= 4). FKBP506 treatment did not alter the SAM-dependence of CSR [^{3}H]ryanodine binding.

3.5. Discussion

Using CSR ryanodine binding and RyR2 current recordings we have shown that SAM activates RyR2. SAM participates in methylation of proteins and other macromolecules, a mechanism by which the localization and function of biological targets is altered (2). A diverse class of enzymes known as methyltransferases catalyzes the transfer of the methyl group from the sulfonium of SAM to the oxygen, nitrogen, or sulfur atom of biological targets (3). We therefore investigated whether SAM activation of RyR2 is associated with channel methylation by incubation of CSR vesicles with SAM containing a radiolabled methyl group. Inclusion of the methyltransferase inhibitor SAH and/or excess unlabled SAM in the incubation buffer reduced the amount of radioactivity incorporated into CSR vesicles by ≥ 95% indicating (i) methyltransferases are present in our CSR preparations, and (ii) SAM provides methyl groups for methylation of CSR components. However, immunoprecipitation of RyR2 from solubilized [^{3}H]SAM treated CSR showed that the amount of radioactivity associated with RyR2 was negligible and nonspecific given that no difference was found compared to samples from immunoprecipitations performed in the absence of an RyR2 specific antibody (Table 2, Fig. 11 B). Furthermore, inclusion of the methyltransferase inhibitors SAH or sinefungin in the binding media did not prevent the SAM-induced increase in CSR ryanodine binding (Fig. 11 A). Together these data suggest SAM activation of RyR2 does not involve channel methylation.

A point of interest is the structural similarity between SAM and ATP (Fig. 13), an important physiological regulator of RyR2. Like ATP and its non-hydrolysable analogue AMPPNP, SAM contains an adenosine moiety raising the possibility that SAM regulates

RyR2 via the adenine nucleotide binding site/s. Using CSR ryanodine binding we found that SAM reduced the extent to which AMPPNP activated RyR2 (Fig. 12 A). Competition experiments were designed to further investigate the interaction between SAM and adenine nucleotide activation of RyR2. The combined effects of ADP and ATP on CSR ryanodine binding were not additive, in line with the expectation for two ligands acting through a common binding site. Likewise, ADP and SAM did not exert additive effects on CSR ryanodine binding (Fig. 12 C), suggesting that SAM acts through binding either the RyR2 adenine nucleotide binding site or a distinct but interacting site on the channel.

Single channel current recordings and analysis are routinely used to clarify the mechanisms underlying channel regulation. A principal goal of the present study, therefore, was to compare the affects of SAM and ATP on RyR2 channel gating using native RyR2 incorporated into phospholipid bilayers. In addition to 0.1 mM SAM, we chose a higher concentration of SAM and ATP (2 mM) shown though ryanodine binding to produce substantial activation of RyR2 (Fig. 12 B). Single channel analyses showed that the effects of SAM on RyR2 P_o, mean open, and closed times followed similar trends to those observed for ATP (Table 3, Fig. 16 C-E). However, unlike ATP, SAM affected RyR2 channel conductance. A concentration dependent increase in the proportion of channel openings to a sub-conductance level ~ 60% γ_{max} was observed in the presence of 0.1 mM and 2 mM SAM (Fig. 16 B), with a much more pronounced effect observed with 2 mM SAM.

Interestingly, we observed that prior incubation of CSR with SAM caused lasting effects on RyR2 conductance while identical treatment of CSR in the absence of SAM

was without effect (Fig. 18). In these experiments, a wash step was included to remove SAM prior to channel incorporation thus, an indirect mechanism distinct from ligand binding likely underlies the SAM induced RyR2 sub-state. In its native membrane the RyR2 is part of a macromolecular complex in association with a number of accessory proteins implicated in channel modulation, and signaling molecules involved in posttranslational protein modification (*99*). It is plausible that SAM alters the interaction between RyR2 and one or more endogenous effector proteins thereby affecting channel conductance. The RyR accessory protein FKBP12/12.6 is associated with RyRs in a 4:1 ratio with one FKBP bound to each RyR monomer. Removal of FKBP12 from the skeletal isoform of the channel (RyR1) increases channel activity, and is associated with an increased frequency of sub-conductance openings (*82, 141*). However, whether removal of FKBPs from RyR2 results in a similar alteration of channel behavior is unclear (*22, 52*). Chen and colleagues attributed SAM activation of smooth muscle RyRs to FKBP methylation causing its dissociation from the channel (*124*). In an attempt to determine whether FKBP dissociation is involved in the SAM related RyR2 sub-conductance state we performed Western blot analysis of CSR proteins and found that immunostaining of the FKBP12.6 band was not reduced by incubation of CSR with 0.1 or 2 mM SAM (Fig. 17 B, *top pane*l). In addition there was no difference in the SAM-induced increase in ryanodine binding to FK506 treated (FKBP stripped) and control CSR (Fig. 17 B, *bottom panel*).

The ability of ATP and its metabolites to activate RyR2 (efficacy) decreases in the order ATP > ADP > AMP > adenine > adenosine (*43, 62*). Although the purine ring is important for agonist activity (*57*), the structural features of adenosine based compounds

which impart efficacy in activating RyR2 are unknown. Several lines of evidence suggest SAM activates RyR2 via the adenine nucleotide binding site/s: (i) SAM contains an adenosine group, (ii) RyR2 activation by SAM and adenine nucleotides is similar in that both compounds enhance Ca^{2+} activation of the channel but have minimal effects on channel activity in the absence of Ca^{2+} (*57*), (iii) the SAM and ATP concentration dependence of CSR ryanodine binding overlap, (iv) SAM and adenine nucleotides have non-additive effects on CSR ryanodine binding, and (v) SAM and ATP have similar effects on mean channel open and closed times.

Studies using native RyR2 channels in phospholipid bilayers have demonstrated that decreasing the number of phosphate groups decreased the ability of adenosine based compounds to activate the channel (*43, 62*). Additional research has used comparative molecular field analysis to correlate the chemical structure of adenosine based molecules with their ability to activate RyR2. This work showed that changes in electrostatic field and steric factors account for 64%, and 36%, respectively, of the total correlation between structure and function. Increasing positive electrostatic potential of the molecule in diffuse regions corresponding to the phosphate groups of ATP was strongly correlated with increasing P_o, meanwhile, increasing negative electrostatic potential distal to the γ phosphate was correlated with increasing P_o. Thus, the effect of electrostatic field on the conformational state of RyR2 is apparently complex. Nevertheless, the high efficacy of ATP was primarily attributed to the negative electrostatic field established by its ionized phosphate groups (*61*). SAM contains a positively charged sulfonium located in the region of the molecule corresponding to the α phosphate in ATP (Fig. 13), yet is equally effective as ATP in activating RyR2. Therefore, our proposal that SAM activates RyR2

via the adenine nucleotide binding site challenges the interpretation that high ligand efficacy at the adenine nucleotide site/s requires a negative electrostatic potential. The methyltransferase inhibitors used in this study (sinefungin and SAH) are adenosine based compounds which have no net charge (Fig. 13). Neither sinefungin nor SAH had an effect on RyR2 activity (Fig. 11 A), an observation which is in accord with an important role of electrostatic interactions in the process of nucleotide activation of RyR2. Our data shed new light on the structure-activity relationship underlying adenine nucleotide regulation of RyR2 and suggest a potential use of SAM as a tool to clarify the structural basis for ligand affinity and efficay at the adenine nucleotide site/s.

Interventions to increase intracellular SAM concentrations were shown to have a positive ionotropic effect in the heart which was at least partially attributed to activation of the SR Ca^{2+} pump (SERCA) upon SAM-dependent N-methylation of membrane phospholipids (*122, 144*). Indeed, investigations of the effect phospholipid N-methylation has on RyR2 activity are lacking, however, the observed inability of methyltransferase inhibitors to block the SAM induced increase in CSR ryanodine binding suggests methyltransferase activity, and thus methylation, is not involved in SAM activation of RyR2. The virtual overlap in the SAM and ATP concentration dependence of CSR [^{3}H]ryanodine binding indicates that both the affinity of SAM for RyR2 and its ability to open the channel are comparable to that of ATP. Therefore, if SAM acts through binding the adenine nucleotide site/s on RyR2, SAM would not function as an effective channel agonist given that cytosolic levels of ATP in cardiac cells (5-10 mM) (*59*) far exceed cellular concentrations of SAM (60-90 μM) (*112*). Our data suggest SAM acts via an indirect yet undetermined mechanism to reduce channel conductance, however, the

functional implication of sub-states in RyRs is unknown, therefore the role of SAM as a physiological regulator of RyR2 is uncertain.

Considering the present data, multiple mechanisms are suggested to account for the effects of SAM on RyR2 activation and conductance. We propose SAM activation of RyR2 results from a direct interaction with the channel, most likely binding the adenine nucleotide site/s. The observed effect of SAM on RyR2 conductance presumably occurs via an indirect mechanism in which SAM reduces channel conductance by causing a conformational change in the RyR2 protein. Such an effect may result from the SAM induced loss of an undetermined RyR2 accessory protein. Determining the mechanism by which SAM causes RyR2 sub-states will further our understanding of the biophysical properties of RyR2 regulation.

CHAPTER 4

INSIGHTS INTO S-ADENOSYL-L-METHIONINE REGULATION OF CARDIAC RYANODINE RECEPTORS: EVIDENCE FOR AN ALLOSTERIC MECHANISM OF SUBSTATE PRODUCTION

4.1. Abstract

S-adenosyl-l-methionine (SAM) can act as a RyR2 channel regulatory ligand in a manner independent from its recognized role as a biological methyl group donor. Channel activation appears to arise from the direct interaction of SAM, via its adenosly moiety, with the RyR2 adenine nucleotide binding sites. In addition to its ability to activate RyR2, recent single channel experiments revealed distinct effects of SAM on RyR2 conductance, which we now explore in greater detail. The effects of SAM on channel conductance are dependent on SAM concentration and membrane holding potential. At negative potentials, *cis* applied SAM induces a clearly resolved subconductance state. The proportion of SAM induced subconductance openings (P_{sub}/P_o), expressed as a proportion of overall channel open probability, increases with decreasing negative potential. Kinetic analysis revealed that changes in the off rate fully accounted for the voltage dependence of the transitions between the full open state and the SAM induced subconductance state. However, at positive potentials SAM causes a striking reduction in channel openings with no distinct effect on channel conductance. Inconsistent with a simple pore block mechanism is the finding that that prevalence of the subconductance state is unaffected by varying the driving force for ion flux. Furthermore, ATP is able to specifically interfere with the effects of SAM at both negative and positive potentials suggesting competition with SAM for a common binding site. Our experimental findings are interpreted in light of an allosteric mechanism whereby SAM interacts with the RyR2

adenine nucleotide binding site. SAM binds to and allosterically stabilizes a channel conformation of reduced conductance and we propose the voltage dependence of the SAM induced subconductance state arises from a voltage-driven alteration in the affinity of the adenine nucleotide binding sites for SAM.

4.2. Introduction

The ryanodine receptor (RyR) is a large homotetrameric intracellular ion channel which mediates the release of Ca^{2+} from the sarcoplasmic reticulum (SR) or other intracellular stores. The subcellular Ca^{2+} signaling which underlies the beat to beat contraction of the heart is regulated through a process of Ca^{2+}-induced-Ca^{2+} release (CICR). Importantly, the basis of CICR regulation is the sensitivity of the cardiac isoform of the Ca^{2+} release channel (RyR2). Although Ca^{2+} is the primary physiological channel activator, alone it is unable to fully activate RyR2 (*59*).

The Ca^{2+} sensitivity of RyR2 is influenced by a number of endogenous effectors including adenine nucleotides. Electron paramagnetic resonance studies have suggested that per RyR monomer, there are two adenine nucleotide binding sites whose availability is altered with conformational changes in the channel protein (*63, 145*). Among these nucleotides, adenosine triphosphate (ATP) is the most potent channel activator (*43, 62*). Although the importance of the purine ring for agonist activity is recognized (*57*), other structural features that influence the efficacy of adenine nucleotides are poorly defined.

S-adenosyl-l-methionine (SAM) is produced when the adenosyl moiety from adenosine triphosphate (ATP) is transferred to methionine forming a sulfonium which readily donates its methyl group through enzyme (methyltransferase) dependent reactions

to numerous biological substrates (*112, 117, 138*). The RyR modulating effects of SAM were first described by Chen and colleagues, who attributed SAM activation of RyRs from coronary artery myocytes to protein methylation and subsequent dissociation of the RyR accessory protein FKBP12 (*124*). However, we have shown that SAM activates a defined channel isoform, RyR2, via a direct physical interaction with a regulatory site on the channel (*137, 146*). Furthermore, observed similarities between SAM- and ATP-enhancement of CSR ryanodine binding, and competition between SAM and adenine nucleotides suggest that this regulatory site is shared by SAM and ATP. In single channel experiments we also observed a previously unreported SAM related subconductance state which could not be attributed to FKBP dissociation (*146*). Subconductance events have been characterized in a variety of both voltage- and ligand-gated ion channels. Although in some cases, such as the GABA- and glycine-activated chloride channels, these subconductance events are intrinsic characteristics of the channel (*78*), many endogenous and exogenous compounds induce channel subconductance events. The mechanisms by which channel effectors induce subconductance levels can broadly be classified as those that interact with the channel conduction pathway (i.e. pore block) or allosteric modulators. The compounds that interact with the channel pore interfere with flux of the conducting ions through the channel. In contrast, allosteric modulators, which may bind some distance from the channel conducting pathway, either induce or stabilize a channel conformation that limits the flux of ions through the pore. Various exogenous RyR regulators modulate channel conductance by producing a voltage dependent reduction in the amplitude of the open full conductance state, or producing one or multiple subconductance states. Ryanoids, and various peptide toxins

(e.g. $IpTx_a$) are proposed to allosterically limit channel conductance, producing a voltage dependent subconductance state upon the binding and stabilization of a distinct protein conformation (allosteric mechanism) (*93, 107*). In contrast, the behavior of a voltage dependent RyR2 subconductance state produced by the tetra butyl ammonium cation (TBA^+) is more consistent with a pore block mechanism whereby TBA^+ interacts with permeant ions (*86*).

This work clarifies the mechanism by which SAM promotes a subconductance state in RyR2. We find that the voltage dependence and kinetics of SAM interaction are inconsistent with a simple pore block mechanism. Furthermore, premeant cations (Cs^+) do not interfere with the SAM related substate, indicating that SAM affects channel conductance through a regulatory (i.e. allosteric) site located on the cytosolic face of RyR2 some distance from the permeation pathway. We also report a specific interaction between SAM and ATP observed at the single channel level; a strong indication that SAM and ATP bind a common regulatory site. Our results are consistent with an allosteric model whereby SAM binds to and stabilizes a voltage dependent subconductance conformation of the RyR2 channel. To account for the voltage dependence of the SAM related substate we propose a voltage driven change in protein conformation alters the affinity of a regulatory site for SAM. In our model we attribute the interaction between SAM and ATP to their binding a common adenine nucleotide regulatory site on RyR2.

4.3. Materials and methods

4.3.1. Materials

Pigs were purchased from Clemson University Research Farm Services. S-(5'-adenosyl)-L-methionine chloride (SAM), S-(5'-adenosyl)-L-homocysteine (SAH), sinefungin, ATP, 4-chloro-m-cresnol (4-CmC) and tetrabutrylammonium bromide (TBA) were obtained from Sigma Aldrich (St. Louis, MO). Phospholipids were purchased from Avanti Polar Lipids (Alabaster, AL).

4.3.2. Isolation of cardiac sarcoplasmic reticulum vesicles

Non-pietrain pigs were euthanized in accordance with the Public Health Services Policy on Humane Care and Use of Laboratory Animals and with the approval of the Institutional Care and Use Committee of the Georgia Institute of Technology. Briefly, following sedation by subcutaneous injection of ketamine (20 mg/kg) and xylazine (2 mg/kg) animals were euthanized by intravenous injection of sodium pentobarbital (100 mg/kg). Heavy CSR vesicles were isolated based on the method of Sitsapesan and Williams (16). Ventricular and septal muscle was cleaned of excess fat and connective tissue, minced and homogenized in an ice-cold buffer containing 300 mM sucrose, and 20 mM piperazine-N,N'-bis(2-ethanesulfonic acid) (PIPES) (pH 7.4), centrifuged at 10,000 × g. The retained supernatant was centrifuged a second time at 87,000 × g and the pelleted membranes were resuspended in a salt solution (400 mM KCl, 0.5 mM $MgCl_2$, 0.5 mM $CaCl_2$, 0.5 mM EGTA, 25 mM PIPES, pH 7.0) containing 10% sucrose w/v. The mixed membrane suspension was layered upon discontinuous sucrose-density

gradients consisting of identical salt solutions containing 20%, 30%, and 40% sucrose w/v and sedimented at 100,000 × g. Heavy CSR membrane vesicles collected at the 30-40% sucrose interface were diluted in 400 mM KCl, pelleted at 87,000 × g, and resuspended in a minimal volume of buffer containing 400 mM sucrose, and 5 mM 4-(2-hydroxyethyl)-1-iperazineethanesulfonic acid (HEPES) (pH 7.2). All steps were performed at 4^{o}C and isolation buffers contained a mixture of protease inhibitors (aprotinin, leupeptin, pepstatin A, benzamidine, and phenylmethylsulphonyl-fluoride). Vesicles were frozen rapidly in liquid N_2 and stored at -80ºC.

4.3.3. Single channel recordings

Muller-Rudin bilayers were formed by painting a lipid mixture (phosphatidylethanolamine, phosphatidylserine, phosphatidylcholine, 5:3:2 ratio by wt, 50 mg/ml dissolved in n-decane) across a 100 - 250 μm aperture in a Delrin cup. To assist in vesicle fusion, an osmotic gradient was established across the bilayer and the *cis* chamber was stirred. Heavy CSR vesicles were added to the *cis* chamber which contained 250 mM cesium methanesulfonate, 10 mM HEPES (pH 7.4), and 1 mM CaCl2. The *trans* chamber contained 50 mM cesium methansulfonate and 10 mM HEPES pH 7.4. After incorporation of channels into the bilayer, the osmotic gradient was abolished by raising the concentration of cesium methansulfonate in the *trans* chamber to 250 mM and the *cis* chamber Ca^{2+} concentration adjusted by adding small aliquots of concentrated EGTA and $CaCl_2$ (21). Small aliquots of concentrated channel regulators were added to the *cis* chamber with stirring prior to data acquisition. Voltage was controlled and channel currents were recorded using an Axoclamp 200B patch clamp amplifier

(Molecular Devices). The *cis* and *trans* chambers were connected to the amplifier head stage by Ag/AgCl electrodes and agar salt bridges. In our experimental setup current is applied to the *cis* chamber with the *trans* chamber held at ground. Therefore in symmetrical cesium methansulfonate a negative membrane potential promotes the flow of Cs^+ from *trans* to *cis*. Current was monitored on an oscilloscope, recorded at 5 kHz and signals were filtered at 1 kHz. Channel data were collected using a pulsing protocol in which the potential was held at 0 mV for 120 ms between steps of 2-s duration each to -50 and + 50 mV (CLAMPEX program, pCLAMP 9.2 software, Molecular Devices, Sunnyvale, CA).

4.3.4. Analysis of data

Single-channel events indicated by current transitions between the closed (c), open subconductance (s), and open full conductance (o) levels were measured from digitized data using manually controlled cursors. Channel activity from at least 30 sweeps was analyzed using the Clampfit program (pCLAMP9.2 software). Open probabilities and lifetimes of closed and open events were determined using the method of 50% threshold analysis. To avoid the complication that subconductance events may arise from unresolved brief channel openings, events shorter than 1.0 ms (3 times the filter rise time) were excluded from analysis. This is a more conservative cut-off than typically employed, but ensured that the amplitude of the filtered events reached >99.8% of the true events(*147*). All channel openings, to either the open full conductance or open subconductance level were included in the determination of P_o. Normalized all points current amplitude histograms (band width = 1 pA) were attained from each 2-minute

recording. In most experiments, components corresponding to the baseline, full open and in the presence of SAM, subconductance currents were readily identified. Each component was fit with a Gaussian function using the Levenberg-Marquardt method. Prevalence of the SAM induced subconductance state was measured by setting two thresholds, one at the subconductance level, and a second at the conductance level. Prevalence of the subconductance state, (P_{sub}/P_o), was calculated by dividing the open probability of subconductance state (P_{sub}) by overall channel open probability (P_o), which included openings to both the open full conductance level and the open subconductance level. Lifetime analysis was carried out only when a single channel incorporated into the bilayer. Closed, open full conductance, and open subconductance lifetimes were fitted to a probability density function (PDF) by the method of maximum likelihood according to the equation

$$f(t) = a_1 \exp(-t/\tau_1) + \ldots + a_n \exp(-t/\tau_n) \quad (1)$$

where a is the area or fractional contribution for that component to the area under the curve, τ is the time constant, an estimate of the mean dwell time of that component, and t is the dwell time. Fits of up to three exponentials were compared by testing the difference in the log (likelihood) against the chi-squared distribution at the 5% level. Analysis of the voltage dependence of the transitions between the open subconductance state and the open full conductance state was based on the assumption that theses transitions arise from the association and dissociation of SAM from the channel. For this purpose, all closed events, and all open events preceded or succeeded by a closed event,

were excluded from analysis using code developed in MATLAB. The rates for SAM association (k_{on}) and dissociation (k_{off}) were derived from single exponential fits to dwell time distributions of the open full conductance and open subconductance states respectively. The SAM concentrations of half maximal efficacy were determined using non-linear curve fitting of Eq. (2) to dose response relationships for P_o and P_{sub}/P_o

$$y = (B_{max} \times [SAM])/ (K_d + [SAM]) \quad (2)$$

All curve fitting was performed using SigmaPlot 9.0 (Systat Software, Point Richmond, CA).

4.3.5. Statistics

Single channel open probabilities (P_o), prevalence of the subconductance state (P_{sub}/P_o), and dwell times are presented as means ± SEM analyzed using Student's paired t-tests. Statistical analysis was performed using SigmaStat 3.1 (Systat Software, Point Richmond, CA). The level of significance was $p < 0.05$ unless otherwise noted.

4.4. Results

4.4.1. SAM differentially affects RyR2 at positive and negative potentials

Under control conditions (10 μM Ca^{2+}) channel open probability (P_o) was 0.431±0.052 at +50 mV and 0.439±0.069 at -50 mV. Channels had a slope conductance of 441± 13 pS (Fig.19). Current reversed at -4.8 mV. The non-zero reversal potential was

likely due to the mixing of chamber solutions upon repeated breakage and reformation of the bilayer prior to successful channel incorporation.

Initial experiments investigated the effect of SAM on single channel currents in lipid bilayers using a sequential pulsing protocol to -50 and +50 mV. Channel activity was better maintained using this alternating voltage protocol compared to a protocol consisting of steps to positive or negative voltages alone. In previous work 2 mM SAM was shown to promote a single, clearly resolved subconductance state, while a lower concentration of SAM (0.1 mM) was relatively ineffective at promoting the substate (*146*). For the purpose of clarifying the mechanism by which SAM affects channel conductance, 2 mM SAM was chosen as it unambiguously promoted the effect of interest (i.e. the subconductance state). Interestingly, membrane potential significantly altered channel response to SAM. The current traces to the left in Figure 20A show channel activity recoded at a holding potential of -50 mV, before and immediately after the addition of 2 mM SAM to the cytosolic chamber (*cis* SAM). At -50 mV, SAM increased channel P_o to 0.824±0.055 and caused a dramatic increase in the appearance of a single clearly resolved subconductance state (~2/3 full conductance) as previously reported (*146*). Channel P_o increased as SAM concentration was increased from 0.3 mM to 10 mM. The dose response curve in the top panel of Figure 21 plateaus around 2 mM SAM and gives a half maximal effective SAM concentration (K_d) of 0.11±0.11 mM. In contrast, at a holding potential of +50 mV, channel P_o decreased exponentially with increasing concentrations of SAM (Fig. 21, bottom panel). Two mM *cis* SAM decreased channel P_o to 0.010±0.002 and did not promote a subconductance state (Fig. 20A, right). None of the SAM concentrations investigated effectively promoted a subconductance

state at positive potentials. For example, 0.3 mM SAM which caused a more moderate (~50%) reduction in channel P_o, had no noticeable effect on channel conductance. Due to the strong inhibitory effect of SAM at positive potentials, channel analysis was primarily limited to recordings at negative holding potentials.

The prevalence of the SAM related substate, expressed as the fraction of open time the channel spent in the subconductance state (P_{sub}/P_o) increased from 0.111±0.019 in the absence of SAM to 0.632±0.050 in 2 mM SAM (Fig. 20 A, left). In contrast to the SAM concentration dependence of overall channel open probability (P_o) which saturated at 2 mM SAM (Fig. 21, *top panel*), P_{sub}/P_o continued to increase with SAM concentrations > 2 mM (Fig. 22A). In the absence of SAM, a fraction of the substate events can be attributed to noise reaching the 50% threshold for the subconductance level and generating a false event. The false event rate is a function of the 50% threshold event amplitude (A), the root mean squared noise of the system in the absence of channel activity (σ_n) and the filter cut-off frequency (f_c) according to equation 3 (*147*).

$$\text{false event rate} \approx f_c \exp[-0.5(A/\sigma_n)^2] \quad (3)$$

At negative potentials where subconductance events were studied, the slope of the substate current-voltage relationship gave a slope conductance of 289±13 pS (Fig. 19). At a holding potential of -50 mV current amplitude of the subconductance state was ~ 14.5 pA with 50% threshold of ~7.25 pA. A σ_n of 2.5 pA and a f_c of 1 kHz yields a false event rate of 15 events per sec. In the absence of SAM the frequency of subconductance

events at -50 mV was 29±4.5, therefore false events accounted for approximately 52% of the subconductance events under control conditions.

In 4 out of 4 experiments, addition of 2 mM SAM to the luminal side (*trans* chamber) had no observable effect on channel conductance or open probability at + 50 mV (control P_o, 0.208 ± 0.105; *trans* SAM P_o, 0.300 ± 0.177) or -50 mV (control P_o, 0.184 ± 0.1; trans SAM P_o, 0.262 ± 0.158) (Fig. 20 B). The methyltransferase inhibitor sinefungin is a structural analogue of SAM, yet when applied to the *cis* chamber, sinefungin had no effect on channel activity at a holding potential of +50 mV (control P_o,0.147 ± 0.097; sinefungin P_o, 0.238 ± 0.063) or -50 mV (control P_o, 0.213 ± 0.154; sinefungin P_o, 0.386 ± 0.195) (Fig. 20 C).

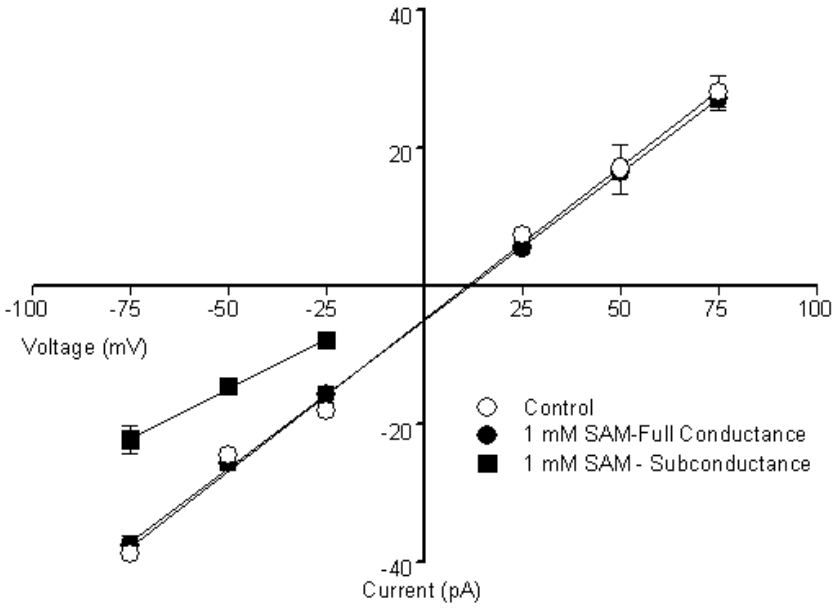

Figure 19. Current-voltage relationship of the maximum conductance and subconductance states. Mean current values of the maximum full conductance state in the absence of SAM (○), maximum full conductance state in the presence of 1 mM SAM (●), and the subconductance state in the presence of 1 mM SAM (■). Data points show the mean ± SEM of 1-6 experiments. The solid lines are linear regression lines.

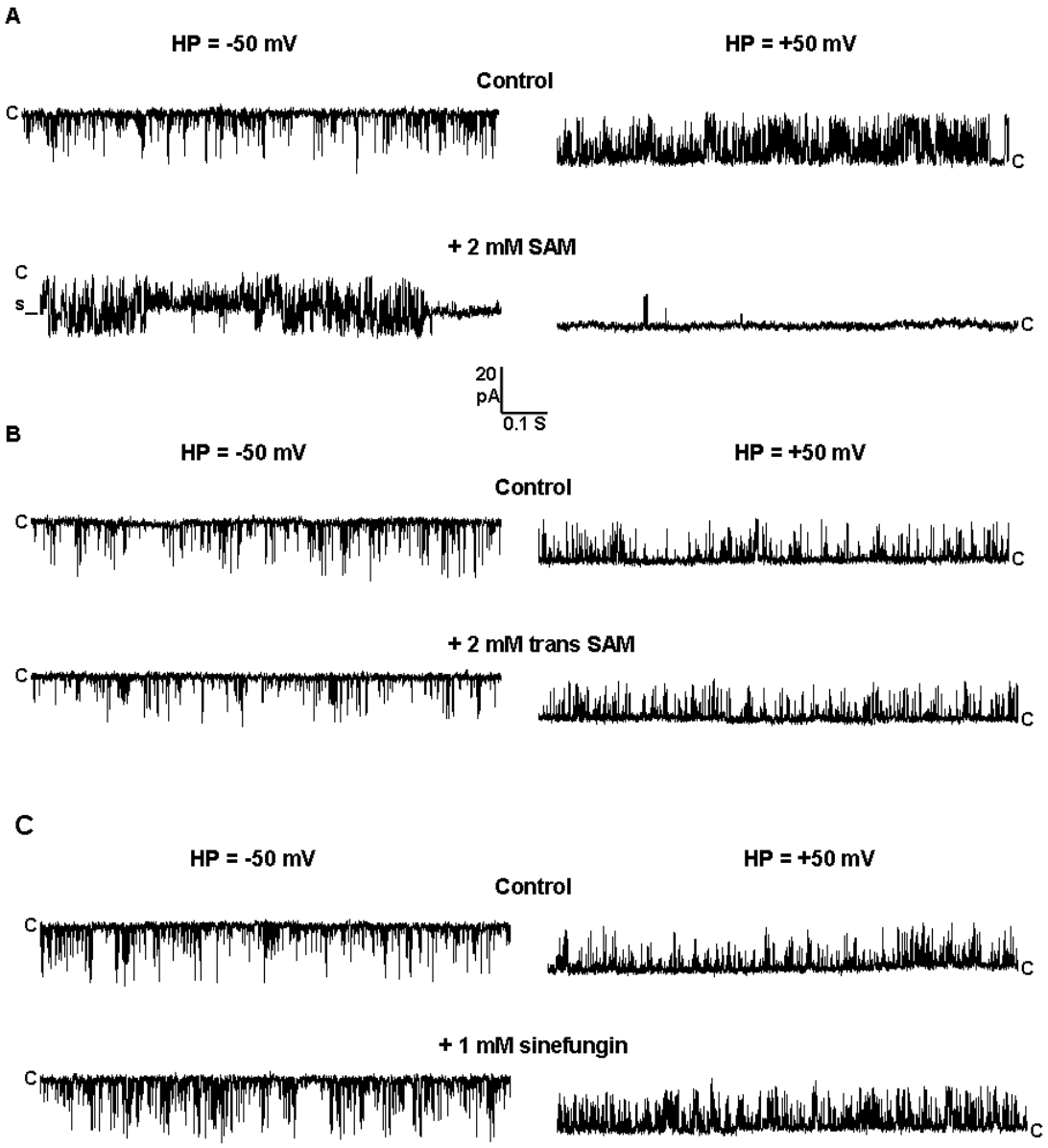

Figure 20. SAM produces a subconductance state from the cytoplasmic face of the channel. Single channel currents shown as downward or upward deflections from closed (c), were recorded in symmetrical 250 mM Cs^+ using a pulsing protocol consisting of steps to ±50 mV. Cytosolic free Ca^{2+} concentration was ~10 μM. (A) A subconductance state (s) became prevalent following the addition of 2 mM cis SAM, but only when current is recorded at a negative holding potential (HP=-50 mV). At a positive potential (HP = +50 mV) 2 mM SAM nearly abolished channel activity. The effects of SAM were observed immediately after ~ 10 sec of chamber stirring. (B) SAM had no effect on channel activity when added to the *trans* chamber. (C) Sinefungin, a structural analogue of SAM, had no effect on channel activity when added to the *cis* chamber.

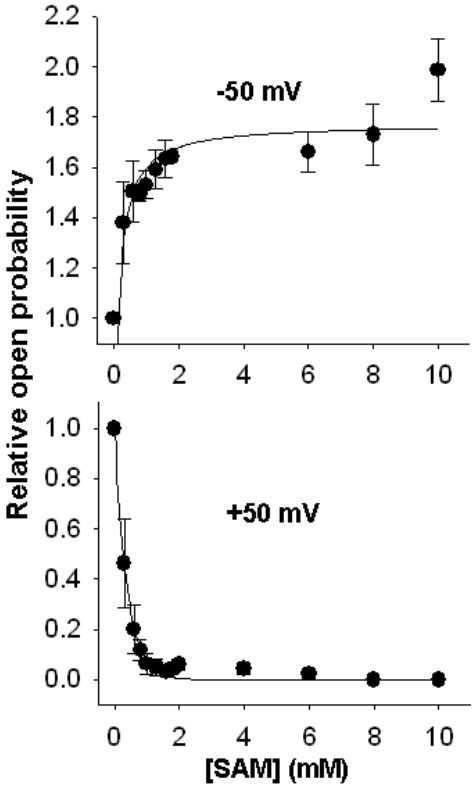

Figure 21. SAM differentially affects channel open probability at negative and positive potentials. At a negative potential of -50 mV, P_o increased with increasing SAM concentration (top panel), whereas at +50 mV, P_o decreased exponentially with increasing SAM concentration (bottom panel). Data points show the means ± SEM of 1-3 experiments. The dose response at -50 mV was fit to a one site saturation ligand binding equation ($y = B_{max}\times/K_d+\times$) with parameter values B_{max} = 1.70±0.149, and K_d = 0.111±0.111. The dose response at +50 mV was fit with an equation for exponential decay (solid line).

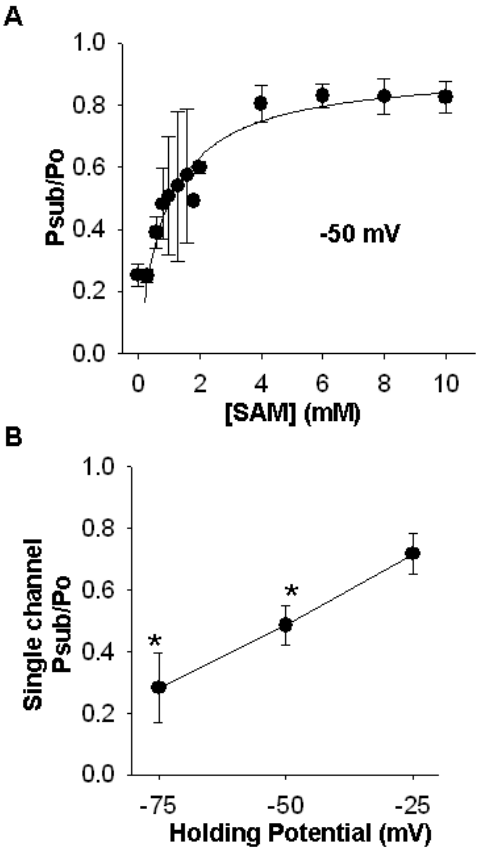

Figure 22. Voltage and SAM concentration dependence of the subconductance state. (A) The proportion of subconductance events (P_{sub}/P_o) observed at -50 mV increased with SAM concentration. The dose response was fit to a one site saturation ligand binding equation (B_{max} = 0.915±0.070, and K_d = 0.887±0.231). Data points show the mean ± SEM from 1-3 experiments. (B) The proportion of subconductance events (P_{sub}/P_o) increased as holding potential became less negative. Data points show the mean ± SEM of 4 experiments. Significantly different from -25 mV *$p<0.05$

4.4.2. The subconductance state is dependent on SAM concentration

Figure 19 shows that the linear current-voltage relationship of the open full conductance state was not altered by SAM (no SAM, slope conductance = 441±13 pS; 1 mM SAM, slope conductance = 428±4 pS). The rarity of events in the presence of SAM at positive potentials makes the conductance measurements here less reliable than at negative potentials. Considering channel openings only at negative potentials yields a substate slope conductance of 289±13 pS, approximately 2/3 full conductance. The dose response curve in Figure 22A shows that the prevalence of the SAM related substate (P_{sub}/P_o) increased with SAM concentration. Equation 2 fit to the SAM dose response curve gives a half maximal effective SAM concentration of 0.887±0.231 mM, and a maximum P_{sub}/P_o value of 0.915±0.07. The prevalence of the SAM related substate was independent of overall channel P_o.

4.4.3. Behavior of the subconductance state is inconsistent with a simple pore block mechanism

SAM was only effective at producing the subconductance state at negative potentials which promote the *trans* to *cis* flux of Cs^+ and therefore do not favor entry of SAM into the conductance pathway. The prevalence of the SAM related substate increased as holding potential was decreased from -75 to -25 mV (in 25 mV increments). In Figure 22 B $P_{sub}/P_{o,}$ in the presence of 2 mM *cis* SAM is plotted as a function of applied negative potential. P_{sub}/P_o increased from 0.284 ± 0.224 at a holding potential of -75 mV to 0.487 ± 0.128 and 0.718 ± 0.13 at -50 mV and -25 mV respectively. The pore block hypothesis attributes the effect of SAM on channel conductance to SAM entering

the conductance pathway thereby directly interfering with the translocation of Cs^+. Based on this hypothesis, the SAM related substate is expected to be sensitive to changes in the driving force for Cs^+ flux through the channel, due to competition between Cs^+ ions and SAM within the conductance pathway. Therefore, P_{sub}/P_o is expected to decrease as the concentration gradient for Cs^+ is increased. Figure 23 shows that P_{sub}/P_o was not significantly altered by a 2.6 fold increase in the *trans* chamber Cs^+ concentration. Increasing *trans* Cs^+ from 250 mM to 650 mM produces a change in driving force equivalent to a 25 mV step increase in the negative potential across the bilayer. In the presence of 2 mM SAM and symmetrical 250 mM CsMS (250/250), P_{sub}/P_o was 0.862 ± 0.034 and remained unchanged after raising the concentration of *trans* CsMs to 450 mM or 650 mM (0.802 ± 0.049 and 0.724 ± 0.071 respectively). The finding that permeant cations do not interfere with SAM binding is inconsistent with the notion of a direct interaction of SAM with the ion permeation pathway.

4.4.4. Voltage dependence of the subconductance state resides in the SAM off rate

SAM appears to interact with both the closed and open full conductance conformations of the RyR2 channel, because opening to the subconductance state occurs from both the closed and the open full conductance state (Fig. 15). Because it is not possible to determine at what instant SAM binds the closed channel, kinetic analysis was limited to SAM's interaction with the open channel. This analysis was based on two assumptions i) dwell time of the subconductance state represents the residence time of SAM on the channel, and thus depends on the rate of SAM dissociation (k_{off}), and ii) dwell time of the open full conductance state represents the unmodified state, and thus

depends on the rate of SAM association (k_{on}). Only transitions between the open full conductance and open subconductance levels were analyzed. The remaining life times of the open full conductance and open subconductance states were well described by a single exponential. The effect of voltage on SAM association and dissociation, shown in Figure 24, revealed that the voltage dependence of the substate resides in the off rate. The rate of SAM dissociation (k_{off}) decreased from 0.581 ±10.148 ms^{-1}at -75 mV to 0.355 ± 0.045 ms^{-1} and 0.187 ± 0.046 ms^{-1}at -50 and -25 mV, respectively. Thus the increase in P_{sub}/P_o that occurred with decreasing negative potential results from a decrease in the rate of SAM dissociation. The SAM association rate (k_{on}) did not change with voltage (-75mV, 0.072 ±0.013 $ms^{-1}mM^{-1}$; -50 mV, 0.089 ±7.7 $\times 10^{-3}$ $ms^{-1}mM^{-1}$; -25mv, 0.117 ± 0.012 $ms^{-1}mM^{-1}$). Indeed, the subconductance openings were visibly prolonged as holding potential was made less negative. Taking the ratio k_{off}/ k_{on} yields a K_d of 1.6 mM, 4 mM, and 8 mM at -25, -50, and -75 mV, respectively. SAM's affinity for the channel decreases as transmembrane potential becomes increasingly negative.

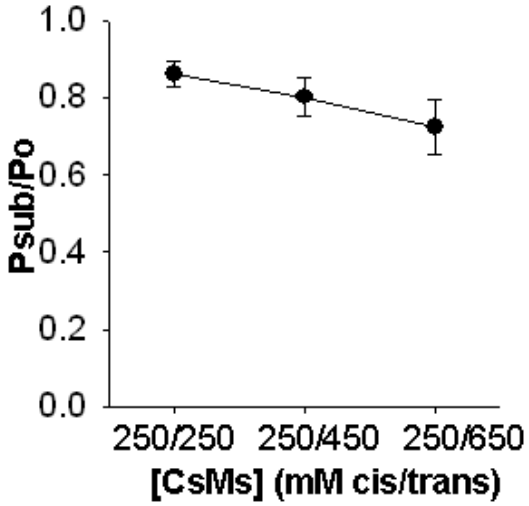

Figure 23. Prevalence of the SAM related subconductance state is unaffected by a change in driving force for ion flux. Single channel currents were recorded at a holding potential of -50 mV in 250 mM symmetrical Cs^+ (250/250), and after increasing *trans* Cs^+ to 450 mM (250/450) and 650 mM (250/650). Data points show means ± SEM of 5-7 experiments.

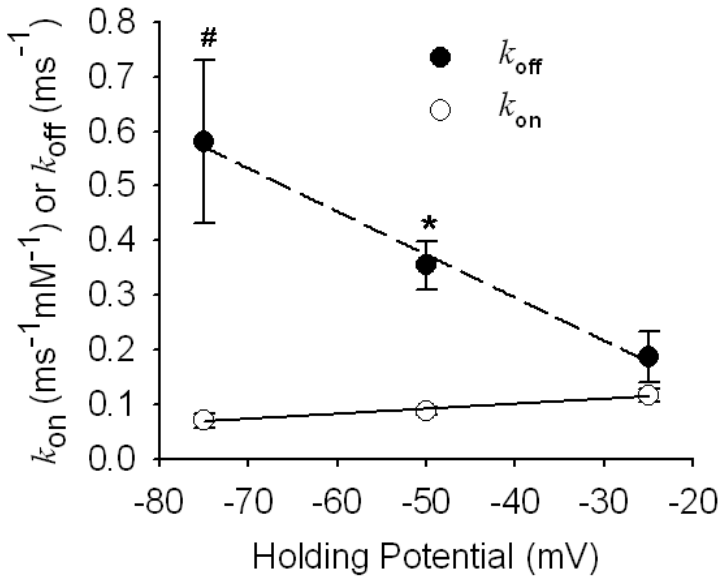

Figure 24. Voltage dependence of the on and off rates for SAM binding RyR2. Channel currents were recorded as described in Figure 21 in the presence of 2 mM SAM. The rate of SAM association (on rate, k_{on} ○) was unaffected by voltage while the rate of SAM dissociation (off rate, k_{off} ●) decreased as holding potential was made less negative. Data points show means ± SEM of 3-8 experiments. Significantly different from -25 mV *$p<0.05$, # $p<0.01$.

4.4.5. ATP interferes with the SAM induced subconductance state

The lack of effect of driving force on the prevalence of the SAM related substate argues against a pore block mechanism and suggests that SAM affects channel conductance by binding to a regulatory site located outside the conduction pathway. Adenine nucleotides compete with the SAM induced increase in CSR [^{3}H]ryanodine binding; a strong indication that SAM and adenine nucleotides interact with a common regulatory site. However, it was unclear whether an interaction between SAM and adenine nucleotides also occurred with respect to the SAM related substate. Representative data from experiments exploring competition between SAM and ATP are shown in Figure 25A. Before SAM addition, the channel displayed flickery gating between the closed and the maximum full conductance state. Following the addition of 2 mM *cis* SAM the channel current fluctuated mainly between the closed state and the SAM related subconductance state. The increased prevalence of the subconductance state in the presence of SAM is reflected in the amplitude histogram as a shift in current distribution to the subconductance level. After subsequent addition of 10 mM *cis* ATP, the vast majority of openings were to the maximum full conductance level. No adjustments in concentration of *cis* Ca^{2+} was made thus, chelation of free Ca^{2+} by ATP reduced overall channel P_o in the presence of 10 mM ATP (Fig. 25 A). The competition between ATP and SAM was evinced by a significant decrease in the prevalence of the SAM related substate. P_{sub}/P_o decreased from 0.828 ± 0.011 in the presence of SAM alone to 0.500 ± 0.048 and 0.244 ± 0.286 following the addition of 5 mM and 10 mM ATP, respectively (Fig. 25B). Furthermore, mean dwell time of the subconductance state decreased from 4.94 ± 0.785 ms in the presence of SAM alone to 2.74 ± 0.362 ms and

2.25 ± 0.192 following the addition of 5 and 10 mM ATP, respectively (Fig. 25C). In the presence of 2 mM *cis* SAM, openings to the full conductance level became very brief giving rise to the slight reduction in the amplitude of the maximum full conductance state in Figure 25 A (+ 2 mM SAM).

ATP was also able to partially reverse the SAM induced inhibition of RyR2 observed at +50 mV. In Figure 26A channel current fluctuations recorded at +50 mV, which were virtually abolished following the addition of 2 mM *cis* SAM, returned, although with lower frequency, upon the subsequent addition of 10 mM *cis* ATP. Summary data from 8 single channel recording experiments are presented in Figure 26B. P_o, which was reduced from 0.448 ± 0.059 to 0.008 ± 0.002 following SAM addition, increased to 0.114 ± 0.023 with the subsequent addition of 10 mM ATP.

4.4.6. The RyR2 agonist 4chloro-m-cresol (4-CmC) does not compete with SAM

A nonspecific agonistic effect on channel P_o could be proposed to explain the ability of ATP to interfere with the SAM related substate at negative potentials, and the SAM induced inhibition at positive potentials. 4-Chloro-m-cresol (4-CmC) is a pharmacological agent which activates RyR with 10-25-fold higher potency compared with the commonly used channel activator, caffeine (*148*). Representative data from experiments exploring competition between SAM and 4-CmC are shown in Figure 27A. Following the addition of 2 mM SAM, P_{sub}/P_o increased significantly from 0.264± 0.024 to 0.843 ± 0.048 and remained elevated at 0.879 ± 0.027 upon subsequent addition of 0.6 mM 4-CmC (Fig. 27 B). An increase in the mean dwell time of the SAM related substate accounted for the effect of 4-CmC on P_{sub}/P_o (Fig. 27 C). In 6 experiments competition

between 4-CmC and SAM was never observed. Similarly, there was no competition between SAM and 4-CmC at a positive holding potential (+50 mV) (Fig. 28 A). In all of 7 experiments SAM caused significant channel inhibition reducing P_o from 0.414 ± 0.113 to 0.015 ± 0.007. With the subsequent addition of 4-CmC, channel inhibition persisted (P_o = 0.012 ± 0.006) (Fig. 28 B). Thus, it is unlikely that the competition between SAM and ATP is due to a nonspecific agonistic effect of ATP, but rather the interaction of SAM and ATP with a common regulatory site on the channel.

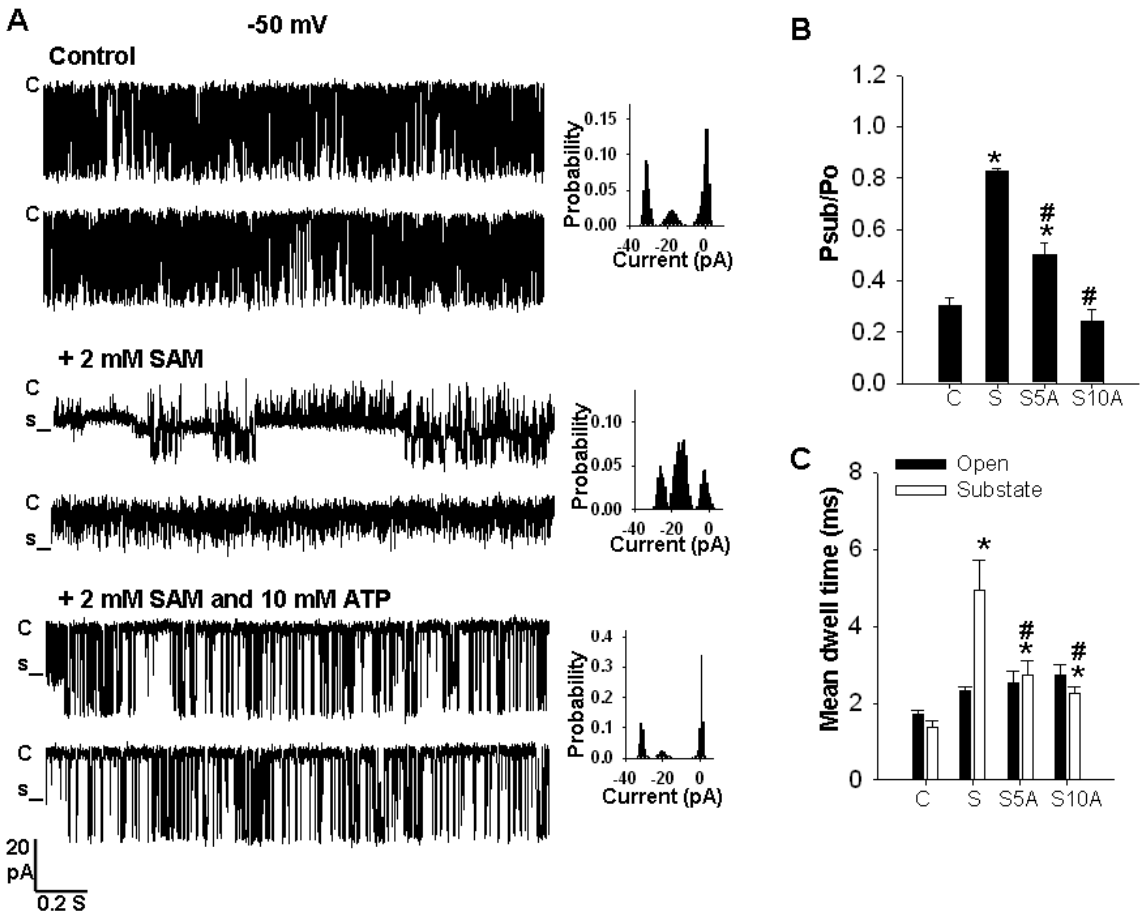

Figure 25. ATP interferes with the SAM related subconductance state. (A) Single channel currents shown as downward deflections from closed (c), were recorded as described in Figure 21at a holding potential of -50 mV. The peaks in the amplitude histograms indicate the predominant conductance states of the channel. The current traces were obtained before (top) and after (middle) the addition of 2 mM *cis* SAM. SAM induced a clearly defined subconductance state (s) which was largely abolished upon the subsequent addition of 10 mM ATP to the *cis* solution (bottom). (B) Proportion of subconductance events for channels recorded as in A in the absence of SAM, following the addition of 2 mM SAM, and the subsequent addition of 5 mM ATP, and 10 mM ATP (C, S, S5A, and S10A respectively). Data are shown as mean ± SEM for 4 experiments. Control vs. SAM *p<0.001, Control vs SAM + 5 mM ATP *p<0.05, #p<0.001, and SAM vs SAM + 10 mM ATP #p<0.001. (C) Mean dwell times in the full open (black bars) and subconductance (white bars) state for channels recorded as in A in the absence of SAM, following the addition of 2 m SAM, and the subsequent addition of 5 mM ATP, and 10 mM ATP (C, S, S5A, and S10A respectively). Data are shown as mean ± SEM for 4 experiments. Control vs. SAM *p<0.01, control vs. SAM + 5 mM ATP *p< 0.05, control vs. SAM +10 mM ATP * p<0.05, SAM vs. SAM + 5 mM ATP # p<0.05, and SAM vs. SAM + 10 mM ATP # p<0.05. Mean open state dwell time were significantly increased over control in the presence of SAM and SAM + ATP p<0.05.

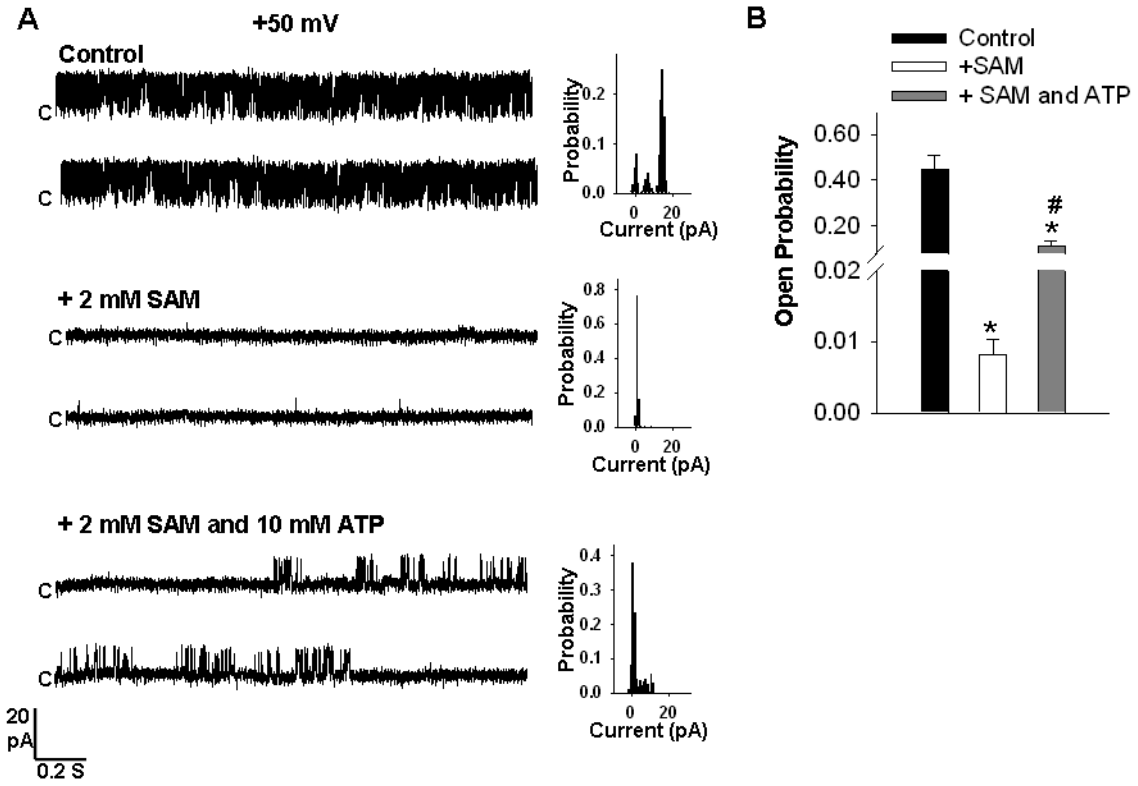

Figure 26. Channel activity is partially restored by ATP following inhibition by SAM at positive holding potential. (A) Single channel currents shown as upward deflections from closed (c), were recorded as described in Figure 21 at a holding potential of +50 mV. The peaks in the amplitude histograms indicate the predominant conductance states of the channel. Current fluctuations (top), which were nearly abolished immediately following the addition of 2 mM SAM to the *cis* solution (middle), were partially restored upon subsequent addition of 10 mM *cis* ATP (bottom). (B) Open probability for channels recorded as in A in the absence of SAM (black bars), following the addition of 2 mM SAM (white bars), and the subsequent addition of 10 mM ATP (grey bars). Data are shown as mean ± SEM of 4 experiments. Significantly different from control *$p<0.001$, significantly different from SAM, #$p<0.001$.

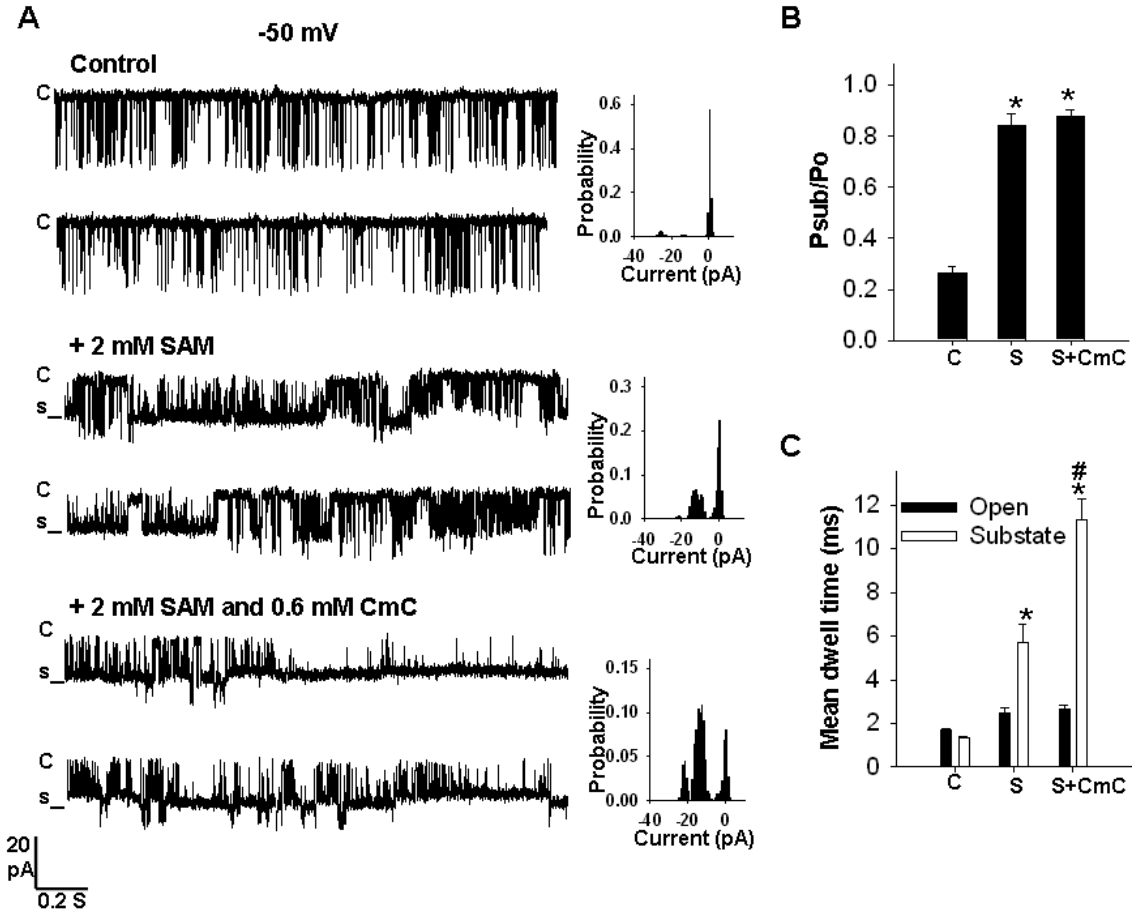

Figure 27. RyR2 agonist 4-chloro-m-cresol (4-CmC) does not interfere with the SAM related subconductance state. (A) Single channel currents shown as downward deflections from closed (c), were recorded as described in Figure 21 at a holding potential of -50mV. The peaks in the amplitude histograms indicate the predominant conductance states of the channel. Following the addition of 2 mM *cis* SAM RyR2 current fluctuated predominantly between the closed (c) and subconductance (s) levels (middle traces), a pattern which persists upon subsequent addition of 0.6 mM cis 4-CmC. (B) Proportion of subconductance events for channels recorded as in A in the absence of SAM, following the addition of 2mM SAM, and the subsequent addition of 0.6 mM 4-CmC (C, S, S + 4-CmC respectively). Data are shown as mean ± SEM for 6 experiments. Significantly different from control *$p<0.001$. (C) Mean dwell times in the full open (black bars) and subconductance (white bars) state for channels recorded as in A in the absence of SAM, following the addition of 2 mM SAM, and the subsequent addition of 0.6 mM 4-CmC (C, S, S + 4-CmC respectively). Data are shown as mean ± SEM for 6 experiments. Significantly different from control *$p<0.001$, significantly different from SAM #$p<0.01$. Open dwell time was significantly increased over control in the presence of SAM plus or minus 4-CmC $p< 0.01$.

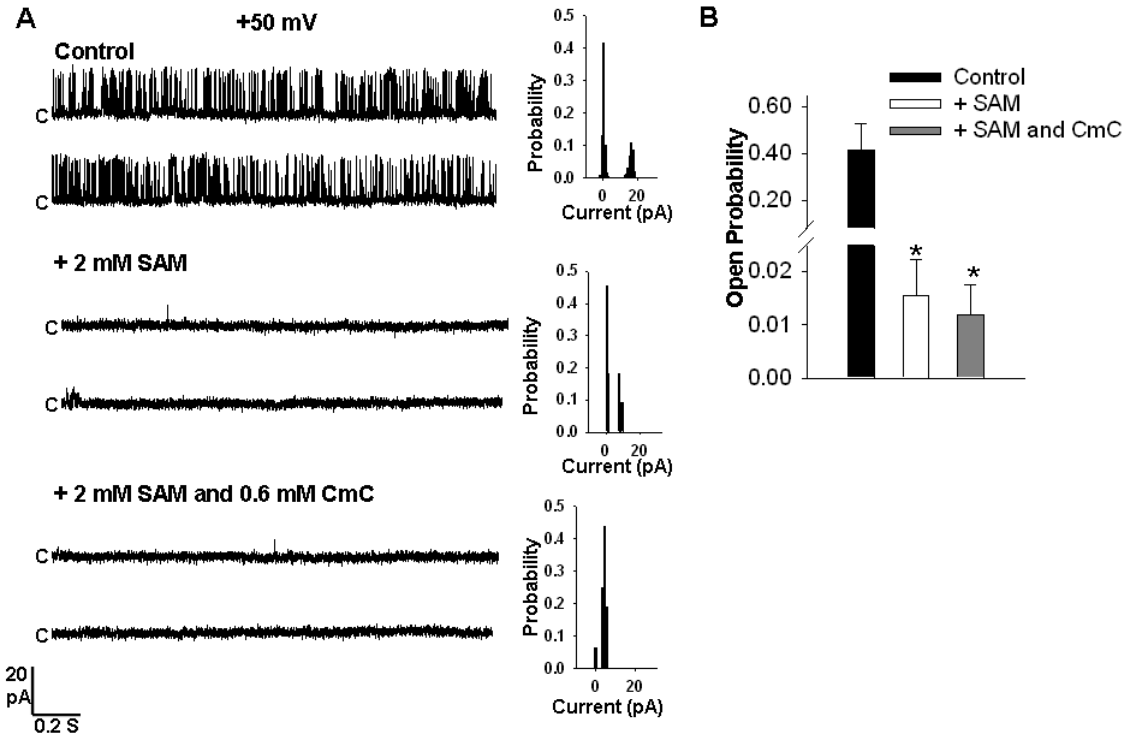

Figure 28. RyR2 agonist 4-chloro-m-cresol (4-CmC) does not restore channel activity following inhibition by SAM at positive holding potential. (A) Single channel currents shown as upward deflections from closed (c), were recorded as described in Figure 21 at a holding potential of +50 mV. The peaks in the amplitude histograms indicate the predominant conductance states of the channel. Current fluctuations (top traces), were nearly abolished immediately following the addition of 2 mM SAM to the *cis* solution (middle traces), and this SAM induced channel inhibition persisted upon the subsequent addition of 0.6 mM *cis* 4-CmC. (B) Open probability for channels recorded as in A in the absence of SAM (black bars), following the addition of 2 mM SAM (white bars), and subsequent addition of 0.6 mM 4-CmC (grey bars). Data are shown as mean ± SEM for 7 experiments. Significantly different from control *$p<0.01$

4.4.7. ATP does not interfere with the effects of an established RyR pore blocker

As an additional control we investigated whether ATP interferes with the TBA^+ related substate. Cytosolic tetra butyl ammonium (TBA^+) produces a RyR2 substate (21% full conductance) at positive voltages via a pore block mechanism (*86, 149*). In Figure 29 single channel currents recorded at +90mV showed a clearly resolvable low amplitude subconductance state in the presence of 0.5 mM *cis* TBA^+. Subsequent addition of 10 mM *cis* ATP did not decrease the prevalence of the TBA^+ related substate. On average P_{sub}/P_o was 0.875 ± 0.066 and 0.912 ± 0.0271 in the presence of 0.5 mM TBA^+ alone and 0.5 mM TBA^+ plus 10 mM ATP, respectively (Fig. 29B). The slight increase in P_{sub}/P_o caused by ATP was accompanied by a significant increase in mean dwell time of the TBA^+ related substate analogous to the effect of 4-CmC on the SAM related substate (Fig. 27 C). Therefore ATP does not interfere with the subconductance state produced by an established RyR2 pore blocker.

4.4.8. ATP activation of RyR2 is not dependent on membrane potential

The lack of an effect of driving force on the prevalence of the SAM related substate and the specific ability of ATP to interfere with the SAM related substate argue for an allosteric mechanism, whereby SAM binding a regulatory site on the channel stabilizes a conformational state having reduced conductance. The effects of SAM on RyR2 are voltage dependent, therefore if ATP and SAM bind a common regulatory site, ATP activation of RyR2 may also vary with membrane potential. The effect of ATP on channel P_o was monitored over a range of voltages from -100 to 100 mV. The single channel current records in Figure 30A show that RyR2 activity was increased by 2 mM

ATP to a similar extent regardless of holding potential (Fig. 30 D). Note the lack of an effect of ATP on channel conductance. At -50 mV, P_o was significantly increased from 0.281 ± 0.093 to 0.699 ± 0.094 in the presence of 2 mM ATP, and was similarly increased at a holding potential of + 50 mV. However, because of high variability among individual channels, these data did not reach significance (control, 0.447 ± 0.129; 2 mM ATP, 0.735 ± 0.084) (Fig. 30 B). ATP increased mean open dwell time from 1.73 ± 0.204 to 8.78 ± 3.01 ms at -50 mV, and from 2.0 ± 0.262 to 13.61 ± 5.808 ms at + 50 mV (Fig. 30 C).

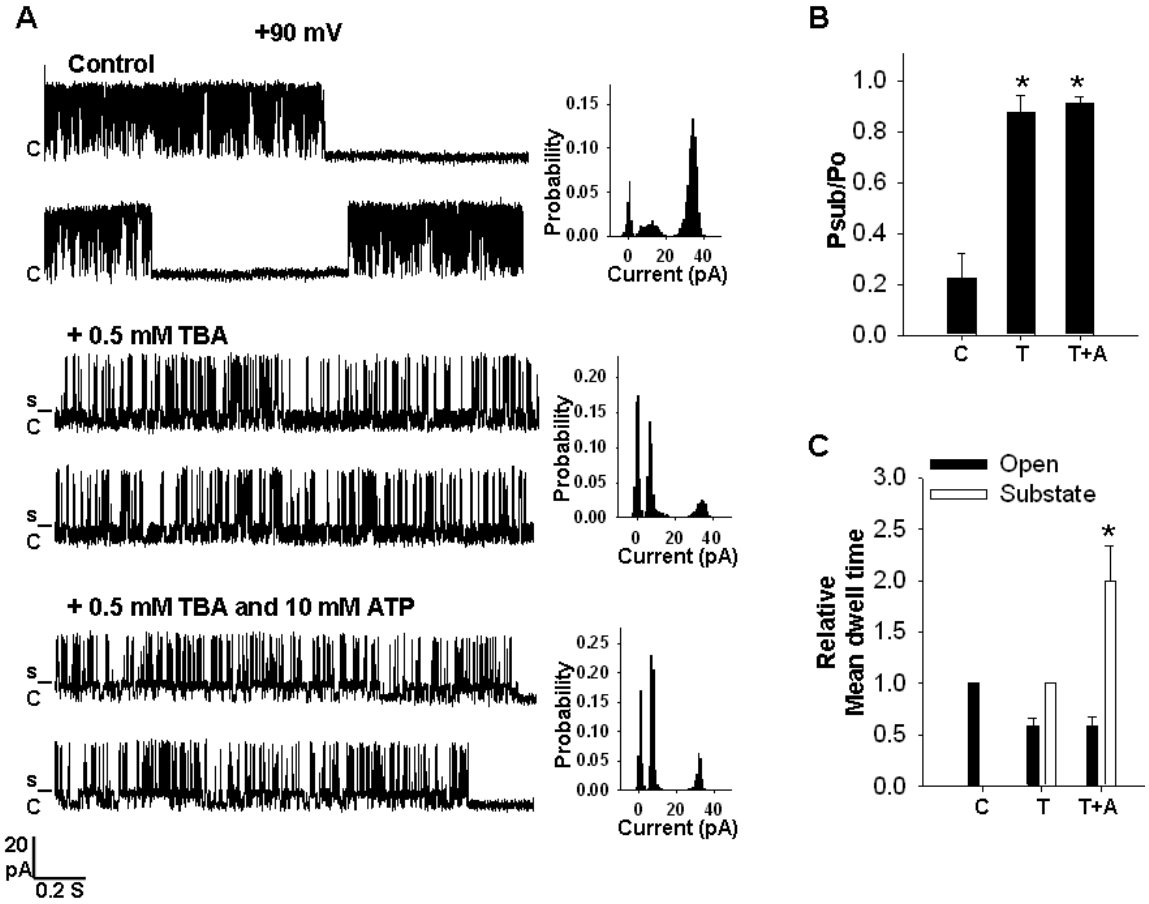

Figure 29. ATP does not interfere with the effects of a known pore blocker. (A) Single channel currents shown as upward deflections from closed (c), were recorded as described in Figure 21 at a holding potential of +90 mV. The peaks in the amplitude histograms indicate the predominant conductance states of the channel. The subconductance state (s) elicited upon the addition of 0.5mM *cis* TBA^+ (middle traces) persists and is prolonged when 10 mM ATP is added to the *cis* solution (bottom traces). (B) Proportion of subconductance events for channels recorded as in A in the absence of TBA^+, in the presence of 0.5 mM TBA^+, and following the addition of 10 mM ATP (C, T, and T+A respectively). Data are shown as mean ± SEM for 4 experiments. Significantly different from control *$p<0.001$. (C) Mean full open state (black bars) and TBA^+ induced subconductance state (white bars) dwell times for channels recorded as in A in the absence of TBA^+, in the presence of 0.5 mM TBA^+, and following the addition of 10 mM ATP (C, T, and T+A respectively). Data are shown as means ± SEM for 4 experiments and are expressed as relative to control to reduce affects of variability between individual channels. Significantly different from TBA^+ *$p< 0.0$. Open dwell time was significantly reduced from control in the presence of TBA^+ plus or minus ATP $p< 0.01$.

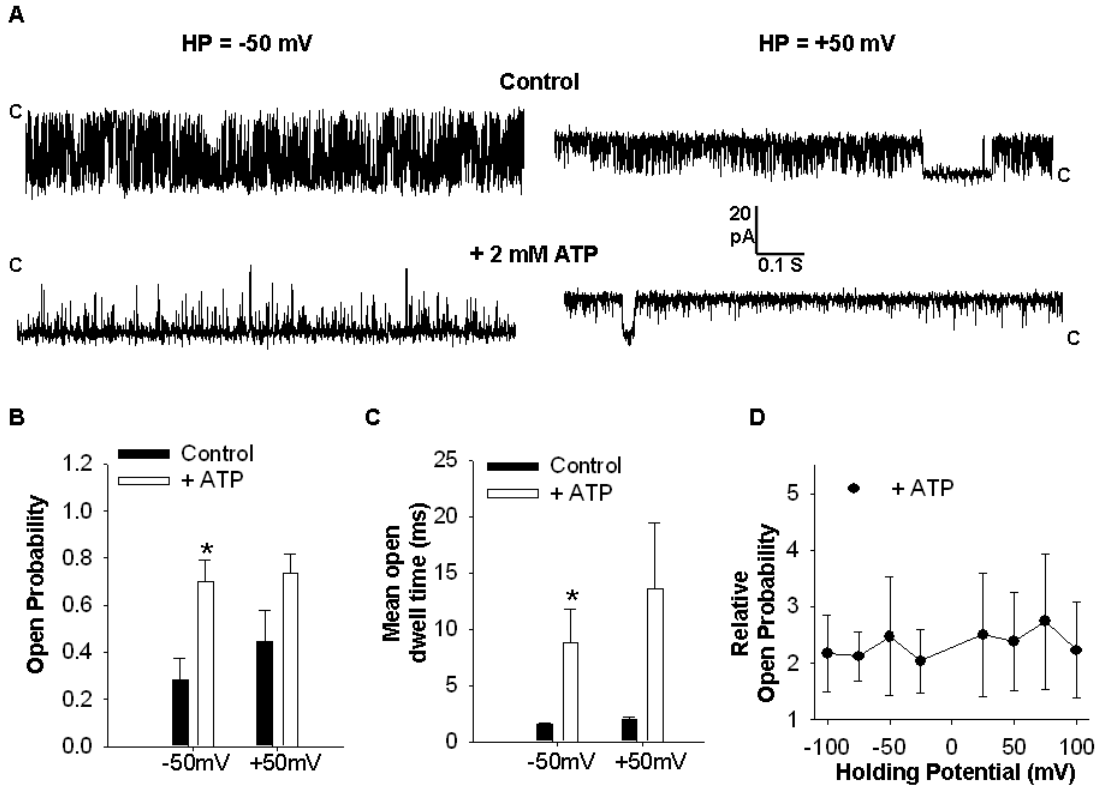

Figure 30. ATP activation of RyR2 is independent of voltage. (A) Single channel currents shown as downward or upward deflections from closed (c), were recorded as described in Figure 21 at ±50 mV. (B) Open probability for channels recorded as in A in the absence (black bars), or presence of 2 mM ATP (white bars). Data are shown as means ± SEM of 6 experiments. Significantly different from control *$p<0.05$. (C) Mean open dwell time for channels recorded as at ±50 mV in the absence (black bars) or presence of 2 mM ATP (white bars). Data are shown as means ± SEM of 6 experiments. Significantly different from control *$p<0.05$. (D) The extent of RyR2 activation by ATP does not change with holding potential. Open probability was analyzed as relative changes from control conditions (no ATP, -50 mV) induced by 2 mM ATP to reduce affects of variability between individual channels. Data are shown as means ± SEM of 6 experiments.

4.4.9. Behavior of the SAM related substate is inconsistent with a gating scheme for open channel block

A final assessment investigated whether a reversible binding process provided a valid description of the SAM related substate. The model in Figure 31 A for reversible discrete block at a single site implies that the binding of SAM to a site in the conductance pathway of the open channel (O) gives rise to a subconductance form of the channel in complex with SAM (S•SAM). Because dwell times in a given state are inversely proportional to the rate constants away from that state, a pore block model predicts that the dwell time of the open full conductance will be dependent on the SAM concentration while the dwell time of the subconductance state will be independent of SAM concentration. The mean dwell time of the open subconductance state was significantly increased in the presence of 2, 4, and 6 mM SAM. However, because of high variability among individual channels, the data at 8 and 10 mM SAM did not reach significance. In contrast, neither the mean dwell time of the open full conductance state or the closed state were affected by SAM. These observations indicate that the one step blocking scheme in Figure 31A is not a valid model of the substate process.

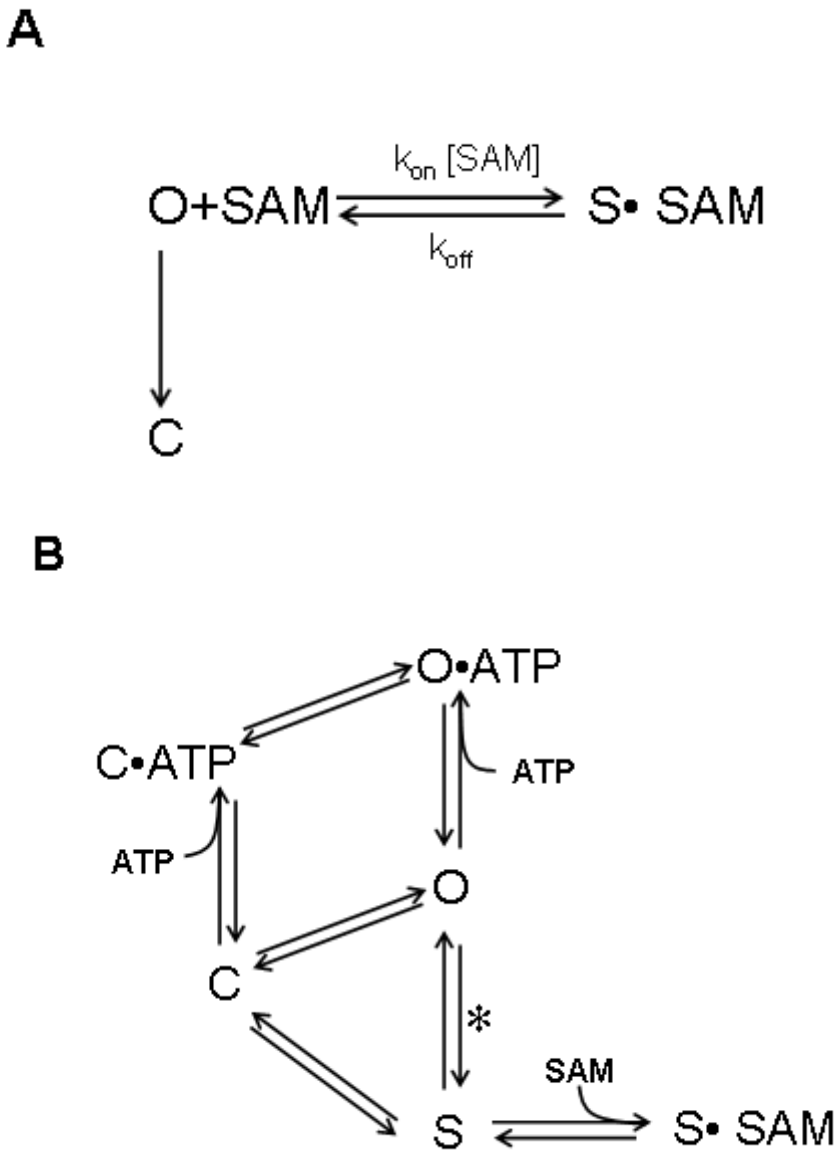

Figure 31. Comparing a pore block and an allosteric model for the SAM related substate process. A) Simple blocking model which entails the binding of SAM to a single site on the open full conductance conformation, O, resulting in a subconductance form of the channel in complex with SAM, S•SAM. B) Allosteric model of subconductance state production by SAM which proposes that SAM preferentially binds to and stabilizes a channel conformation of reduced conductance (described in detail in *Discussion*).

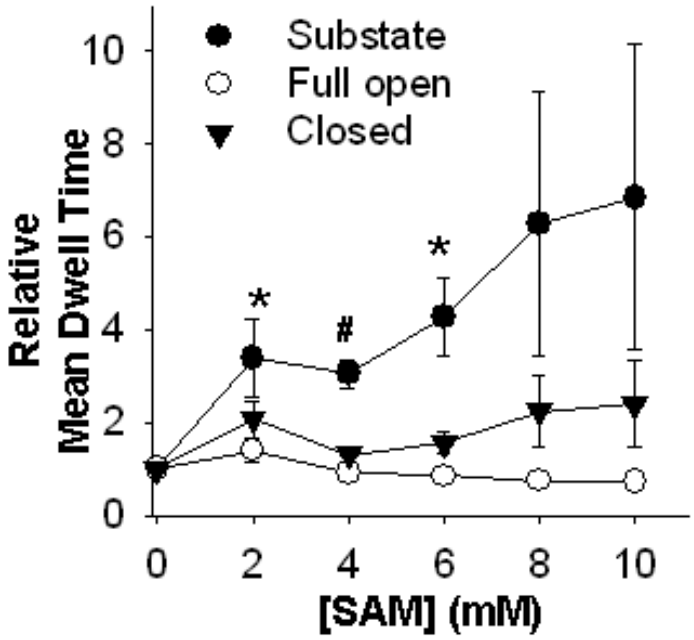

Figure 32. Relationship between SAM concentrations and mean state dwell times. Relative Mean dwell times of the subconductance (●), maximum full conductance (○) and closed (▼) states as a function of SAM concentration for channels recoded as in Figure 21 at -50 mV. Dose response curves show that duration of the subconductance state increased with increasing SAM concentration. Durations of the maximum full conductance and closed state were independent of SAM concentration. Data are shown as mean ± SEM from 2-3 experiments. * (substate), $p<0.05$ versus 0 mM SAM; # (substate), $p<0.01$ versus 0 mM SAM.

4.5. Discussion

We have previously reported that SAM directly activates RyR2 in a manner independent from its recognized role as a biological methyl group donor (*146*). Several lines of evidence suggest that SAM and ATP share a common binding site. RyR2 activation by SAM and ATP is similar in that both compounds enhance Ca^{2+} activation of the channel but have minimal effects on channel activity in the absence of Ca^{2+} and the dose response curves for SAM and ATP enhancement of CSR [^{3}H]ryanodine binding virtually overlap. Most convincingly, the adenine nucleotides ADP and AMP, which compete for ATP activation of RyR2, similarly compete with SAM activation of RyR2 in the presence of sub-activating, maximally-activating, and inhibitory Ca^{2+} concentrations.

Measurements of single channel activity revealed that SAM activation of RyR2 is associated with effects on channel conductance. The effects of SAM on native RyR2 channel conductance in symmetric 250 mM cesium methanesulfonate were dependent on SAM concentration and membrane holding potential. SAM was effective in producing a single, clearly resolved subconductance state (~2/3 full conductance) only from the cytosolic side, and only at negative potentials which favor *cis* to *trans* Cs^+ fluxes. The subconductance state was voltage dependent, becoming less prevalent with higher negative potentials.

Two mechanisms vie to explain the effect of SAM on RyR2 conductance: i) SAM interferes directly with ion permeation via binding within the conduction pathway, or ii) the binding of SAM at a regulatory (or allosteric) site stabilizes or induces a reduced conductance conformation of the channel. Evidence for entry of SAM into the conduction pathway of RyR2 was lacking. Experiments investigated whether permeant

ions (Cs^+) interfere with the SAM related substate. This approach has clarified the mechanism underlying 'blocking' phenomena in other ion channels. For example, Armstrong provided strong support for the notion that intracellular TEA^+ blocks K^+ channels through a direct interaction with the permeation pathway by showing that the TEA^+ dissociation rate is increased by external K^+ especially at membrane potentials that elicit inward K^+ currents. The SAM related substate was unchanged by a 2.6 fold increase in *trans* Cs^+ concentration (change in driving force equivalent to a 25 mV step increase in the negative potential across the bilayer) (Fig. 25). This lack of interference between permeant ions and the interaction of SAM with the channel is a strong indication that SAM affects channel conductance via a regulatory (allosteric) site on the cystolic face of the channel some distance from the ion conduction pathway.

Secondly, behavior of the SAM related substate was inconsistent with a reversible binding scheme. A simple two state model describing a reversible binding reaction is shown in Figure 34 A. The significance of this model is that it is only realistic in the case of direct pore block (i.e. the physical interaction of the 'blocking' species with the permeation pathway). According to this scheme SAM binding to the open full conductance state (O) results in partial channel block which manifests as a subconductance state (S). This mechanism predicts that the lifetime of the open state (O) will be inversely proportional to the rate of SAM binding, which in turn is dependent on the concentration of SAM, whereas lifetime of the subconductance state (S) is determined by the residence time of SAM at its site, a parameter which is independent of SAM concentration. Thus, for the case of direct pore block, the lifetime of the open full conductance and subconductance states should be inversely proportional to and

independent of SAM concentration, respectively. However, duration of the open full conductance state was unaffected by SAM concentration, whereas the duration of the subconductance state increased as a function of SAM concentration.

The state diagram in Figure 31 B is an allosteric model which accounts for, i) the interconversion between the closed (C), open (O), and subconductance (S) states, ii) the increased lifetime of the subconductance state with increasing SAM concentration, iii) the voltage dependent behavior of the SAM related subconductance state at negative potentials, and iv) the competition between ATP and SAM. It was clear from single channel current recordings that RyR2 can enter the subconductance state (S) from either the open full conductance state (O) or the closed state (C), hence the triangular scheme which allows for interconversion between all three states. Although conductance levels are shown as single states (O, S, C) in the diagram, this is not meant to imply a direct correspondence between channel conductance and channel state (or conformation). In other words RyR2 may adopt multiple distinct conformations which can not be distinguished based on conductance alone.

SAM does not appear to induce the change in channel conformation (to the subconductance conformation). Rather, SAM binds to and stabilizes an inherent subconductance conformation. When bound by SAM (S•SAM) the subconductance conformation is more energetically favorable (stable). Support for this interpretation is based upon the presence of brief infrequent openings to the subconductance state even in the absence of SAM which increase in duration as a function of SAM concentration.

The scheme depicted in Figure 31 B, attributes the apparent voltage dependence of SAM's interaction (increase in k_{off} with increasing negative potentials) to a voltage

dependent (*) equilibrium between at least two inherent channel conformations (the open full conductance state (O) and the subconductance state (S)). By this allosteric mechanism, voltage indirectly influences SAM binding. The regulatory site has a high affinity for SAM when the channel is in the S conformation and a low affinity for SAM when the channel is in the O conformation. Higher negative potentials shift the equilibrium towards the O conformation giving rise to the apparent increase in k_{off} as voltage becomes more negative. Due to the brevity and low frequency of subconductance openings in the absence of SAM it was not possible to directly investigate the voltage dependence of the substate in the absence of SAM.

The proposed allosteric model also addresses the competitive effects of SAM and ATP on RyR2 activity. Measurements of [^{3}H]ryanodine binding showed that the characteristics of SAM and ATP activation of RyR2 both involve an enhancement of Ca^{2+} activation of the channel, and the dose response curves virtually overlapped. The adenine nucleotides, ADP and AMP, which competed for ATP activation of RyR2, similarly competed for SAM activation of the channel. At the single channel level competition was observed as an interference of ATP with the SAM related subconductance state. This was a specific competition between ATP and SAM. The RyR2 agonist 4-CMC did not interfere with the SAM related subconductance state. The competition between SAM and ATP can be attributed to the existence of a regulatory site to which either SAM or ATP can bind. Presumably this regulatory site is specific for adenine nucleotides, and SAM and ATP interact with this site via their common structural feature, the adenosine moiety. Others have shown that concentrations of ATP $\leq EC_{50}$ primarily increased channel P_o by increasing the frequency of channel openings

while [ATP] ≥ EC_{50} progressively increased P_o by increasing the duration of channel openings (*43*). Thus, ATP is shown interacting with the open full conductance state (O) and the closed state (C). The lack of effect of membrane potential on ATP activation (Fig. 30) indicates that ATP is unable to bind its regulatory site when the channel is in the S conformation.

Within the limits of an allosteric model involving SAM binding the adenine nucleotide binding site, one of two possibilities may explain the voltage dependent effect of SAM. The first possibility purports the existence of a subconductance state which interconverts in a voltage dependent manner with the open full conductance state. Although indirect, support for this interpretation comes from the observation that a clearly defined subconductance state is observed with low frequency in channel currents recorded in the absence of SAM. Alternatively, the adenine nucleotide binding site lies within the membrane electric field. However support for this interpretation is lacking as ATP activation of RyR2 was not dependent on membrane holding potential. In summary, the effects of SAM and ATP are mediated through a common binding site and a direct effect of voltage on protein conformation accounts for the voltage dependent effects of SAM. This work underscores the complexity of ion channel gating and its modulation; it affirms the notion that channels exist in manifold conformations with distinct ion permeation properties.

CHAPTER 5

PERSPECTIVE AND FUTURE DIRECTIONS

5.1. Summary of presented work

The goal of this dissertation was to clarify the mechanism by which SAM regulates RyR2. Initial experiments aimed at characterizing the effect of SAM on RyR2 employed [^{3}H]ryanodine binding to cardiac SR vesicles. CSR vesicle [^{3}H]ryanodine binding was increased by SAM at concentrations as low as 75 μM. The Ca^{2+} concentration dependence of CSR [^{3}H]ryanodine binding revealed that SAM activation of RyR2 is Ca^{2+} dependent; SAM increased Ca^{2+} activation of the channel, but alone did not activate. Saturation analysis indicated that low concentrations of SAM primarily enhanced CSR [^{3}H]ryanodine binding by increasing the affinity of RyR2 for ryanodine, while higher concentrations of SAM also increased the number of channels which bind ryanodine. Additional experiments investigated the effects of SAM on RyR2 in the presence of other physiological RyR2 effectors. Alone SAM and the nonhydrolysable ATP analogue AMPPNP enhanced CSR [^{3}H]ryanodine binding however, combined their effects were not additive. This was an early indication of an interaction between SAM and ATP.

Because SAM is well-known for its role as a biological methyl group donor I explored whether methylation mediated the effect of SAM on RyR2 activity. SAH and sinefungin are methyltransferase inhibitors; SAH works by mass action while sinefungin competes with the SAM binding site on the enzyme. Neither SAH nor sinefungin interfered with the SAM induced increase in CSR [^{3}H]ryanodine binding. The

incorporation of methyl groups into CSR incubated with a radiolabeled SAM (S-adenosyl-L-[methyl-^{3}H]-methionine) was investigated. Scintillation counts (radioactivity) remained elevated after multiple wash steps indicating methylation of some CSR component(s). However, imunoprecipitation showed that no amount of the radioactivity was specifically associated with RyR2. This was direct evidence that RyR2 was not methylated in the presence of SAM, and that methyltransferase activity was not required for SAM activation of RyR2.

With confidence that SAM activation of RyR2 is independent from its function as a methyl group donor, interest shifted to the structural similarity between SAM and ATP. Several lines of evidence suggested that SAM and ATP share a common binding site. RyR2 activation by SAM and ATP was similar in that both compounds enhance the Ca^{2+} activation of the channel but have minimal effects on channel activity in the absence of Ca^{2+} and the dose response curves for SAM and ATP enhancement of CSR [^{3}H]ryanodine binding virtually overlapped. Most convincingly, the adenine nucleotides ADP and AMP, which competed for ATP activation of RyR2, similarly competed with SAM activation of RyR2 in the presence of sub-activating, maximally-activating, and inhibitory Ca^{2+} concentrations.

At the single channel level, 100 μM cytosolic SAM increased RyR2 P_o, consistent with results from CSR [^{3}H]ryanodine binding. The aim to compare the kinetics of SAM and ATP activation of RyR2 was encumbered by the unexpected observation that SAM promoted a subconductance state having an amplitude ~ 2/3 of the open full conductance level. The subconductance state was SAM concentration dependent, accounting for almost 60% of the overall channel P_o in the presence of 2 mM SAM. Cytosolic SAM did

not affect the open full conductance level and luminal SAM had no effect on channel activity.

SAM has a net positive charge and a molecular weight close to that of the charged local anesthetic lidocaine, and two quaternary amines (QX572 and QX314) which affect RyR2 conductance via a direct interaction with the permeation pathway (i.e. pore block). However, the SAM related substate process was incompatible with the hypothesis that SAM affects channel conductance via pore block. Firstly, premeant cations did not appear to interfere with SAM binding as the prevalence of the SAM related subconductance state was unaffected by a change in the driving force for ion flux. This lack of interference between permeant cations and the interaction of SAM with the channel was a strong indication that SAM affects channel conductance via a regulatory (allosteric) site on the cytosolic face of the channel some distance from the ion conduction pathway. Further analysis revealed that the duration of the subconductance state increased as a function of SAM concentration. This behavior is consistent with the notion that SAM binds to and stabilizes an inherent RyR2 subconductance conformation.

The kinetics of SAM and ATP activation could not be compared as originally planned due to the confounding effect of SAM on RyR2 conductance. Both SAM and ATP increased channel P_o, however only SAM induced a subconductance state, thus the SAM related substate could be used as gauge for determining whether SAM and ATP bind a common regulatory site on the channel. ATP caused a decrease in the prevalence of the SAM related subconductance state. This competition was dose dependent (10 mM ATP more effective than 5 mM ATP) and specific to ATP. The RyR2 agonist 4-CmC did not interfere with the SAM related subconductance state. Furthermore, ATP did not

interact with the effects of a known RyR2 pore blocker, TBA^+. Together these data suggested that SAM and ATP share a common binding site.

In summary, SAM is a RyR2 channel agonist which induces a subconductance state. This work indicates that SAM modulates RyR2 channel gating through a direct physical interaction with a site located on the cytosolic face of the channel, and that SAM and ATP share a common binding site. Unlike ATP, the interaction of SAM with RyR2 is voltage dependent. I have proposed an allosteric model whereby voltage driven changes in channel conformation alter the affinity of a putative regulatory site (possibly the adenine nucleotide site) for SAM. By this mechanism, the direct effect of voltage on protein conformation gives rise to the voltage dependent subconductance behavior produced by SAM.

5.2. Future direction and implications

A working model for SAM regulation of RyR must first consider the mode of interaction. SAM is an established methyl group donor and SAM mediated methylation of RyR2 would be a novel mechanism of RyR2 channel regulation with potential implications for the physiological and pathological control of cardiac function. However, this work showed that SAM regulation of RyR2 does not involve methylation. Methyltransferase inhibitors did not block SAM activation of RyR2 and methylation of the channel was not detected. Furthermore, if SAM regulated RyR2 via methylation a delayed effect would be expected. However, direct measurements of channel activity showed that the effects of SAM are immediate and independent of exposure time to SAM. These findings establish SAM as a novel RyR2 regulatory ligand.

Direct measurements of RyR2 channel activity revealed a SAM related subconductance state. Initial speculation that SAM binding causes the dissociation of a RyR2 regulatory protein was based on apparent irreversibility of the subconductance state (*146*). In repeated single channel experiments, an increased proportion of subconductance events were detected under control conditions if the bilayer apparatus was not thoroughly washed at the end of the preceding experiment (personal observation). Efficient removal of SAM from even the single channel recording apparatus appears to require very thorough washing. Thus in retrospect, I attribute the relatively high proportion of subconductance events in SAM pretreated channels (*146*) to incomplete removal of SAM from the CSR.

Two remaining mechanisms vied to explain the SAM related subconductance state. The pore block mechanism attributes the effect of SAM on RyR2 conductance to a direct interference with ion permeation via SAM binding within the conduction pathway. The alternative allosteric mechanism envisions the binding of SAM to a regulatory (or allosteric) site stabilizes or induces a reduced conductance conformation of the channel.

Findings from this research make a pore block mechanism for the effect of SAM of RyR2 conductance improbable. The interference between permeant ions and the SAM related substate was investigated. This approach has clarified the mechanism underlying 'blocking' phenomena in other ion channels. For example, Armstrong provided strong support for notion that intracellular TEA^+ blocks K^+ channels by binding a site located in the permeation pathway by showing that the TEA^+ dissociation rate is increased by external K^+ especially at membrane potentials that elicit inward K^+ currents (*97*). The prevalence of the SAM related subconductance state was unchanged when the driving

force for cation (Cs^+) flux was increased under asymmetric conditions (elevated *trans* Cs^+). Therefore, permeant ions did not appear to interfere with SAM reaching its binding site on the channel. Additionally, behavior of the SAM related substate was inconsistent with a simple reversible binding scheme for open channel block. According to the model in Figure 33, SAM binds in or very near the conduction pathway producing a subconductance state (S) by direct interference with ion permeation (either by physical occlusion or electrostatic repulsion). This reversible binding scheme predicts the duration of the open full conductance state to be inversely proportional to SAM concentration. However, mean dwell time of the open full conductance state was not dependent on SAM concentration. Rather, the mean dwell time of the subconductance state increased with SAM concentration. Therefore I conclude that SAM does not directly interact with the permeation pathway of the channel. I propose that the subconductance state represents a channel conformation with altered permeation properties, which becomes more energetically favorable when bound by SAM.

The state diagram in Figure 34 is a summary of the experimental findings. It is clear from single channel current recordings that RyR2 can enter the subconductance state (S) from either the open full conductance state (O) or the closed state (C), hence the triangular scheme (in black) which allows for interconversion between all three states. Although conductance levels are shown as single states (O, S, C) in the diagram, this is not meant to imply a direct correspondence between channel conductance and channel state (or conformation). In other words RyR2 may adopt multiple distinct conformations which can not be distinguished based on conductance alone.

SAM does not appear to induce the change in channel conformation (to the subconductance conformation). Rather, SAM binds to and stabilizes an inherent subconductance conformation (shown in blue). When bound by SAM (S•SAM) the subconductance conformation is more energetically favorable (stable). Support for this interpretation is based upon the presence of brief infrequent openings to the subconductance state even in the absence of SAM which increased in duration as a function of SAM concentration.

SAM only effectively produced the subconductance state from the cytosolic face of RyR2, and only at negative holding potentials which favor luminal to cytosolic cation fluxes. The substate became less prevalent with higher negative potentials. A voltage dependent (V) equilibrium between at least two inherent channel conformations (the open full conductance state (O) and the subconductance state (S) in Figure 34 can account for the apparent voltage dependence of SAM's interaction (k_{on} and k_{off}). I propose that the regulatory site has a high affinity for SAM when the channel is in the S conformation and a low affinity for SAM when the channel is in the O conformation. Higher negative potentials shift the equilibrium towards the O conformation giving rise to the apparent increase in k_{off} as voltage becomes more negative.

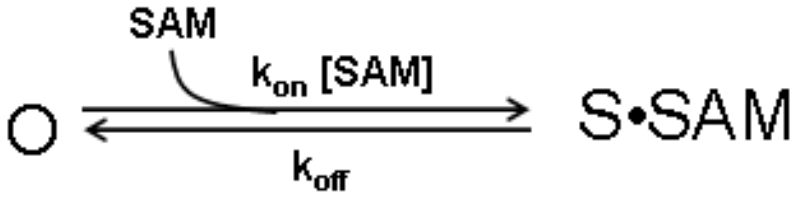

Figure 33. Predictions based upon a pore block mechanism for the SAM related subconductance state. The gating scheme for open channel block predicts the duration of the open full conductance state (O) will decrease as the concentration of SAM in increased, while the duration of the SAM bound subconductance state (S•SAM) will be independent of SAM concentration.

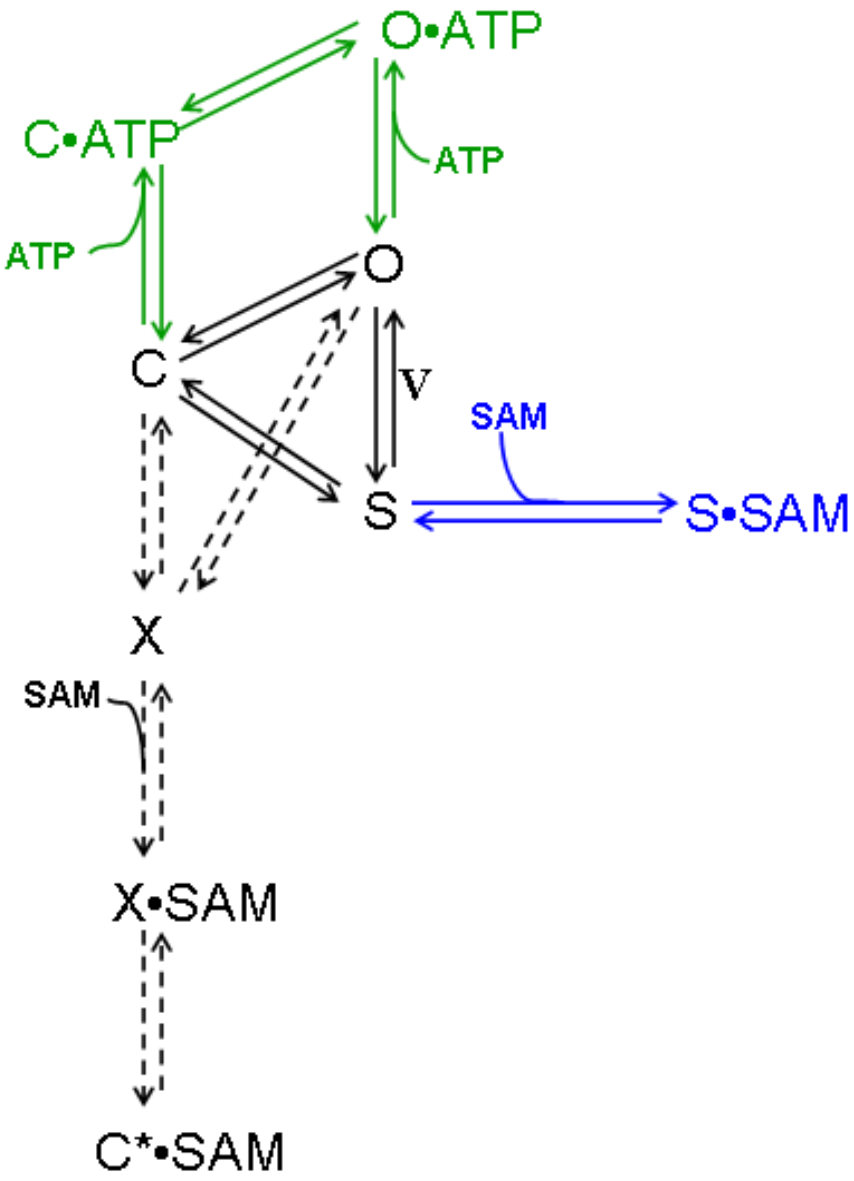

Figure 34. Allosteric model of the SAM related subconductance state. SAM binds to and stabilizes and inherent subconductance state (S). The model proposes a voltage dependent (V) equilibrium between the open full conductance (O) and inherent subconductance state (S) to account for the voltage dependence of SAM's interaction with the channel. SAM and ATP bind a common regulatory site; SAM has a high affinity for this site when the channel is in the S conformation while ATP has a high affinity for this site when the channel is in the O conformation. SAM inhibition (C*•SAM; inactivated state) of RyR2 at positive potentials could be accommodated in our model by postulating a pathway whereby positive voltages promote one or more different channel conformations (X) which lead into a distinct gating pathway (dotted arrows).

My model also addresses the competitive effects of SAM and ATP on RyR2 activity. Measurements of [^{3}H]ryanodine binding showed that the characteristics of SAM and ATP activation of RyR2 both involved an enhancement of Ca^{2+} activation of the channel, and the dose response curves virtually overlapped. The adenine nucleotides, ADP and AMP, which competed for ATP activation of RyR2, similarly competed for SAM activation of the channel. At the single channel level competition was observed as an interference of ATP with the SAM related subconductance state. This was a specific competition between ATP and SAM. The RyR2 agonist 4-CmC did not interfere with the SAM related subconductance state. I attribute the competitive effects of SAM and ATP to the existence of a regulatory site to which either SAM or ATP can bind. Presumably this regulatory site is specific for adenine nucleotides; SAM and ATP interact with this site via their common structural feature, the adenosine moiety. Others have shown that concentrations of ATP $\leq EC_{50}$ primarily increased channel P_o by increasing the frequency of channel openings while [ATP] $\geq EC_{50}$ progressively increased P_o by increasing the duration of channel openings (*43*). Thus, ATP is shown interacting with the open full conductance state (O) and the closed (C) (Fig.34, green). The lack of effect of membrane potential on ATP activation indicated that ATP is unable to bind its regulatory site when the channel is in the S conformation. ATP activation of RyR2 was not voltage dependent and ATP did not produce a subconductance state. Although perplexing, these observations are not irreconcilable with our allosteric model. My model suggests that ATP, by stabilizing the full open state of the channel, reduces the availability of the high SAM affinity S state.

In summary, the effects of SAM and ATP are mediated through a common binding site and a direct effect of voltage on protein conformation accounts for the voltage dependent effect of SAM. This work underscores the complexity of ion channel gating and its modulation; it affirms the notion that channels exist in manifold conformations with distinct ion permeation properties.

Questions remain regarding the inhibitory effect of SAM on RyR2 at positive potentials. Channel activity was virtually abolished in the presence of 2 mM cytosolic SAM. SAM 'inactivation' (C*•SAM; inactivated state) of RyR2 at positive potentials could be accommodated in the model by postulating a mechanism whereby positive voltages impose different forces on the channel protein giving rise to one or more different channel conformations (X) which lead into a distinct gating pathway (Fig. 34, dotted arrows). Importantly, competition between SAM and ATP was also observed at positive potentials suggesting that SAM 'inactivation' of RyR2 is likewise mediated via a regulatory site shared by ATP. Due to channel inactivation, the interaction of SAM with RyR2 at positive potentials was not amenable to kinetic analysis. However, by 'locking' the channel open with ryanodine it may be possible to analyze the interaction of SAM with ryanodine-modified RyR2 at positive potentials in spite of SAMs strong inhibitory effect. This approach was used to investigate the interaction of ruthenium red with RyR1 (*100*). In the presence of 0.3 mM SAM, channel P_o was reduced by approximately 50% compared to the over 90% reduction in P_o observed in the presence of 2 mM SAM. It may therefore be possible to gain insight into the interaction of SAM with RyR2 at positive potentials by analyzing channel activity in the presence of micromolar SAM concentrations which promote only a moderate reduction in channel activity.

As this work has demonstrated, direct measurements of channel activity can provide insights that might not be detected by ryanodine binding measurements. There are some discrepancies between the effects of SAM on RyR2 revealed from ryanodine binding measurements and single channel recordings. Ryanodine binding did not saturate with up to 10 mM SAM, however channel P_o reached a plateau at ~2 mM SAM. Although there is evidence to suggest that the high affinity ryanodine binding site is available only when the channel is open (*27, 28, 92*), more recent findings indicate that ryanodine does not bind within the channel pore (*89, 93, 150*). Therefore, although measurements of ryanodine binding correlate reasonably well with RyR activation levels, it is not surprising to find equilibrium ryanodine binding measurements are not a direct reflection of channel open time. One can reconcile the inhibitory effect of SAM observed in direct measurements of RyR2 activity at positive potentials with the SAM induced increase in CSR ryanodine binding by the fact that a transmembrane potential of 0 mV is expected during ryanodine binding measurements.

SR membrane is highly permeable to monovalent cations and anions suggesting that the potential across the SR in resting muscle is close to 0 mV (*151*). The question arises as to whether SAM produces a subconductance state when transmembrane potential is held at 0 mV. This investigation may be informative. The disparate effects of SAM on RyR2 activity at positive and negative potentials demonstrated that SAM interacts with RyR2 in a voltage dependent manner. Therefore at 0 mV holding potential I would expect SAM regulation of RyR2 to differ from the effects described in this work.

Both cardiac and skeletal RyRs (RyR2 and RyR1, respectively) are activated by millimolar concentrations of adenine nucleotides; however the activation characteristics

of the two isoforms have a number of important differences. A major difference is that adenine nucleotides activate RyR1in the absence of Ca^{2+} (*43, 152, 153*), while RyR2 requires Ca^{2+} for adenine nucleotide activation (*43, 61*). A similar discrepancy in the requirement of Ca^{2+} for SAM activation of the RyR1 and RyR2 would provide additional evidence that SAM binds ATP sites on the channel.

Adenosine antagonizes ATP activation of both RyR1 and RyR2 by a mechanism in which adenosine is a relatively weak agonist that competes for ATP binding sites on the channel (*43, 61, 153*). However, adenosine is noted to be a weaker activator of RyR1 compared to RyR2 (*61, 153*). Furthermore, the relative affinities for ATP and adenosine are quite different in RyR2 and RyR1; in RyR1, the ratio of the dissociation constants $K_{ATP}/K_{adenosine}$ is ~ 6, while in RyR2 $K_{ATP}/K_{adenosine}$ is ~1 (*153*). Thus adenosine is a more potent inhibitor of ATP activation of RyR1 compared to RyR2. A comparison of the effect of adenosine on SAM activation of RyR1 and RyR2 would be informative. Based on the hypothesis that SAM and ATP share a common binding site I expect adenosine to more effectively antagonize SAM activation of RyR1.

Although our data suggest SAM and ATP share a common binding site we can not rule out the possibility that these two molecules interact with distinct sites which are allosterically coupled. Sequence analysis of RyR1 predicts at least eight adenine nucleotide consensus binding motifs per monomer (*69*) however, the characteristics of RyR activation by ATP, and direct binding studies suggest the presence of only two ATP binding sites per RyR monomer (*43, 63*). Mutagenesis of two predicted ATP binding sequences, GXGXXG (amino acids 2370-2375 of RyR1), and YSGK (amino acids 3937-3940 of RyR1), which are conserved among all RyR isoforms, did not alter the ATP

induced increase in [^{3}H]ryanodine binding to any of the RyR1 mutants (*69*). Thus far the combined use of functional assays and molecular biology has not identified which, if any, of the predicted consensus motifs confers sensitivity of RyR to ATP. Although low resolution reconstructions of RyR have been obtained (*154*), high resolution crystallographic means will be required to confidently locate ATP binding sites by structural means.

An important question concerns the significance of SAM regulation of RyR2. Our findings indicate that SAM and ATP regulate RyR2 via a common binding site. The overlap of the SAM and ATP dose-response curves indicates the regulatory site has similar affinity for these two molecules. Therefore, SAM regulation of RyR2 is unlikely of physiological relevance given that cytosolic levels of ATP in cardiac cells (5-6 mM) (*58*) far exceed cellular concentrations of SAM (60-90 μM) (*112*). However, the notion that SAM regulates RyR2 via adenine nucleotide regulatory sites has important implications for clarifying the structural basis of ATP regulation of the channel and provides insight into the molecular characteristics (i.e. steric factors, charge distribution) required of ligands acting through the adenine nucleotide regulatory sites. Furthermore, study of the SAM related subconductance state provides insight into mechanisms of RyR2 gating. The finding that SAM stabilizes a subconductance conformation of RyR2 suggests substates may be an inherent characteristic of RyR channel gating.

4.3. Closing

RyR2 plays a critical role in the contractile performance of the heart and recent compelling evidence positions RyR2 as a potential target for the treatment of cardiac

arrhythmias and heart disease. However, uncertainty remains regarding the structural motifs involved in RyR2 modulation by even its principal physiological ligands, Ca^{2+} and ATP. Therefore, the interaction of SAM with the ATP regulatory site(s) is a novel finding which has exciting implications for clarifying the structure-activity relationship underlying ATP regulation of RyR2. The SAM related subconductance state is of special interest because it appears to involve an allosteric mechanism of gating modification. Patterns in the transitions between RyR2 conductance states in the presence of SAM may provide insight into the structure-activity relationship of RyR2 which can aid in the development of therapeutic strategies targeting this channel.

REFERENCES

1. Sandow, A. (1965) Excitation-contraction coupling in skeletal muscle, *Pharmacol Rev 17*, 265-320.
2. Ringer, S. (1883) A further Contribution regarding the influence of the different Constituents of the Blood on the Contraction of the Heart, *J Physiol 4*, 29-42 23.
3. Heilbrunn, L. V. (1940) The action of calcium on muscle protoplasm, *Physiol Zool 13*, 88-94.
4. Heilbrunn, L. V., and Wiercinski, F. J. (1947) The action of various cations on muscle protoplasm, *J Cell Physiol 29*, 15-32.
5. Rossi, D., Barone, V., Giacomello, E., Cusimano, V., and Sorrentino, V. (2008) The sarcoplasmic reticulum: an organized patchwork of specialized domains, *Traffic 9*, 1044-1049.
6. Ebashi, S., and Lipmann, F. (1962) Adenosine Triphosphate-Linked Concentration of Calcium Ions in a Particulate Fraction of Rabbit Muscle, *J Cell Biol 14*, 389-400.
7. Franzini-Armstrong, C., and Nunzi, G. (1983) Junctional feet and particles in the triads of a fast-twitch muscle fibre, *J Muscle Res Cell Motil 4*, 233-252.
8. Franzini-Armstrong, C. (1964) Fine Structure of Sarcoplasmic Reticulum and Tranverse Tubular System in Muscle Fibers, *Fed Proc 23*, 887-895.
9. Jenden, D. J., and Fairhurst, A. S. (1969) The pharmacology of ryanodine, *Pharmacol Rev 21*, 1-25.
10. Fleischer, S., Ogunbunmi, E. M., Dixon, M. C., and Fleer, E. A. (1985) Localization of Ca2+ release channels with ryanodine in junctional terminal cisternae of sarcoplasmic reticulum of fast skeletal muscle, *Proc Natl Acad Sci U S A 82*, 7256-7259.
11. Franzini-Armstrong, C. (1980) Structure of sarcoplasmic reticulum, *Fed Proc 39*, 2403-2409.
12. Radermacher, M., Rao, V., Grassucci, R., Frank, J., Timerman, A. P., Fleischer, S., and Wagenknecht, T. (1994) Cryo-electron microscopy and three-dimensional reconstruction of the calcium release channel/ryanodine receptor from skeletal muscle, *J Cell Biol 127*, 411-423.
13. Smith, J. S., Coronado, R., and Meissner, G. (1985) Sarcoplasmic reticulum contains adenine nucleotide-activated calcium channels, *Nature 316*, 446-449.
14. Smith, J. S., Coronado, R., and Meissner, G. (1986) Single channel measurements of the calcium release channel from skeletal muscle sarcoplasmic reticulum. Activation by Ca2+ and ATP and modulation by Mg2+, *J Gen Physiol 88*, 573-588.
15. Bers, D. M. (2004) Macromolecular complexes regulating cardiac ryanodine receptor function, *J Mol Cell Cardiol 37*, 417-429.
16. Hamilton, S. L. (2005) Ryanodine receptors, *Cell Calcium 38*, 253-260.
17. Franzini-Armstrong, C., Protasi, F., and Ramesh, V. (1998) Comparative ultrastructure of Ca2+ release units in skeletal and cardiac muscle, *Ann N Y Acad Sci 853*, 20-30.

18. Fill, M., and Copello, J. A. (2002) Ryanodine receptor calcium release channels, *Physiol Rev 82*, 893-922.
19. Tripathy, A., Xu, L., Mann, G., and Meissner, G. (1995) Calmodulin activation and inhibition of skeletal muscle Ca2+ release channel (ryanodine receptor), *Biophys J 69*, 106-119.
20. Bers, D. M., Li, L., Satoh, H., and McCall, E. (1998) Factors that control sarcoplasmic reticulum calcium release in intact ventricular myocytes, *Ann N Y Acad Sci 853*, 157-177.
21. Brillantes, A. B., Ondrias, K., Scott, A., Kobrinsky, E., Ondriasova, E., Moschella, M. C., Jayaraman, T., Landers, M., Ehrlich, B. E., and Marks, A. R. (1994) Stabilization of calcium release channel (ryanodine receptor) function by FK506-binding protein, *Cell 77*, 513-523.
22. Marx, S. O., Reiken, S., Hisamatsu, Y., Jayaraman, T., Burkhoff, D., Rosemblit, N., and Marks, A. R. (2000) PKA phosphorylation dissociates FKBP12.6 from the calcium release channel (ryanodine receptor): defective regulation in failing hearts, *Cell 101*, 365-376.
23. Beard, N. A., Wei, L., and Dulhunty, A. F. (2009) Ca(2+) signaling in striated muscle: the elusive roles of triadin, junctin, and calsequestrin, *Eur Biophys J 39*, 27-36.
24. Marx, S. O., Reiken, S., Hisamatsu, Y., Gaburjakova, M., Gaburjakova, J., Yang, Y. M., Rosemblit, N., and Marks, A. R. (2001) Phosphorylation-dependent regulation of ryanodine receptors: a novel role for leucine/isoleucine zippers, *J Cell Biol 153*, 699-708.
25. Salama, G., Menshikova, E. V., and Abramson, J. J. (2000) Molecular interaction between nitric oxide and ryanodine receptors of skeletal and cardiac sarcoplasmic reticulum, *Antioxid Redox Signal 2*, 5-16.
26. Sun, J., Yamaguchi, N., Xu, L., Eu, J. P., Stamler, J. S., and Meissner, G. (2008) Regulation of the cardiac muscle ryanodine receptor by O(2) tension and S-nitrosoglutathione, *Biochemistry 47*, 13985-13990.
27. Meissner, G. (1994) Ryanodine receptor/Ca2+ release channels and their regulation by endogenous effectors, *Annu Rev Physiol 56*, 485-508.
28. Chu, A., Diaz-Munoz, M., Hawkes, M. J., Brush, K., and Hamilton, S. L. (1990) Ryanodine as a probe for the functional state of the skeletal muscle sarcoplasmic reticulum calcium release channel, *Mol Pharmacol 37*, 735-741.
29. Mueller, P., Rudin, D. O., Tien, H. T., and Wescott, W. C. (1962) Reconstitution of cell membrane structure in vitro and its transformation into an excitable system, *Nature 194*, 979-980.
30. Sitsapesan, R., and Williams, A. J. (1994) Gating of the native and purified cardiac SR Ca(2+)-release channel with monovalent cations as permeant species, *Biophys J 67*, 1484-1494.
31. Ashley, R. H., and Williams, A. J. (1990) Divalent cation activation and inhibition of single calcium release channels from sheep cardiac sarcoplasmic reticulum, *J Gen Physiol 95*, 981-1005.
32. Rousseau, E., Smith, J. S., Henderson, J. S., and Meissner, G. (1986) Single channel and 45Ca2+ flux measurements of the cardiac sarcoplasmic reticulum calcium channel, *Biophys J 50*, 1009-1014.

33. Tinker, A., Lindsay, A. R., and Williams, A. J. (1992) A model for ionic conduction in the ryanodine receptor channel of sheep cardiac muscle sarcoplasmic reticulum, *J Gen Physiol 100*, 495-517.
34. Lindsay, A. R., Manning, S. D., and Williams, A. J. (1991) Monovalent cation conductance in the ryanodine receptor-channel of sheep cardiac muscle sarcoplasmic reticulum, *J Physiol 439*, 463-480.
35. Tinker, A., and Williams, A. J. (1992) Divalent cation conduction in the ryanodine receptor channel of sheep cardiac muscle sarcoplasmic reticulum, *J Gen Physiol 100*, 479-493.
36. Tinker, A., Lindsay, A. R., and Williams, A. J. (1992) Block of the sheep cardiac sarcoplasmic reticulum Ca(2+)-release channel by tetra-alkyl ammonium cations, *J Membr Biol 127*, 149-159.
37. Buck, E., Zimanyi, I., Abramson, J. J., and Pessah, I. N. (1992) Ryanodine stabilizes multiple conformational states of the skeletal muscle calcium release channel, *J Biol Chem 267*, 23560-23567.
38. Sutko, J. L., Airey, J. A., Welch, W., and Ruest, L. (1997) The pharmacology of ryanodine and related compounds, *Pharmacol Rev 49*, 53-98.
39. Tinker, A., Sutko, J. L., Ruest, L., Deslongchamps, P., Welch, W., Airey, J. A., Gerzon, K., Bidasee, K. R., Besch, H. R., Jr., and Williams, A. J. (1996) Electrophysiological effects of ryanodine derivatives on the sheep cardiac sarcoplasmic reticulum calcium-release channel, *Biophys J 70*, 2110-2119.
40. Welch, W., Williams, A. J., Tinker, A., Mitchell, K. E., Deslongchamps, P., Lamothe, J., Gerzon, K., Bidasee, K. R., Besch, H. R., Jr., Airey, J. A., Sutko, J. L., and Ruest, L. (1997) Structural components of ryanodine responsible for modulation of sarcoplasmic reticulum calcium channel function, *Biochemistry 36*, 2939-2950.
41. Meissner, G., Darling, E., and Eveleth, J. (1986) Kinetics of rapid Ca2+ release by sarcoplasmic reticulum. Effects of Ca2+, Mg2+, and adenine nucleotides, *Biochemistry 25*, 236-244.
42. Xu, L., Mann, G., and Meissner, G. (1996) Regulation of cardiac Ca2+ release channel (ryanodine receptor) by Ca2+, H+, Mg2+, and adenine nucleotides under normal and simulated ischemic conditions, *Circ Res 79*, 1100-1109.
43. Kermode, H., Williams, A. J., and Sitsapesan, R. (1998) The interactions of ATP, ADP, and inorganic phosphate with the sheep cardiac ryanodine receptor, *Biophys J 74*, 1296-1304.
44. Hill, A. P., Kingston, O., and Sitsapesan, R. (2004) Functional regulation of the cardiac ryanodine receptor by suramin and calmodulin involves multiple binding sites, *Mol Pharmacol 65*, 1258-1268.
45. Meissner, G., and Henderson, J. S. (1987) Rapid calcium release from cardiac sarcoplasmic reticulum vesicles is dependent on Ca2+ and is modulated by Mg2+, adenine nucleotide, and calmodulin, *J Biol Chem 262*, 3065-3073.
46. Xu, L., and Meissner, G. (1998) Regulation of cardiac muscle Ca2+ release channel by sarcoplasmic reticulum lumenal Ca2+, *Biophys J 75*, 2302-2312.
47. Xu, L., and Meissner, G. (2004) Mechanism of calmodulin inhibition of cardiac sarcoplasmic reticulum Ca2+ release channel (ryanodine receptor), *Biophys J 86*, 797-804.

48. Laver, D. R., Baynes, T. M., and Dulhunty, A. F. (1997) Magnesium inhibition of ryanodine-receptor calcium channels: evidence for two independent mechanisms, *J Membr Biol 156*, 213-229.
49. Timerman, A. P., Onoue, H., Xin, H. B., Barg, S., Copello, J., Wiederrecht, G., and Fleischer, S. (1996) Selective binding of FKBP12.6 by the cardiac ryanodine receptor, *J Biol Chem 271*, 20385-20391.
50. Lam, E., Martin, M. M., Timerman, A. P., Sabers, C., Fleischer, S., Lukas, T., Abraham, R. T., O'Keefe, S. J., O'Neill, E. A., and Wiederrecht, G. J. (1995) A novel FK506 binding protein can mediate the immunosuppressive effects of FK506 and is associated with the cardiac ryanodine receptor, *J Biol Chem 270*, 26511-26522.
51. Jeyakumar, L. H., Ballester, L., Cheng, D. S., McIntyre, J. O., Chang, P., Olivey, H. E., Rollins-Smith, L., Barnett, J. V., Murray, K., Xin, H. B., and Fleischer, S. (2001) FKBP binding characteristics of cardiac microsomes from diverse vertebrates, *Biochem Biophys Res Commun 281*, 979-986.
52. Xiao, J., Tian, X., Jones, P. P., Bolstad, J., Kong, H., Wang, R., Zhang, L., Duff, H. J., Gillis, A. M., Fleischer, S., Kotlikoff, M., Copello, J. A., and Chen, S. R. (2007) Removal of FKBP12.6 does not alter the conductance and activation of the cardiac ryanodine receptor or the susceptibility to stress-induced ventricular arrhythmias, *J Biol Chem 282*, 34828-34838.
53. Xiao, B., Sutherland, C., Walsh, M. P., and Chen, S. R. (2004) Protein kinase A phosphorylation at serine-2808 of the cardiac Ca2+-release channel (ryanodine receptor) does not dissociate 12.6-kDa FK506-binding protein (FKBP12.6), *Circ Res 94*, 487-495.
54. Li, Y., Kranias, E. G., Mignery, G. A., and Bers, D. M. (2002) Protein kinase A phosphorylation of the ryanodine receptor does not affect calcium sparks in mouse ventricular myocytes, *Circ Res 90*, 309-316.
55. Stange, M., Xu, L., Balshaw, D., Yamaguchi, N., and Meissner, G. (2003) Characterization of recombinant skeletal muscle (Ser-2843) and cardiac muscle (Ser-2809) ryanodine receptor phosphorylation mutants, *J Biol Chem 278*, 51693-51702.
56. Barg, S., Copello, J. A., and Fleischer, S. (1997) Different interactions of cardiac and skeletal muscle ryanodine receptors with FK-506 binding protein isoforms, *Am J Physiol 272*, C1726-1733.
57. Meissner, G. (1984) Adenine nucleotide stimulation of Ca2+-induced Ca2+ release in sarcoplasmic reticulum, *J Biol Chem 259*, 2365-2374.
58. Swain, J. L., Sabina, R. L., McHale, P. A., Greenfield, J. C., Jr., and Holmes, E. W. (1982) Prolonged myocardial nucleotide depletion after brief ischemia in the open-chest dog, *Am J Physiol 242*, H818-826.
59. Laver, D. R. (2006) Regulation of ryanodine receptors from skeletal and cardiac muscle during rest and excitation, *Clin Exp Pharmacol Physiol 33*, 1107-1113.
60. Chan, W. M., Welch, W., and Sitsapesan, R. (2003) Structural characteristics that govern binding to, and modulation through, the cardiac ryanodine receptor nucleotide binding site, *Mol Pharmacol 63*, 174-182.

61. Chan, W. M., Welch, W., and Sitsapesan, R. (2000) Structural factors that determine the ability of adenosine and related compounds to activate the cardiac ryanodine receptor, *Br J Pharmacol 130*, 1618-1626.
62. Ching, L. L., Williams, A. J., and Sitsapesan, R. (1999) AMP is a partial agonist at the sheep cardiac ryanodine receptor, *Br J Pharmacol 127*, 161-171.
63. Dias, J. M., Szegedi, C., Jona, I., and Vogel, P. D. (2006) Insights into the regulation of the ryanodine receptor: differential effects of Mg2+ and Ca2+ on ATP binding, *Biochemistry 45*, 9408-9415.
64. Saraste, M., Sibbald, P. R., and Wittinghofer, A. (1990) The P-loop--a common motif in ATP- and GTP-binding proteins, *Trends Biochem Sci 15*, 430-434.
65. Mao, L., Wang, Y., Liu, Y., and Hu, X. (2004) Molecular determinants for ATP-binding in proteins: a data mining and quantum chemical analysis, *J Mol Biol 336*, 787-807.
66. Patel, S., Joseph, S. K., and Thomas, A. P. (1999) Molecular properties of inositol 1,4,5-trisphosphate receptors, *Cell Calcium 25*, 247-264.
67. Betzenhauzer, M. J., Wagner, Larry E., Park, Hyung Seo, and Yule, David I. (2009) ATP regulation of type-1 inositol (1,4,5)-trisphosphate receptor activity does not require walker a-type ATP-binding motifs, *J Biol Chem*.
68. Nunn, D. L., and Taylor, C. W. (1990) Liver inositol, 1,4,5-trisphosphate-binding sites are the Ca2(+)-mobilizing receptors, *Biochem J 270*, 227-232.
69. Du, G. G., Oyamada, H., Khanna, V. K., and MacLennan, D. H. (2001) Mutations to Gly2370, Gly2373 or Gly2375 in malignant hyperthermia domain 2 decrease caffeine and cresol sensitivity of the rabbit skeletal-muscle Ca2+-release channel (ryanodine receptor isoform 1), *Biochem J 360*, 97-105.
70. Brandt, N. R., Caswell, A. H., Brandt, T., Brew, K., and Mellgren, R. L. (1992) Mapping of the calpain proteolysis products of the junctional foot protein of the skeletal muscle triad junction, *J Membr Biol 127*, 35-47.
71. Ogawa, Y. (1994) Role of ryanodine receptors, *Crit Rev Biochem Mol Biol 29*, 229-274.
72. Otsu, K., Willard, H. F., Khanna, V. K., Zorzato, F., Green, N. M., and MacLennan, D. H. (1990) Molecular cloning of cDNA encoding the Ca2+ release channel (ryanodine receptor) of rabbit cardiac muscle sarcoplasmic reticulum, *J Biol Chem 265*, 13472-13483.
73. Betzenhauser, M. J., Wagner, L. E., 2nd, Iwai, M., Michikawa, T., Mikoshiba, K., and Yule, D. I. (2008) ATP modulation of Ca2+ release by type-2 and type-3 inositol (1, 4, 5)-triphosphate receptors. Differing ATP sensitivities and molecular determinants of action, *J Biol Chem 283*, 21579-21587.
74. Hamill, O. P., and Sakmann, B. (1981) Multiple conductance states of single acetylcholine receptor channels in embryonic muscle cells, *Nature 294*, 462-464.
75. Hanke, W., Boheim, G., Barhanin, J., Pauron, D., and Lazdunski, M. (1984) Reconstitution of highly purified saxitoxin-sensitive Na+-channels into planar lipid bilayers, *EMBO J 3*, 509-515.
76. Barrett, J. N., Magleby, K. L., and Pallotta, B. S. (1982) Properties of single calcium-activated potassium channels in cultured rat muscle, *J Physiol 331*, 211-230.

77. Siegelbaum, S. A., Camardo, J. S., and Kandel, E. R. (1982) Serotonin and cyclic AMP close single K+ channels in Aplysia sensory neurones, *Nature 299*, 413-417.
78. Bormann, J., Hamill, O. P., and Sakmann, B. (1987) Mechanism of anion permeation through channels gated by glycine and gamma-aminobutyric acid in mouse cultured spinal neurones, *J Physiol 385*, 243-286.
79. Mak, D. O., and Foskett, J. K. (1997) Single-channel kinetics, inactivation, and spatial distribution of inositol trisphosphate (IP3) receptors in Xenopus oocyte nucleus, *J Gen Physiol 109*, 571-587.
80. Mak, D. O., McBride, S., Raghuram, V., Yue, Y., Joseph, S. K., and Foskett, J. K. (2000) Single-channel properties in endoplasmic reticulum membrane of recombinant type 3 inositol trisphosphate receptor, *J Gen Physiol 115*, 241-256.
81. Liu, Q. Y., Lai, F. A., Rousseau, E., Jones, R. V., and Meissner, G. (1989) Multiple conductance states of the purified calcium release channel complex from skeletal sarcoplasmic reticulum, *Biophys J 55*, 415-424.
82. Ahern, G. P., Junankar, P. R., and Dulhunty, A. F. (1994) Single channel activity of the ryanodine receptor calcium release channel is modulated by FK-506, *FEBS Lett 352*, 369-374.
83. Carter, S., Colyer, J., and Sitsapesan, R. (2006) Maximum phosphorylation of the cardiac ryanodine receptor at serine-2809 by protein kinase a produces unique modifications to channel gating and conductance not observed at lower levels of phosphorylation, *Circ Res 98*, 1506-1513.
84. Hille, B. (2001) Classical Mechanisims of Block, In *Ion Channels of Excitable Membranes* 3 ed., Sinauer Associates, Inc., Sunderland.
85. Woodhull, A. M. (1973) Ionic blockage of sodium channels in nerve, *J Gen Physiol 61*, 687-708.
86. Tinker, A., Lindsay, A. R., and Williams, A. J. (1992) Large tetraalkyl ammonium cations produce a reduced conductance state in the sheep cardiac sarcoplasmic reticulum Ca(2+)-release channel, *Biophys J 61*, 1122-1132.
87. Xu, L., Jones, R., and Meissner, G. (1993) Effects of local anesthetics on single channel behavior of skeletal muscle calcium release channel, *J Gen Physiol 101*, 207-233.
88. Tinker, A., and Williams, A. J. (1993) Charged local anesthetics block ionic conduction in the sheep cardiac sarcoplasmic reticulum calcium release channel, *Biophys J 65*, 852-864.
89. Welch, W., Ahmad, S., Airey, J. A., Gerzon, K., Humerickhouse, R. A., Besch, H. R., Jr., Ruest, L., Deslongchamps, P., and Sutko, J. L. (1994) Structural determinants of high-affinity binding of ryanoids to the vertebrate skeletal muscle ryanodine receptor: a comparative molecular field analysis, *Biochemistry 33*, 6074-6085.
90. Welch, W., Sutko, J. L., Mitchell, K. E., Airey, J., and Ruest, L. (1996) The pyrrole locus is the major orienting factor in ryanodine binding, *Biochemistry 35*, 7165-7173.
91. Bidasee, K. R., and Besch, H. R., Jr. (1998) Structure-function relationships among ryanodine derivatives. Pyridyl ryanodine definitively separates activation potency from high affinity, *J Biol Chem 273*, 12176-12186.

92. Tanna, B., Welch, W., Ruest, L., Sutko, J. L., and Williams, A. J. (1998) Interactions of a reversible ryanoid (21-amino-9alpha-hydroxy-ryanodine) with single sheep cardiac ryanodine receptor channels, *J Gen Physiol 112*, 55-69.
93. Tanna, B., Welch, W., Ruest, L., Sutko, J. L., and Williams, A. J. (2000) The interaction of a neutral ryanoid with the ryanodine receptor channel provides insights into the mechanisms by which ryanoid binding is modulated by voltage, *J Gen Physiol 116*, 1-9.
94. Moczydlowski, E., Hall, S., Garber, S. S., Strichartz, G. S., and Miller, C. (1984) Voltage-dependent blockade of muscle Na+ channels by guanidinium toxins, *J Gen Physiol 84*, 687-704.
95. Armstrong, C. M. (1966) Time course of TEA(+)-induced anomalous rectification in squid giant axons, *J Gen Physiol 50*, 491-503.
96. Armstrong, C. M. (1969) Inactivation of the potassium conductance and related phenomena caused by quaternary ammonium ion injection in squid axons, *J Gen Physiol 54*, 553-575.
97. Armstrong, C. M. (1971) Interaction of tetraethylammonium ion derivatives with the potassium channels of giant axons, *J Gen Physiol 58*, 413-437.
98. Schild, L., Ravindran, A., and Moczydlowski, E. (1991) Zn2(+)-induced subconductance events in cardiac Na+ channels prolonged by batrachotoxin. Current-voltage behavior and single-channel kinetics, *J Gen Physiol 97*, 117-142.
99. Zucchi, R., and Ronca-Testoni, S. (1997) The sarcoplasmic reticulum Ca2+ channel/ryanodine receptor: modulation by endogenous effectors, drugs and disease states, *Pharmacol Rev 49*, 1-51.
100. Ma, J. (1993) Block by ruthenium red of the ryanodine-activated calcium release channel of skeletal muscle, *J Gen Physiol 102*, 1031-1056.
101. Xu, L., Tripathy, A., Pasek, D. A., and Meissner, G. (1999) Ruthenium red modifies the cardiac and skeletal muscle Ca(2+) release channels (ryanodine receptors) by multiple mechanisms, *J Biol Chem 274*, 32680-32691.
102. Lamy, C., Goodchild, S. J., Weatherall, K. L., Jane, D. E., Liegeois, J. F., Seutin, V., and Marrion, N. V. (2010) Allosteric block of KCa2 channels by apamin, *J Biol Chem 285*, 27067-27077.
103. Goodchild, S. J., Lamy, C., Seutin, V., and Marrion, N. V. (2009) Inhibition of K(Ca)2.2 and K(Ca)2.3 channel currents by protonation of outer pore histidine residues, *J Gen Physiol 134*, 295-308.
104. Zamudio, F. Z., Gurrola, G. B., Arevalo, C., Sreekumar, R., Walker, J. W., Valdivia, H. H., and Possani, L. D. (1997) Primary structure and synthesis of Imperatoxin A (IpTx(a)), a peptide activator of Ca2+ release channels/ryanodine receptors, *FEBS Lett 405*, 385-389.
105. Fajloun, Z., Kharrat, R., Chen, L., Lecomte, C., Di Luccio, E., Bichet, D., El Ayeb, M., Rochat, H., Allen, P. D., Pessah, I. N., De Waard, M., and Sabatier, J. M. (2000) Chemical synthesis and characterization of maurocalcine, a scorpion toxin that activates Ca(2+) release channel/ryanodine receptors, *FEBS Lett 469*, 179-185.
106. Valdivia, H. H., Kirby, M. S., Lederer, W. J., and Coronado, R. (1992) Scorpion toxins targeted against the sarcoplasmic reticulum Ca(2+)-release channel of skeletal and cardiac muscle, *Proc Natl Acad Sci U S A 89*, 12185-12189.

107. Tripathy, A., Resch, W., Xu, L., Valdivia, H. H., and Meissner, G. (1998) Imperatoxin A induces subconductance states in Ca2+ release channels (ryanodine receptors) of cardiac and skeletal muscle, *J Gen Physiol 111*, 679-690.
108. Chen, L., Esteve, E., Sabatier, J. M., Ronjat, M., De Waard, M., Allen, P. D., and Pessah, I. N. (2003) Maurocalcine and peptide A stabilize distinct subconductance states of ryanodine receptor type 1, revealing a proportional gating mechanism, *J Biol Chem 278*, 16095-16106.
109. Samso, M., Trujillo, R., Gurrola, G. B., Valdivia, H. H., and Wagenknecht, T. (1999) Three-dimensional location of the imperatoxin A binding site on the ryanodine receptor, *J Cell Biol 146*, 493-499.
110. Chiang, P. K., Gordon, R. K., Tal, J., Zeng, G. C., Doctor, B. P., Pardhasaradhi, K., and McCann, P. P. (1996) S-Adenosylmethionine and methylation, *FASEB J 10*, 471-480.
111. Lu, S. C. (2000) S-Adenosylmethionine, *Int J Biochem Cell Biol 32*, 391-395.
112. Hoffman, D. R., Cornatzer, W. E., and Duerre, J. A. (1979) Relationship between tissue levels of S-adenosylmethionine, S-adenylhomocysteine, and transmethylation reactions, *Can J Biochem 57*, 56-65.
113. Eloranta, T. O., and Raina, A. M. (1977) S-adenosylmethionine metabolism and its relation to polyamine synthesis in rat liver. Effect of nutritional state, adrenal function, some drugs and partial hepatectomy, *Biochem J 168*, 179-185.
114. Paik, W. K., Paik, D. C., and Kim, S. (2007) Historical review: the field of protein methylation, *Trends Biochem Sci 32*, 146-152.
115. Finkelstein, J. D. (1990) Methionine metabolism in mammals, *J Nutr Biochem 1*, 228-237.
116. Coronado, R., Ahern, C. A., Sheridan, D. C., Cheng, W., Carbonneau, L., and Bhattacharya, D. (2004) Functional equivalence of dihydropyridine receptor alpha1S and beta1a subunits in triggering excitation-contraction coupling in skeletal muscle, *Biol Res 37*, 565-575.
117. Bedford, M. T., and Richard, S. (2005) Arginine methylation an emerging regulator of protein function, *Mol Cell 18*, 263-272.
118. Mumby, M. (2001) A new role for protein methylation: switching partners at the phosphatase ball, *Sci STKE 2001*, PE1.
119. Becchetti, A., Kemendy, A. E., Stockand, J. D., Sariban-Sohraby, S., and Eaton, D. C. (2000) Methylation increases the open probability of the epithelial sodium channel in A6 epithelia, *J Biol Chem 275*, 16550-16559.
120. Stockand, J. D., Zeltwanger, S., Bao, H. F., Becchetti, A., Worrell, R. T., and Eaton, D. C. (2001) S-adenosyl-L-homocysteine hydrolase is necessary for aldosterone-induced activity of epithelial Na(+) channels, *Am J Physiol Cell Physiol 281*, C773-785.
121. Beltran-Alvarez, P., Pagans, S., and Brugada, R. (2011) The cardiac sodium channel is post-translationally modified by arginine methylation, *J Proteome Res 10*, 3712-3719.
122. Gupta, M. P., Panagia, V., and Dhalla, N. S. (1988) Phospholipid N-methylation-dependent alterations of cardiac contractile function by L-methionine, *J Pharmacol Exp Ther 245*, 664-672.

123. Panagia, V., Gupta, M. P., Ganguly, P. K., and Dhalla, N. S. (1988) Methionine-induced positive inotropic effect in rat heart: possible role of phospholipid N-methylation, *Circ Res 62*, 51-55.
124. Chen, Y. F., Zhang, A. Y., Zou, A. P., Campbell, W. B., and Li, P. L. (2004) Protein methylation activates reconstituted ryanodine receptor-ca release channels from coronary artery myocytes, *J Vasc Res 41*, 229-240.
125. Ledbetter, M. W., Preiner, J. K., Louis, C. F., and Mickelson, J. R. (1994) Tissue distribution of ryanodine receptor isoforms and alleles determined by reverse transcription polymerase chain reaction, *J Biol Chem 269*, 31544-31551.
126. Neylon, C. B., Richards, S. M., Larsen, M. A., Agrotis, A., and Bobik, A. (1995) Multiple types of ryanodine receptor/Ca2+ release channels are expressed in vascular smooth muscle, *Biochem Biophys Res Commun 215*, 814-821.
127. Jiang, D., Xiao, B., Li, X., and Chen, S. R. (2003) Smooth muscle tissues express a major dominant negative splice variant of the type 3 Ca2+ release channel (ryanodine receptor), *J Biol Chem 278*, 4763-4769.
128. Zalk, R., Lehnart, S. E., and Marks, A. R. (2007) Modulation of the ryanodine receptor and intracellular calcium, *Annu Rev Biochem 76*, 367-385.
129. McGarry, S. J., and Williams, A. J. (1994) Adenosine discriminates between the caffeine and adenine nucleotide sites on the sheep cardiac sarcoplasmic reticulum calcium-release channel, *J Membr Biol 137*, 169-177.
130. Meissner, G., and el-Hashem, A. (1992) Ryanodine as a functional probe of the skeletal muscle sarcoplasmic reticulum Ca2+ release channel, *Mol Cell Biochem 114*, 119-123.
131. Brooks, S. P., and Storey, K. B. (1992) Bound and determined: a computer program for making buffers of defined ion concentrations, *Anal Biochem 201*, 119-126.
132. Balog, E. M., Fruen, B. R., Shomer, N. H., and Louis, C. F. (2001) Divergent effects of the malignant hyperthermia-susceptible Arg(615)-->Cys mutation on the Ca(2+) and Mg(2+) dependence of the RyR1, *Biophys J 81*, 2050-2058.
133. Paik, W. K., and Kim, S. (1967) Enzymatic methylation of protein fractions from calf thymus nuclei, *Biochem Biophys Res Commun 29*, 14-20.
134. Edinger, R. S., Yospin, J., Perry, C., Kleyman, T. R., and Johnson, J. P. (2006) Regulation of epithelial Na+ channels (ENaC) by methylation: a novel methyltransferase stimulates ENaC activity, *J Biol Chem 281*, 9110-9117.
135. Santoni, V., Verdoucq, L., Sommerer, N., Vinh, J., Pflieger, D., and Maurel, C. (2006) Methylation of aquaporins in plant plasma membrane, *Biochem J 400*, 189-197.
136. Franzini-Armstrong, C., and Protasi, F. (1997) Ryanodine receptors of striated muscles: a complex channel capable of multiple interactions, *Physiol Rev 77*, 699-729.
137. Kampfer, A. J., and Balog, E. M. (2008) S-Adenosyl-l-methionine activates the cardiac ryanodine receptor, *Biochem Biophys Res Commun 371*, 606-609.
138. Boisvert, F. M., Chenard, C. A., and Richard, S. (2005) Protein interfaces in signaling regulated by arginine methylation, *Sci STKE 2005*, re2.

139. Fruen, B. R., Kane, P. K., Mickelson, J. R., and Louis, C. F. (1996) Chloride-dependent sarcoplasmic reticulum Ca2+ release correlates with increased Ca2+ activation of ryanodine receptors, *Biophys J 71*, 2522-2530.
140. Sitsapesan, R., and Williams, A. J. (1990) Mechanisms of caffeine activation of single calcium-release channels of sheep cardiac sarcoplasmic reticulum, *J Physiol 423*, 425-439.
141. Ahern, G. P., Junankar, P. R., and Dulhunty, A. F. (1997) Subconductance states in single-channel activity of skeletal muscle ryanodine receptors after removal of FKBP12, *Biophys J 72*, 146-162.
142. Laemmli, U. K. (1970) Cleavage of structural proteins during the assembly of the head of bacteriophage T4, *Nature 227*, 680-685.
143. Timerman, A. P., Ogunbumni, E., Freund, E., Wiederrecht, G., Marks, A. R., and Fleischer, S. (1993) The calcium release channel of sarcoplasmic reticulum is modulated by FK-506-binding protein. Dissociation and reconstitution of FKBP-12 to the calcium release channel of skeletal muscle sarcoplasmic reticulum, *J Biol Chem 268*, 22992-22999.
144. Ganguly, P. K., Panagia, V., Okumura, K., and Dhalla, N. S. (1985) Activation of Ca2+-stimulated ATPase by phospholipid N-methylation in cardiac sarcoplasmic reticulum, *Biochem Biophys Res Commun 130*, 472-478.
145. Dias, J. M., and Vogel, P. D. (2009) Effects of small molecule modulators on ATP binding to skeletal ryanodine receptor, *Protein J 28*, 240-246.
146. Kampfer, A. J., and Balog, E. M. (2010) S-adenosyl-L-methionine regulation of the cardiac ryanodine receptor involves multiple mechanisms, *Biochemistry 49*, 7600-7614.
147. Colquhoun, D., and J., S. F. (1995) Fitting and Statistical Analysis of Single-Channel Records, In *Single-Channel Recording* (Sakmann, B., and Neher, E., Eds.) 2 ed., Plenum Press, New York.
148. Herrmann-Frank, A., Richter, M., Sarkozi, S., Mohr, U., and Lehmann-Horn, F. (1996) 4-Chloro-m-cresol, a potent and specific activator of the skeletal muscle ryanodine receptor, *Biochim Biophys Acta 1289*, 31-40.
149. Prod'hom, B., Pietrobon, D., and Hess, P. (1989) Interactions of protons with single open L-type calcium channels. Location of protonation site and dependence of proton-induced current fluctuations on concentration and species of permeant ion, *J Gen Physiol 94*, 23-42.
150. Tanna, B., Welch, W., Ruest, L., Sutko, J. L., and Williams, A. J. (2005) Voltage-sensitive equilibrium between two states within a ryanoid-modified conductance state of the ryanodine receptor channel, *Biophys J 88*, 2585-2596.
151. Meissner, G. (1983) Monovalent ion and calcium ion fluxes in sarcoplasmic reticulum, *Mol Cell Biochem 55*, 65-82.
152. Meissner, G., Rousseau, E., Lai, F. A., Liu, Q. Y., and Anderson, K. A. (1988) Biochemical characterization of the Ca2+ release channel of skeletal and cardiac sarcoplasmic reticulum, *Mol Cell Biochem 82*, 59-65.
153. Laver, D. R., Lenz, G. K., and Lamb, G. D. (2001) Regulation of the calcium release channel from rabbit skeletal muscle by the nucleotides ATP, AMP, IMP and adenosine, *J Physiol 537*, 763-778.

154. Wagenknecht, T., and Radermacher, M. (1995) Three-dimensional architecture of the skeletal muscle ryanodine receptor, *FEBS Lett 369*, 43-46.